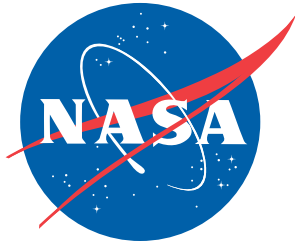NASA/CR-2012-217347 (Corrected Copy)

Composite Structures
Damage Tolerance Analysis Methodologies

James B. Chang, Vinay K. Goyal, John C. Klug and Jacob I. Rome
The Aerospace Corporation, El Segundo, California

March 2012

NASA STI Program . . . in Profile

Since its founding, NASA has been dedicated to the advancement of aeronautics and space science. The NASA scientific and technical information (STI) program plays a key part in helping NASA maintain this important role.

The NASA STI program operates under the auspices of the Agency Chief Information Officer. It collects, organizes, provides for archiving, and disseminates NASA's STI. The NASA STI program provides access to the NASA Aeronautics and Space Database and its public interface, the NASA Technical Report Server, thus providing one of the largest collections of aeronautical and space science STI in the world. Results are published in both non-NASA channels and by NASA in the NASA STI Report Series, which includes the following report types:

- TECHNICAL PUBLICATION. Reports of completed research or a major significant phase of research that present the results of NASA programs and include extensive data or theoretical analysis. Includes compilations of significant scientific and technical data and information deemed to be of continuing reference value. NASA counterpart of peer-reviewed formal professional papers, but having less stringent limitations on manuscript length and extent of graphic presentations.

- TECHNICAL MEMORANDUM. Scientific and technical findings that are preliminary or of specialized interest, e.g., quick release reports, working papers, and bibliographies that contain minimal annotation. Does not contain extensive analysis.

- CONTRACTOR REPORT. Scientific and technical findings by NASA-sponsored contractors and grantees.

- CONFERENCE PUBLICATION. Collected papers from scientific and technical conferences, symposia, seminars, or other meetings sponsored or co-sponsored by NASA.

- SPECIAL PUBLICATION. Scientific, technical, or historical information from NASA programs, projects, and missions, often concerned with subjects having substantial public interest.

- TECHNICAL TRANSLATION. English-language translations of foreign scientific and technical material pertinent to NASA's mission.

Specialized services also include creating custom thesauri, building customized databases, and organizing and publishing research results.

For more information about the NASA STI program, see the following:

- Access the NASA STI program home page at *http://www.sti.nasa.gov*

- E-mail your question via the Internet to help@sti.nasa.gov

- Fax your question to the NASA STI Help Desk at 443-757-5803

- Phone the NASA STI Help Desk at 443-757-5802

- Write to:
  NASA STI Help Desk
  NASA Center for AeroSpace Information
  7115 Standard Drive
  Hanover, MD 21076-1320
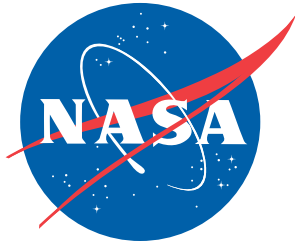
Composite Structures
Damage Tolerance Analysis Methodologies

James B. Chang, Vinay K. Goyal, John C. Klug and Jacob I. Rome
The Aerospace Corporation, El Segundo, California

Acknowledgments

The continuous encouragement from Dr. Ivatury Raju of National Aeronautics and Space Administration (NASA) Engineering and Safety Center (NESC) is highly appreciated. The administrative support from Mr. Allan Cohen of Aerospace Civil and Commercial Group is acknowledged.

ERRATA
NASA/CR–2012-217347

Issue Date: 06/04/2014

Cover, Title Page, and Report Documentation Page: Author name spelling corrected from Vanay to Vinay.

Foreword

This report presents the results of a literature review as part of the development of composite hardware fracture control guidelines funded by NASA Engineering and Safety Center (NESC) under contract NNL04AA09B. J. B. Chang is the principal investigator.

The objectives of the overall development tasks are to provide a broad information and database to the designers, analysts, and testing personnel who are engaged in space flight hardware production.

The literature review concentrated on the state-of-the-art damage tolerance analysis methods that have the potential to be used in the damage tolerance demonstration for fracture-critical composite hardware in manned and unmanned spaceflight systems.

Table of Contents

List of Figures

List of Tables

Acronyms

1-D	One-dimensional
2-D	Two-dimensional
3-D	Three-dimensional
ADAM-C	Aerospace Damage Analysis Methodology for Composites
ASTM	American Society for Testing and Materials
BAI	Burst Strength after Impact
CMH	Composite Material Handbook
COPV	Composite Overwrapped Pressure Vessel
COSAP	COPV Stress Analysis Program
da/dN	crack growth rates
DCB	Double Cantilever Beam
DF	Material Degradation Factor
ECT	End Crack Torsion
ED	Edge Delamination
ELS	End Load Split
ENF	End-Notched Flexure
ERR	Energy Release Rate
FCI	Fracture Critical Item
FEA	Finite Element Analysis
FEM	Finite Element Model
FRMM	Fixed Ratio Mixed Mode
Gr/Ep	Graphite/Epoxy
IFM	Inherent Flaw Model
LaRC	Langley Research Center
LEFM	Linear Elastic Fracture Mechanics
MIL-HDBK	Military Handbook
ML	Mar-Lin Model
MMB	Mixed-Mode Bending
NASA	National Aeronautics and Space Administration
NESC	NASA Engineering and Safety Center
NESC	NASA Engineering and Safety Center
PFA	Progressive Failure Analysis
PS	Point Strain Model
PSM	Point Stress Model
SSP	Space Station Program
UEL	User Element Subroutine
VCCT	Virtual Crack Slosure Technique
WN	Whitney and Nuismer
WN-PSM	Whitney and Nuismer Point Stress Model
WWFE	World-Wide Failure Exercise

1.0 Introduction

The National Aeronautics and Space Administration (NASA) requires that all payload that used the Space Shuttle and all equipment installed in the International Space Station comply with the fracture control requirements specified in NASA-STD-5003, *Fracture Control Requirements for Payloads Using the Space Shuttle* and SSP 30558B, *Fracture Control Requirements for Space Station*. In a general fracture control standard, NASA-STD-5007, *General Fracture Control Requirements for Manned Spaceflight Systems*, fracture critical items (FCIs) shall be demonstrated to have adequate damage tolerance capabilities, i.e., to have adequate "safe-life." This requirement is applicable to all FCIs independent of materials.

NASA-STD-5007 has been replaced by NASA-STD-5019, *Fracture Control Requirements for Spaceflight Hardware*. In this standard, fracture control of the composite and bonded structures specified in MSFC-RQMT-3479, *Fracture Control Requirements for Composite and Bonded Vehicle and Payload Structures*, shall be applied to all fracture critical composite hardware. The detail requirements specified in these standards are shown in NASA-STD-5019.

In fracture control for hardware items made of metal, the primary failure mode that should be considered is the crack propagation leading to catastrophic failure. Cracks or crack-like defects are the "damage" to be assessed. Damage tolerance demonstration consists of life and residual strength predictions that are obtained by performing fatigue crack growth analysis and static fracture strength analysis. Linear elastic fracture mechanics (LEFM) principle is the base for such analyses. The primary parameter used in LEFM is the crack-tip stress intensity factor, which is a function of the crack size, crack geometry and applied loading conditions. Crack growth analysis computer codes used in the aerospace industry, including CRKGRO (Chang *et al.*, 1981) and FLAGRO (Hu, 1980), all contain various K-solutions and a large database of fracture properties (K_c) and crack growth rates (da/dN). The capabilities of crack-growth life predictions using LEFM have been shown to be adequate when correlated with experimental results (Chang, 1981). NASGRO (JSC-22267B, *Fatigue Crack Growth Computer Program NASGRO®*, 2001), a derivative code from FLAGRO, is widely used for space flight hardware.

In fracture control of composite hardware, it is generally agreed that analytical methods that can be used for damage tolerance demonstration of composite structures are not as mature as the metallic counterparts. It is known that tensile failures of composite structures are primarily K associated with fiber breaking. On the other hand, compression and shear failures of composite structures are often associated with matrix cracking and local delamination. Furthermore, a commonly used composite material system such as graphite/epoxy (Gr/Ep) is very brittle and highly susceptible to impact damage. Therefore, the evaluations of damage tolerance capabilities of composite hardware are much more complicated than their metallic counterparts.

To meet fracture control requirements levied in NASA-STD-5003 and SSP 30558B, it is common practice in the spacecraft industry to perform acceptance proof tests on all flight composite structures at a 1.2 × limit load level. For many applications, it has been shown to be a viable option to meet the requirement set forth in those standards. However, unless there is reasonable compensation for the effect of environment, proof tests are required to be conducted at the service environment. In some cases, to perform a proof test at a specific environment is both costly and time consuming. For example, a composite cryogenic tank adapter used in an upper stage vehicle should be proof tested at cryogenic temperature. However, due to facility

limitations and other technical concerns, it may be decided to conduct a damage tolerance test program instead (Sollars, 1987). Furthermore, to avoid a high proof load causing matrix cracking and fiber breakage, there is a limit for a proof test level for composite structural items. NASA-STD-5003 specifies that the proof test level should be limited to less than 80 percent of ultimate strength. For a marginal design, the proof load should be ≤1.1 × limit load; in this case, the "1.2 × limit load" requirement cannot be met. Hence, damage tolerance testing is the only viable option if damage tolerance analysis is not acceptable by most fracture-control authorities.

The aircraft industry has traditionally used the "building block" approach to demonstrate the damage tolerance capability of fracture critical airframe structures (Whitehead and Dee, 1983). In the building block approach, one would run different level tests in concert with damage tolerance analysis. This approach is currently being adopted by the space industry for the same purpose (Konno *et al.*, 2001). Because there are many impact threat events, such as tool drop, runway debris, hail, lighting strikes, etc. in the operation of an aircraft, impact damage is the predominant "defect" to be considered. Compressive strength after impact is used as the allowable for composite wing and other critical airframe structural designs. Many attempts have been made by investigators to predict residual strength for those structures (Rhoades *et al.*, 1978; Byers, 1980; Smith and Wilson, 1985; Horton *et al.*, 1988; Madan, 1988). Another important defect that needs to be evaluated is delamination. The growth of delamination in compression-compression fatigue spectrum applied structures such as upper wing covers was the focus of research in the 1970s and 1980s (Rybicki and Kanninen, 1977; Chai and Babcock, 1985). From this research, a few growth models have been proposed.

For spaceflight composite structures such as satellite trusses and platforms and launch vehicle fairings, delaminations are very critical defects since these structures are also subjected to compression loads. For other composite hardware items such as overwrapped pressure vessels and pressurized structures, impact damage and other types of mechanical damage including surface cuts and scratches are potential damages that need to be considered. Damage tolerance testing on some of the above-mentioned composite hardware could be very costly. Thus, the use of damage-tolerance analysis technologies to demonstrate the damage tolerance ability of composite FCIs should be encouraged. Accordingly, this state-of-the-art review was conducted; the results are presented in this document.

2.0   Residual Strength Prediction Methodologies

Damage tolerance analysis methods reviewed in this task cover two categories: residual strength analysis and "safe-life" analysis. Defects included are surface cuts and/or scratches, delamination and impact damage. The residual strength analysis methods are presented in this section while the life prediction methods are discussed in Section 3.

2.1   Surface Cuts and Scratches

2.1.1   *Closed Form Solutions for Surface Cuts and Scratches*

For laminated composite structures, it has been observed by many investigators that defects such as cuts, scratches and impact damage will in general not grow under tensile cyclic loading. In these cases, damage tolerance assessments require the consideration of the residual strength

instead of "safe-life." A few methods and models have been developed for predicting the residual strength of these types of damage.

- LEFM (Classic) Method
- Inherent Flaw Model
- Point Stress Model
- Point Strain Model
- Mar-Lin (ML) Model

2.1.1.1   Brief Description of Closed Form Solutions

LEFM (Classic) Method

The LEFM method uses the crack-tip stress intensity factor, **K**, to characterize the crack behavior in an isotropic body. This method has been routinely used to predict the residual strength of cracked metallic spaceflight structures since the 1970s. For a through-the-thickness cut in a quasi-isotropic composite laminate plate subjected to tensile load, attempts have been made to use the same parameter, **K**. In this case, the cut is treated as a crack.

Based on the LEFM method, the strain in the fiber direction at a distance r directly ahead of a cut (crack) tip can be written in the following infinite series (Poe, 1983).

$$\varepsilon_1 = Q(2\pi r)^{-1/2} + O(r^0) \tag{2.1}$$

where

$$Q = K_c \xi / E_x \tag{2.2}$$

and

$$\xi = \left(1 - \sqrt{\nu_{xy}\nu_{yx}}\right)\left(\sqrt{E_x/E_y}\sin^2\alpha + \cos^2\alpha\right) \tag{2.3}$$

In Equations (2.2) and (2.3), K_c is the critical stress intensity factor (or fracture toughness) of the composite laminate, x and y are Cartesian coordinates with x perpendicular to the cut; E is modulus of elasticity, ν is Poisson's ratio, and α is the angle that the fiber makes to the x-axis (perpendicular to the crack).

Inherent Flaw Model

The inherent flaw model (IFM) was originally developed by Waddoups *et al.* (1971) (Aronsson, 1986) for predicting the residual strength of notched laminates with infinite width under tensile load. It has been extended to finite width by introducing a finite-width correction factor. For a composite laminate with a notch (crack) of length 2a and inherent damage zone size, c_o, symmetrically on both sides of the crack tip, the notched tensile strength σ_N^{IFM} is given by

$$\sigma_N^{IFM} = \frac{\sigma_o}{Y}\sqrt{\frac{c_o}{a + c_o}} \tag{2.4}$$

3

where σ_o is the unnotched tensile strength and Y is a finite-width correction factor.

While the material is considered homogeneous, orthotropic and linear elastic, the following relation-ship between σ_N^{IFM} and the critical strain-energy release rate (fracture toughness), G_c, is obtained (Aronsson, 1986) from the equation:

$$\sigma_N^{IFM} = \frac{\sigma_o}{Y\sqrt{1 + \frac{\pi a \sigma_o^2}{C G_c}}} \tag{2.5}$$

where

$$C = \sqrt{\frac{A_{11}A_{22}}{2}\left(\sqrt{\frac{A_{22}}{A_{11}}} + \frac{2A_{12} + A_{66}}{2A_{11}}\right)} \tag{2.6}$$

In Equation (2.6), A_{ij} are the in-plane laminate stiffnesses as determined from laminate plate theory (Ashton and Whitney, 1970). A linear relationship between c_o and G_c may further be obtained from

$$c_o = \frac{C}{\pi\sigma_o^2}G_c \tag{2.7}$$

Point Stress Model

The Point Stress Model (PSM) was derived by Whitney and Nuismer (WN) who considered the exact elasticity solution of the normal stress ahead of a notch. By approximating the exact solution of the normal stress ahead of the notch (crack) with the asymptotic solution, the model can be extended to notched laminates with finite geometry. This is justified if the notch length is sufficiently large compared to the size of the damage zone size d_o (Agarwal and Giare, 1982; Zweben, 1973).

For a tension loaded laminate with a notch length 2a, an approximate expression for the unnotched tensile strength according to the Whitney and Nuismer Point Stress Model (WN-PSM) is given by (Aronsson, 1986):

$$\sigma_N^{PSC} = \frac{\sigma_o}{Y}\sqrt{\frac{2d_o}{a}} \tag{2.8}$$

where d_o is the characteristic length defined in the PSM (Whitney and Nuismer, 1974; Nuismer and Whitney, 1975).

The finite-width correction factor, Y, used in the calculations was obtained from (Brown, 1970):

$$Y\left(\frac{a}{w}\right) = 1.09 - 1.73\left(\frac{a}{w}\right) + 8.2\left(\frac{a}{w}\right)^2 - 14.2\left(\frac{a}{w}\right)^3 + 14.6\left(\frac{a}{w}\right)^4 \tag{2.9}$$

4

This factor was derived originally for an isotropic material and is used for the quasi-isotropic laminates considered here.

The WN-PSM (Nuismer and Whitney, 1975; Whitney and Nuismer, 1974), predicts failure when the stress at a characteristic dimension, d_1, ahead of the crack tip equals or exceeds σ_o. The residual notched strength is given by

$$\sigma_n^\infty = \sigma_o \sqrt{1 - \left(\frac{a}{a + d_1}\right)^2} \tag{2.10}$$

The two parameters in this model, σ_o and d_1, are usually determined by tests.

PSM

The PSM proposed by Poe and Sova (Poe, 1983; Poe and Sova, 1980), may also be formulated with a characteristic dimension, d_2. This model predicts failure when the strain at a distance ahead of the notch (crack) tip equals or exceeds the fiber failure strain. The notched failure stress is given by

$$\sigma_n^\infty = \frac{\sigma_o}{\sqrt{1 + \frac{a\xi^2}{2d_2}}} \tag{2.11}$$

where ξ is a functional that depends on elastic constants and the orientation of the principal load carrying plies. The characteristic dimension relates to a material toughness parameter, which was found to be relatively independent of lay-up. The two parameters that must be determined for this model are the fiber failure strain and d_2.

ML Model

The Mar-Lin (ML) model (Lin and Mar, 1977; Mar and Lin, 1977) allows the singularity, n, in the stress intensity factor to be a value other than square-root. The notched failure stress is given by

$$\sigma_n^\infty = \frac{H_c}{(2a)^n} \tag{2.12}$$

where H_c is the composite fracture toughness. In general, H_c and the exponent n are the two parameters that must be determined by test. In studies, the exponent, n, was related to the theoretical singularity of a crack in the matrix, with the tip at the fiber/matrix interface. In this case, the singularity is a function of the ratio of fiber and matrix shear moduli and Poisson's ratios. Using this method, the singularities for a range of typical fiber/matrix combinations were determined to be between 0.25 and 0.35.

2.1.1.2   Comparison of Various Closed Form Models

The following discussions are taken from CMH-17, Composite Materials Handbook Volume 3. In this reference, predictions for both small notch (2a ~ 1.2 in. (3 cm)) and large notch (2a up to

20 in. (0.5 m)) sizes are compared. The former notch sizes are characteristic of much of the data collected for composites to date. Four models are compared; LEFM (Classical), WN (point stress), point strain (PS), and ML. As a baseline for comparing changes in notch length predicted by the four models, curves are generated based on average experimental results (finite width corrected) for the IM6/937A tape material with $W/2a = 4$ and a lay-up of [+45/90/–45/0/+30/–30/0/–45/90/+45]. This will ensure that all theories agree for at least one crack length.

Figure 1 shows a comparison of the four models for small crack notches. Only a small difference is seen between PS and WN models. A close examination of the LEFM and ML curves indicates that the singularity has a significant effect on curve shape. For notch lengths less than the baseline point, ML predictions are less than those of Classical. For notch lengths greater than the baseline point, the opposite is true, and models tend to segregate based on singularity, i.e., WN, PS and Classical yield nearly the same predictions.

Figure 2 shows that singularity dramatically affects differences between predictions in the large notch length range. The ratio of notched strength predictions for models with the same order of singularity becomes a constant. For example, WN and LEFM become functionally equivalent, and the relationship

$$K_{IC} = \sigma_o \sqrt{2\pi d_1} \qquad (2.13)$$

will yield a value for K_{IC} such that the two models compare exactly for large notches.
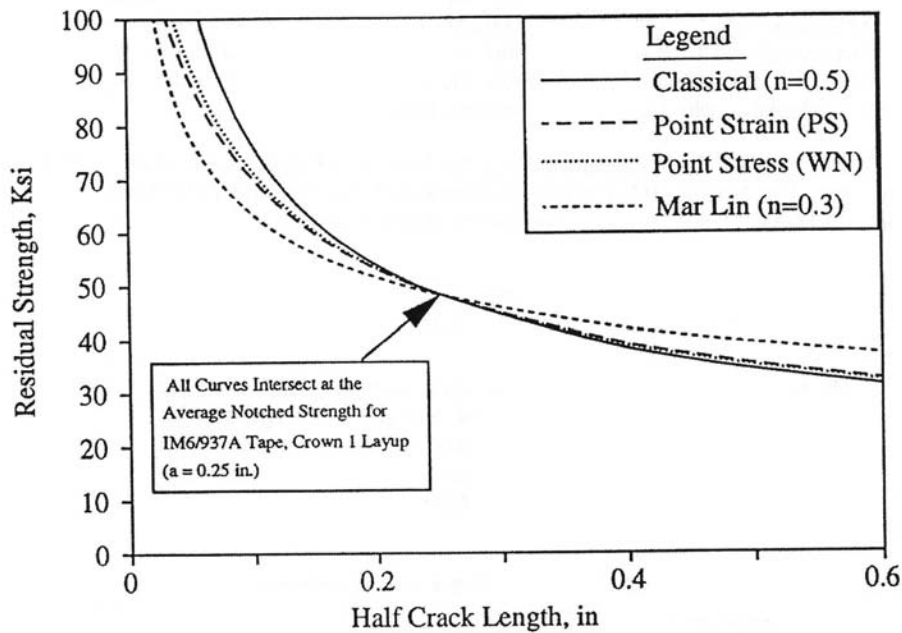
Figure 1. Comparison of curve shapes for notched strength prediction theories in small notch range.

6
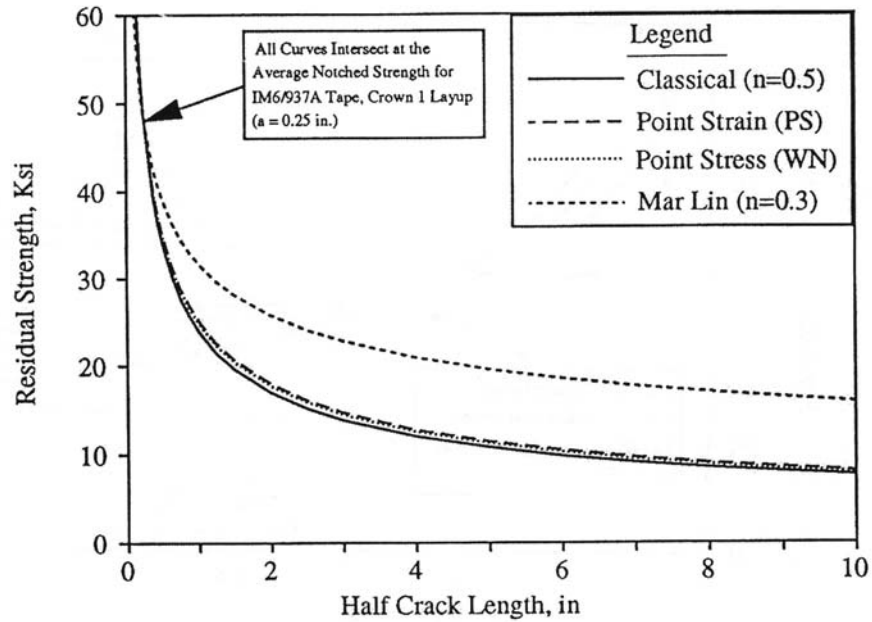
Figure 2. Comparison of curve shapes for notched strength prediction theories in large crack notch.

2.1.2   Finite Element Analysis (FEA) Methods for Surface Cuts and Scratches

The FEA method provides flexibility and accuracy for multiple configurations.

2.1.2.1   Conventional FEA Methods

Two conventional FEA methods exist to account for the effects of damage progression on load redistribution in finite element models (FEM). Progressive damage methods that degrade various stiffness properties of individual elements as specified failure criteria are met (Dopker *et al.*, 1995) have shown some success in modeling damage growth in specimen configurations. The magnitude of the calculations, however, provides a significant obstacle to incorporating them into the complex models required for stiffened structures.

Notched Strength Modeling Using FEA

In order to achieve a truly general notched strength model, the physical basis of failure must be considered, and an extensive study of subcritical damage is an essential element of this process. To this end, a notched strength model was developed by Kortschot and Beaumont (1991) based on experimental results that illustrate the dependence of notched strength on subcritical damage. The model was finite element based and used to determine the modified notch tip stress distributions. The failure criterion was complemented by theoretical predictions of damage growth.

The approach of this method is to calculate the stress distribution near the notch tip for a FEM that includes a subcritical damage region. Using stress results from the FEA, the stress concentration factor, K_t, can be determined. The failure criterion is derived from curve fitting the finite element results to test data.

An example of this method uses a one-quarter model of the specimen using appropriate boundary conditions, as shown in Figure 3. Two-dimensional (2-D), eight-noded quadrilateral plane stress elements were used. Two layers of elements were superimposed with one layer of elements

7

given the properties of a 0º ply and the other given the properties of a 90º ply. Corresponding elements in the two layers shared all nodes and hence deformed identically except in the area representing the delamination region where the 90º ply was disconnected from the 0º ply. In addition, the elements of the 90º ply were continuous across the split in the 0º ply, as illustrated in Figure 4. Although this geometry is quite complicated, it is a direct representation of the observed subcritical damage in [90/0]$_s$ laminates.

The FEM was constructed to yield information about the tensile stress distribution in the 0º ply near the notch tip. The model produced stress contour maps that displayed finite maximum stresses for all values of $\ell/a \neq 0$, where ℓ is the split length and a is the crack length (V-notch). The stress concentration factor, K_t, was determined as the maximum stress in the 0º ply divided by the remote stress on the laminate for each ℓ/a ratio. The relationship between K_t and ℓ/a was approximated very closely by the empirical function

$$K_t = 8.16(\ell/a)^{-0.284} \tag{2.14}$$
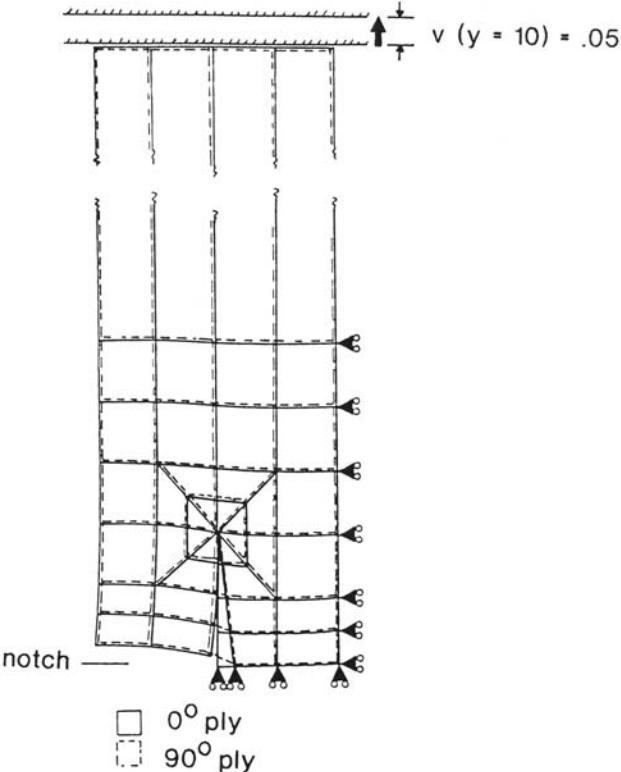
Figure 3. Finite element mesh for $\ell/a = 1$.
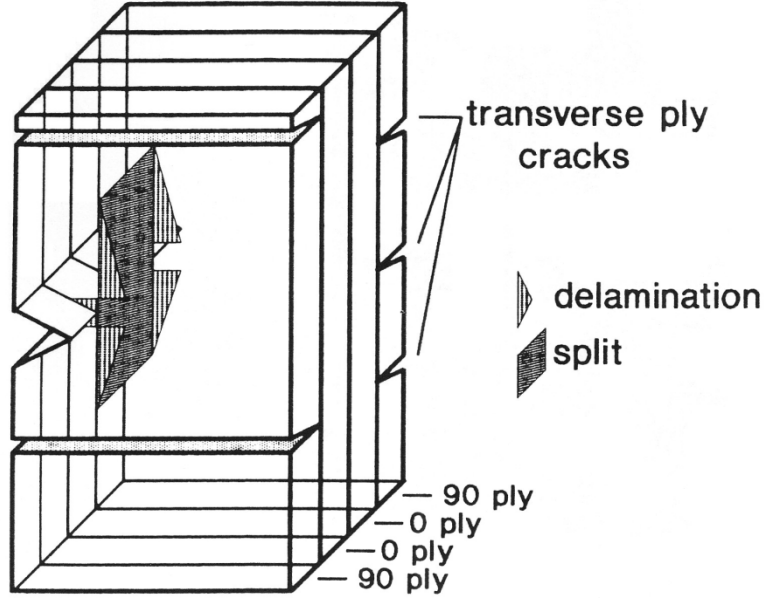
Figure 4. Schematic of typical subcritical damage in a $[90/0]_s$ laminate.

In order to derive a failure criterion, that is, to discover what aspect of the 0º ply stress field is constant at failure, the terminal stress distributions for a variety of specimens must be compared. To do this in a simplified way, the peak stress in the 0º ply immediately prior to failure, σ_{0p}, was calculated for all specimens. A value for terminal ℓ/a was obtained from a radiograph of the failed specimen and substituted into Equation (2.14). The remote stress at failure, $\sigma_{\infty f}$, was then multiplied by K_t to obtain σ_{0p}. The predicted failure stress can be expressed as

$$\sigma_{\infty f}(\text{ predicted }) = \frac{\sigma_{0f}}{K_t} \tag{2.15}$$

where

$K_t = 8.16(\ell/a)\text{-}0.284,$

$\sigma_{\infty f}$ = remote failure stress of the laminate; and
σ_{0f} = failure stress of 0º ply.

Strain Softening Models

Strain softening models (Llorca and Elices, 1992; Mazars and Bazant, 1988) have been successfully used to simulate the fracture of concrete and other materials by providing the ability to capture the global load redistribution that occurs as the notch-tip region is softened by damage formation, without the computational concerns of detailed progressive damage models. A range of softening laws has been proposed. However, determination of the strain softening material laws through trial and error requires a large number of tests, and can be computationally intensive. Basham *et al.* have presented an approach to determine these laws using energy methods and relatively few tests (Basham *et al.*, 1993).

This method is a generalized continuum approach that is compatible with complex FEMs required to properly approximate structural configurations. The approach allows the capture of

9

load redistribution due to local damage formation and growth. One approach is the use of nonlinear springs that undergo reductions in bending stiffness as damage occurs. The models can be calibrated using small-notch test results, and then extended to large-notch configurations. Modeling and calibrating the stiffness reductions are of concern for most structural configurations, where out-of-plane loading, load eccentricities, and bending loads are common (Kongshavn and Poursartip, 1999).

Non-local Damage Theory Using Strain Softening

Nahan and Kennedy have used the damage induced strain softening approach for degradation of laminate properties to simulate crack growth in laminate plates (Nahan and Kennedy, 2000). This approach defines bulk plate damage as a linear variation of orthotropic damage through the plate thickness. A damage term is defined that can range from zero, being a no damage condition, to one, which corresponds to complete material failure. A bulk laminate stress-strain softening relationship is derived and incorporated into a FEM of the laminate. The FEA will generate a simulated load history, in which the damage can be observed to develop at the notch-tip and propagate to eventual failure. The theory performs well in predicting tension fracture over a wide range of notch sizes as shown in Figure 5.
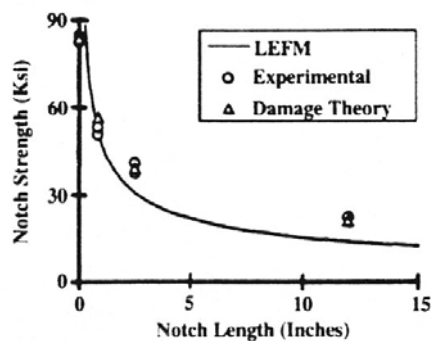
Figure 5. Non-local damage theory predictions versus tested strength.

Predicting Crack Growth Using Micropolar Strain Softening

In another study, Kennedy used micropolar strain softening for predicting damage growth in composite plates with different notch geometries (Kennedy, 1999). The micropolar approach differs from classical elasticity theory in that the deformation of the body is described by a displacement vector and an independent microrotation vector (Eringen, 1968). The theory prevents singularities due to localization of deformation in strain softening materials under simple stress states.

An eight-node, isoparametric quadrilateral element, as shown in Figure 6, was developed for carrying out the plain strain micropolar elasticity analysis. The element is similar to that used in classical elasticity theory, except the addition of a rotation degree of freedom, ϕ_l, at each node.

The theory was used to predict damage growth in a rectangular laminate plate with notches consisting of a circular hole, an elliptical hole, and a sharp crack. In all cases, the results showed that the specimen size had a relatively weak effect on the failure load predicted, which indicates that the usefulness of this model is limited to materials with this characteristic.

10
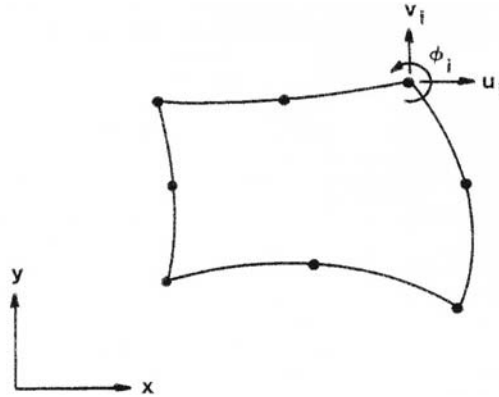
Figure 6. 2-D eight-noded isoparametric quadrilateral element.

Finite Element Solution Issues

Finite element solutions for problems involving strain softening material laws involve a number of complexities not often associated with static structural analysis. Specifically, singular stiffness matrices are encountered when material failure is occurring in a sufficiently large area and/or when the structure is buckling. A solver with a variety of robust, nonlinear solution algorithms that is capable of modeling strain-softening response for orthotropic materials should be selected. Arc-length methods, such as Riks (1979), have proven useful in dealing with snap-through stability problems, and were useful in initial efforts to model tension loaded strain softening problems.

Solving the problem dynamically minimizes a number of numerical difficulties because damping and inertial forces can smooth out system response and greatly reduce numerical noise in the solution process. As the maximum load is reached, local failure occurs, thus accelerating parts of the system, and the numerical integration in time can be stopped when a minimum acceleration related to system failure has been achieved. This has proven to be a very accurate failure criterion for compression-loaded structural systems (Dopker *et al.*, 1995).

Element Size and Formulation

Strain-softening laws and the finite element size are interrelated, due to the effect of element size on notch-tip strain distribution. A great amount of mesh sensitivity has been found when strain is incorporated into FEAs based on classical plasticity theory. The sensitivity occurs because as the mesh is refined, there is a tendency for the damage zone to localize to a zero volume, which can lead to the physically impossible condition of structural failure with zero energy dissipation. It has been found that larger elements (i.e., ≥ 0.20 in. (0.5 cm)) result in less-severe, but broader, stress concentrations and in strain-softening curves with steeper unloading segments (Scholz *et al.*, 1997). Element size, therefore, is another parameter in the strain softening approach that must be determined. Fortunately, damage in composite materials typically localizes on a relatively large scale, e.g. relative to plastic yielding at a crack tip in metal. Element sizes required to accurately predict notch-length and finite-width effects in compression are typically larger than those required for tension.

Element formulation and strain softening laws are also interrelated. Limited studies of 4-, 8-, and 9-noded shell elements found that higher order elements lead to higher fracture strengths and large damage zones (Dopker *et al.*, 1994).

11

2.2   Delaminations

Delamination, often referred to as interlaminar fracture, is one of the few instances where fracture mechanics formalism is applicable to fiber-reinforced composites on a global scale (Anderson, 1991). A delamination surface can be treated as a crack, where the resistance of the material to the propagation of the delamination is the critical strain-energy release rate (fracture toughness), G_c. Since the delamination typically is confined to the matrix material, e.g., between plies, continuum theory is applicable, and the delamination growth is self similar, i.e., keeping the same aspect ratio. For composite structures under compressive loads, one of the most predominant failure modes is the growth of delamination. This type of "crack" has been studied extensively by the aircraft industry since the aircraft wing and other control surfaces are generally loaded in both tension and compression.

2.2.1   Closed Form Solutions for Delaminations

Closed form solutions are often used in the determination of the critical strain-energy release rates, G_c, of a composite laminate specimen. Typical specimens include the double cantilever beam (DCB) specimen, the end-notched flexure (ENF) specimen and the edge delamination (ED) specimen. An advantage of the DCB specimen configuration is that it permits measurements of Mode I, Mode II, or mixed-mode fracture toughness (see Figure 7). The ENF specimen has essentially the same geometry as the DCB specimen, but the latter is loaded in three-point bending, which imposes Mode II displacements of the crack faces. The ED specimen simulates the conditions in an actual structure – tensile stresses normal to the ply are highest at the free edge; thus, delamination zones often initiate at the edges of a panel.

For pure Mode I loading, elastic beam theory leads to the following expression for energy release rate (ERR):

$$G_I = \frac{P_I^2 a^2}{B\ E\ I} \tag{2.16}$$

where B is the beam's thickness, and

$$E\ I = \frac{2P_I a^3}{3 \cdot \Delta_I} \tag{2.17}$$

(a) Mode I.

(b) Mode II
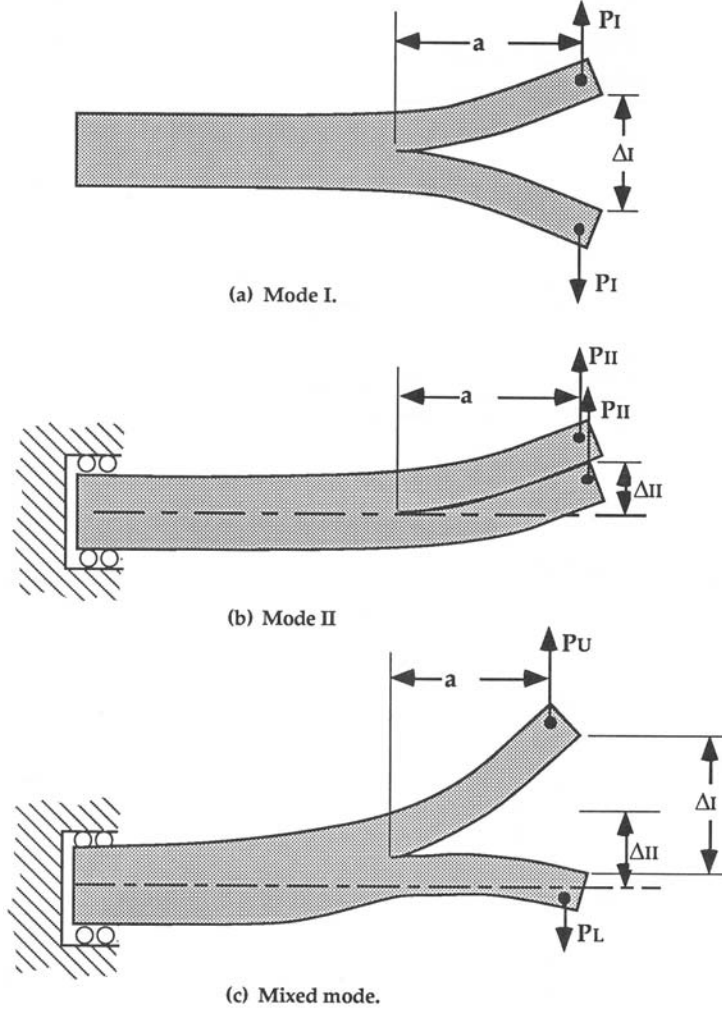
(c) Mixed mode.

Figure 7. Mode I, II and mixed-mode loading of DCB specimens.

Assuming linear beam theory, the corresponding relationship for Mode II is given by

$$G_{II} = \frac{3P_{II}^2 a^2}{4\,B\,E\,I} \qquad (2.18)$$

Mixed-mode loading conditions can be achieved by unequal tensile loading of the upper and lower portions of the specimens. The applied loads can be resolved into Mode I and Mode II components as follows:

$$P_I = |P_L| \qquad (2.19a)$$

$$P_{II} = \frac{|P_U| - |P_L|}{2} \qquad (2.19b)$$

where P_U and P_L are the upper and lower loads, respectively. The components of G can be computed by inserting P_I and P_{II} into Equations (2.16), (2.17) and (2.18) above.

Linear beam theory may result in erroneous estimates of G, particularly when the specimen displacements are large. In this case, the area method provides an alternative measure of G. Figure 8 schematically illustrates a typical load-displacement curve, where the specimen is periodically unloaded. The loading portion of the curve is typically nonlinear, but the unloading curve is usually linear and passes through the origin. G can be estimated from the incremental area inside the load-displacement curve, divided by the change in crack area:

$$G = \frac{\Delta U}{B\,\Delta a} \tag{2.20}$$

The Mode I and Mode II components of G can be inferred from the $P_I - \Delta_I$ and $P_{II} - \Delta_{II}$ curves, respectively.

(Chai, 1982). The one-dimensional (1-D) thin film model is shown below.
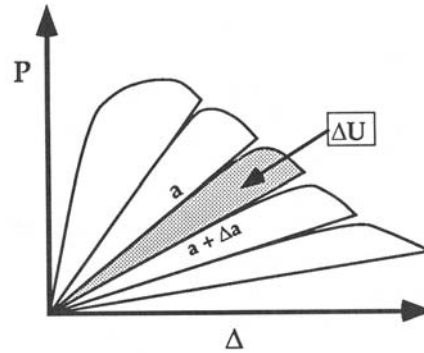
Figure 8. Schematic load-displacement curve for a delamination toughness measurement.

2.2.1.1   Thin-Film Models

Three delamination models derived by Chai in the early 1980s include the 1-D Thin-Film Model, Thick-Column Model and the 2-D Elliptical Model (Chai, 1982). The 1-D thin-film model is shown below.

Consider the three stages in thin-film delamination and buckling as shown in Figure 9. The delaminated film of thickness h and length ℓ is part of an infinitely thick body characterized by Young's Modulus, E, and Poisson's ratio, ν. The strain-energy release rate, G, can be expressed as

$$G = \frac{Eh\left(1 - \nu^2\right)}{2}\left(\varepsilon_0 - \varepsilon_{cr}\right)\left(\varepsilon_0 - 3\varepsilon_{cr}\right) \tag{2.21}$$

where ε_0 is the compressed strain and ε_{cr} is the critical buckling strain.

14
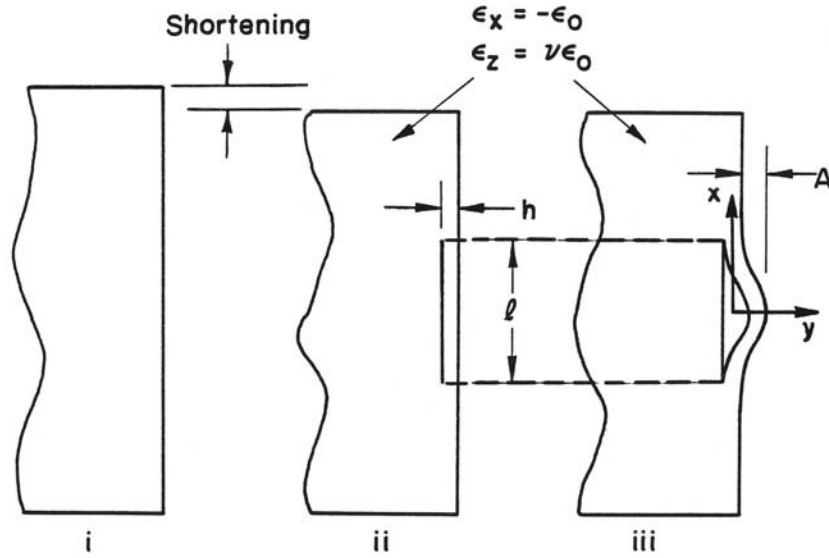
Figure 9. Thin-film model – three configurations.

The thin-film model provides a simple means of predicting delamination growth, but it has very limited application due to its simplifying assumptions such as infinite thickness and through the thickness delamination.

2.2.2   FEA Methods for Delaminations

The FEA method provides flexibility and accuracy for multiple configurations. Analyses methods have been presented that utilize conventional continuum elements. Other methods use singular elements that contains singularity to predict delaminations.

2.2.2.1   Conventional FEA for Delaminations

Analyses that use conventional continuum elements, such as, quadrilateral and triangular shell elements or hexagonal and pentagonal solid elements, are referred to as conventional methods. One such method for predicting delaminations in a composite structure using conventional elements is the Virtual Crack Closure Technique (VCCT), first presented by Rybicki and Kanninen in a classic paper (Rybicki and Kanninen, 1977).

Calculation of Stress Intensity Factor by FEA

In their paper in 1977, Rybicki and Kanninen presented a method for evaluating stress intensity factors using a modified crack closure integral and a constant strain finite element analysis.

The method uses Irwin's crack closure integral. The assumption is that if a crack extends by a small amount Δc, the energy absorbed in the process is equal to the work required to close the crack to its original length (Irwin, 1958). The following is the mathematical interpretation

$$
\begin{aligned}
G = {} & \lim_{\Delta c \to 0} \frac{1}{2\Delta c} \int_0^{\Delta c} \sigma_y (\Delta c - r, 0)\, \overline{v}(r, \pi)\, dr \\
& + \lim_{\Delta c \to 0} \frac{1}{2\Delta c} \int_0^{\Delta c} \tau_{xy} (\Delta c - r, 0)\, \overline{u}(r, \pi)\, dr
\end{aligned}
\tag{2.22}
$$

15

where G is the energy release rate, σ_y and τ_{xy} are the stresses near the crack tip, u and v are the relative sliding and opening displacements between points on the crack faces, and Δc is the crack extension at the crack tip. The above equation can also be expressed as $G = G_I + G_{II}$.

Taking the limit and using the stress intensity factors K_I and K_{II} gives

$$G_I = \frac{K_I^2}{E}\beta \text{ and } G_{II} = \frac{K_{II}^2}{E}\beta \tag{2.23-2.24}$$

where $\beta = 1$ for plane stress and $1 - v^2$ for plane strain and E is Young's modulus.

Rybicki used constant strain elements near the crack tip, and found a good match comparing with the other results, using more complex methods. The finite element approach for evaluating G_I and G_{II} from Equation (2.22) is based on the nodal forces and displacements as shown in Figure 10.

In equation form, the work required to close the crack an amount Δc is

$$G_I = \lim_{\Delta c \to 0} \frac{1}{2\Delta c} \overline{F}_c \cdot (v_c - v_d) \text{ and } G_{II} = \lim_{\Delta c \to 0} \frac{1}{2\Delta c} \overline{T}_c \cdot (u_c - u_d) \tag{2.25-2.26}$$

where the value of F_c and T_c are the y- and x-forces, respectively, that are required to hold nodes c and d together.
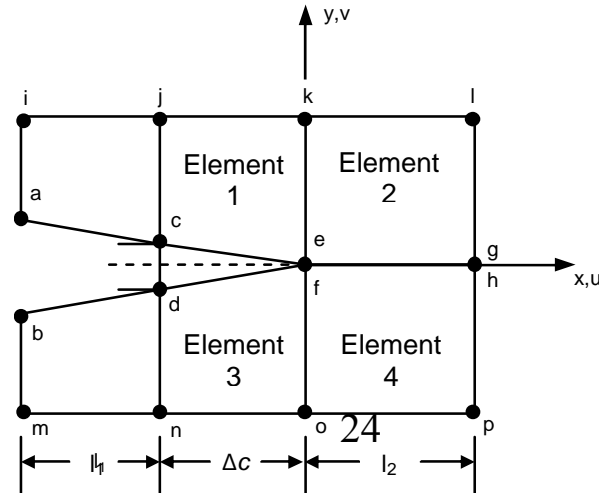
Figure 10. Finite element nodes near crack tip.

The energy domain integral methodology (Shih *et al.*, 1986; Moran and Shih, 1987) is a general framework for numerical analysis of the *J*-integral, energy release rate. This approach is extremely versatile, as it can be applied to both quasistatic and dynamic problems with elastic, plastic, or viscoplastic material responses, as well as thermal loading. Moreover, the domain integral formulation is relatively simple to implement numerically, and it is very efficient. This approach is very similar to the VCCT.

Taking account of plastic strain, thermal strain, body forces, and crack face tractions leads to the following general expression for J in two dimensions:

$$J = \int_{A^*} \left\{ \left[\sigma_{ij} \frac{\partial u_j}{\partial x_1} - w \delta_{1i} \right] \frac{\partial q}{\partial x_i} + \left[\sigma_{ij} \frac{\partial \varepsilon_{ij}^p}{\partial x_1} - \frac{\partial w^p}{\partial x_1} + \alpha \sigma_{ij} \frac{\partial \Theta}{\partial x_1} - F_i \frac{\partial u_j}{\partial x_1} \right] q \right\} dA - \int_{\Gamma_+ + \Gamma_-} \sigma_{2j} \frac{\partial u_j}{\partial x_1} q \, d\Gamma \quad (2.27)$$

where α is the coefficient of thermal expansion, Θ is the temperature relative to ambient, the super-script p denotes the plastic strain, and q is an arbitrary but smooth function that is equal to unity on Γ_o and zero on Γ_1 (Figure 11).

Inertia can be taken into account by incorporating T, the kinetic energy density, into the group of terms that are multiplied by q. For a linear or nonlinear elastic material under quasistatic conditions, in the absence of body forces, thermal strains, and crack face tractions, Equation (2.27) reduces to

$$J = \int_{A^*} \left[\sigma_{ij} \frac{\partial u_j}{\partial x_1} - w \delta_{1i} \right] \frac{\partial q}{\partial x_i} dA \quad (2.28)$$
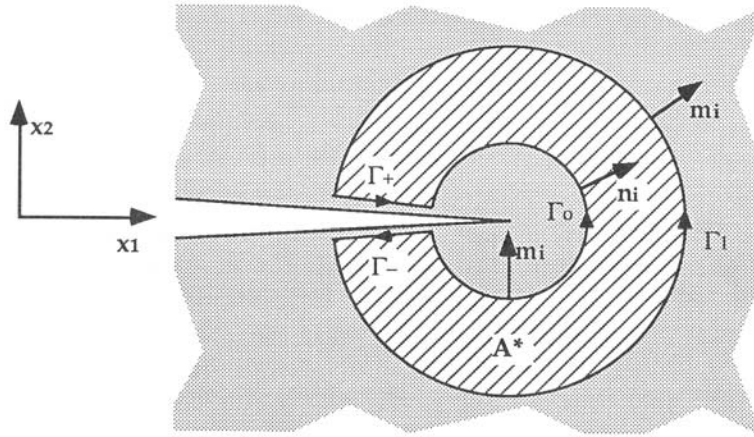
Figure 11. Inner and outer contours, which form a closed contour around the crack tip when connected by Γ_+ and Γ_- (Anderson, 1991).

Equation (2.28) is equivalent to Rice's path-independent J-integral. When the sum of the additional terms in the more general expression (Equation (2.27)) is nonzero, J is path dependent. The variable, q, can be interpreted as a normalized virtual displacement. The q function is merely a mathematical device that enables the generation of an area integral, which is better suited to numerical calculations.

Implementing J-Integral into FEA

The domain integral approach can be implemented into finite elements with some modifications (Shih *et al.*, 1986; Dodds and Vargas, 1988). In 2-D problems, one must define the area over which the integration is to be performed. The inner contour, Γ_o is often taken as the crack tip, in which case A* corresponds to the area inside of Γ_1. The boundary of Γ_1 should coincide with element boundaries. An analogous situation applies in three dimensions, where it is necessary to

define the volume of integration. The latter situation is somewhat more complicated, however, since $J(\eta)$ is usually evaluated at a number of locations along the crack front.

In the absence of thermal strains, path-dependent plastic strains, and body forces within the integration volume or area, the *J* integral is expressed as follows:

$$J = \sum_{A^* \text{ or } V^*} \sum_{p=1}^{m} \left\{ \left[\left(\sigma_{ij} \frac{\partial u_j}{\partial x_1} - w\delta_{1i} \right) \frac{\partial q}{\partial x_i} \right] det\left(\frac{\partial x_j}{\partial \xi_k} \right) \right\}_p w_p - \sum_{\text{crack faces}} \left(\sigma_{2j} \frac{\partial u_j}{\partial x_1} q \right) w \qquad (2.29)$$

where the spatial derivatives of q are given by

$$\frac{\partial q}{\partial x_i} = \sum_{I=1}^{n} \sum_{k=1}^{2 \text{ or } 3} \frac{\partial N_I}{\partial \xi_k} \frac{\partial \xi_k}{\partial x_j} \qquad (2.30)$$

and m is the number of Gaussian points per element, w_p are w are weighting factors, n is the number of nodes per element, q_i are the nodal values of q_i, ξ_i are the parametric coordinates for the element, and N_I are the element shape functions. The quantities within $\{\ \}_p$ are evaluated at the Gaussian points. Note that the integration over crack faces is only necessary when there are nonzero tractions.

Finite Element Mesh Design

Although many commercial codes have automatic mesh generation capabilities, producing a properly designed FEM always requires some human intervention. Crack problems, in particular, require skill on the part of the user. Figure 12 shows several common element types for crack problems. At the crack tip, four-sided elements (in 2-D problems) are often degenerated down to triangles, as Figure 13 illustrates. An analogous situation occurs in three dimensions, where a brick element is degenerated to a wedge.

(a) 8-node 2-D element.   (b) 9-node 2-D element.

(b) 20 node brick element.   (d) 27-node brick element.
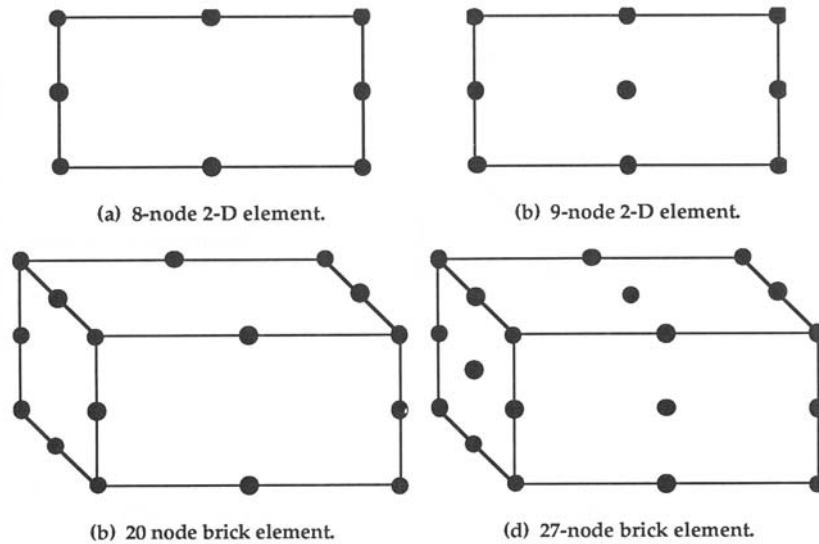
Figure 12. Isoparametric elements that are commonly used in 2-D and three-dimensional (3-D) crack problems.
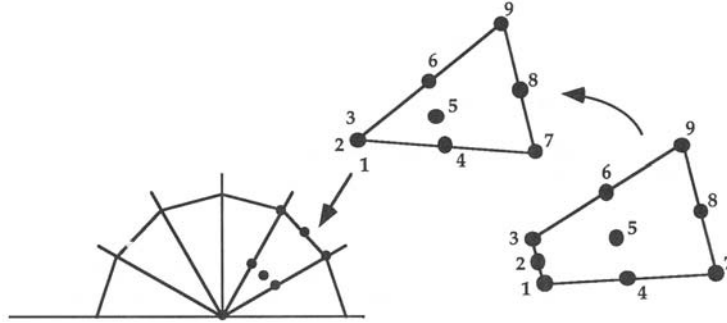
Figure 13. Degeneration of a quadrilateral element into a triangle at the crack tip.

Using the Strain Softening Method to Perform Progressive Delamination Analysis

Using the strain-softening method, Davila *et al.*, have developed a method to simulate progressive debonding or delamination using decohesion elements (Davila *et al.*, 2001). The onset of damage and the growth of delamination can be simulated without previous knowledge about the location, size, and direction of propagation of the delaminations. The approach has been found to be well suited to nonlinear progressive failure analyses where both ply damage and delaminations are present.

The approach consists of placing interfacial decohesion elements between composite layers. A decohesion failure criterion that combines aspects of strength-based analysis and fracture mechanics is used to simulate delamination by softening the element. As the delamination grows, the tractions across the interface will grow to a maximum value, then decrease and eventually vanish when complete decohesion occurs. The work of normal and tangential separation can be related to the critical values of ERR.

Davila *et al*. developed an 8-node decohesion element and implemented it in ABAQUS™ to perform the analyses (de Moura *et al*., 2000; 1997). The decohesion element models the interface between sublaminates or between two bonded components. The element consists of a zero-thickness volumetric element in which the kinematics of the elements that are being connected on the top and bottom faces are correctly modeled. The element represents damage by a material response using a cohesive zone ahead of the crack tip to predict the delamination growth. The interface elements have been formulated to deal with mixed-mode delamination growth problems.

An example comparing this approach with a beam solution and test data uses a DCB to determine interlaminar fracture toughness in Mode I (G_{IC}). A Gr/Ep specimen made of a unidirectional fiber-reinforced laminate containing a thin insert at the mid-plane near the loaded end is chosen. The specimen was 15 cm (6 in.) long and 2 cm (0.8 in.) wide with an initial crack length of 5.5 cm (2.2 in.). A plot of the reaction force as a function of the applied end displacement, d, is shown in Figure 14. The beam solution was developed by Mi and Crisfield (Mi and Crisfield, 1996) for isotropic adhered materials and used plane stress assumptions. After the initiation of delamination, fiber bridging in the test specimen caused a small drift in the response compared to the FEM and analytical results. The results of the decohesion method were in good agreement with the test data.
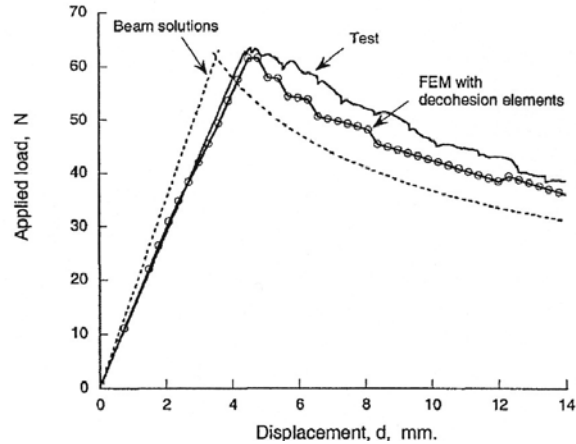
Figure 14. Load-deflection response of DCB test.

A parametric study revealed that the accuracy of the prediction was reduced when the element sizes in the region of strain softening were greater than a prescribed value. Poor results were obtained when the element size was greater than 1.25 mm (0.5 in.).

2.2.2.2   *FEA With Singular Element Formulation*

In contrast to the conventional delamination prediction approach presented in the previous section, the following approach uses singular elements to predict delamination growth along a crack tip.

Davidson developed a crack-tip element methodology for predicting delamination growth in laminated composite structures (Davidson, 1998). First, the toughness versus mode mix relation was determined experimentally. The definition of mode mix sought was the one that, when applied to all experimental results, produced a single-valued toughness versus mode mix curve. The mode mix definition was found from the results of a series of delamination toughness tests, and obtained within the construct of a crack-tip element analysis. This approach allowed for the possibility that the singular field-based decomposition was valid; it also allowed for the possibility that an alternative definition was valid. This alternative definition was based on parameters that uniquely defined the loading at the crack tip but which were insensitive to the details of the near-tip damage. The second component of the methodology consisted of analyzing the structure of interest and assessing delamination growth. This was also done using the crack tip element analysis and incorporated the experimentally determined definition of mode mix. One of the attractions of this approach is that it removes the need for detailed 2-D and 3-D FEAs.

Total Energy Release Rate

Consider the crack tip element of Figure 15 that represents a 3-D portion of the crack tip region in a general interfacial fracture problem. The crack lies locally in the x-y plane at constant z, the element is in a state of plane stress or plane strain with respect to the y coordinate direction. The crack front may be straight or curved with the length of the element in the y direction assumed to be sufficiently short such that there is no significant variation in the loading and in the orientation of the edges of the element with respect to y. It is assumed that the lengths of the cracked and uncracked regions comprising the element are large with respect to their thicknesses but are sufficiently small such that geometric nonlinearities are negligible.

20
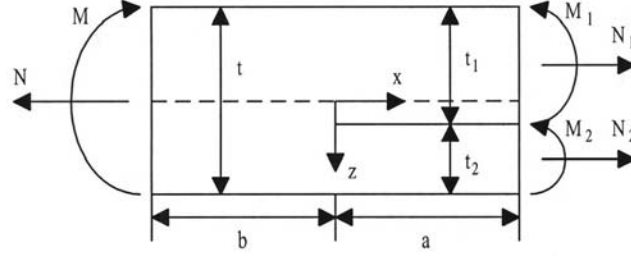
Figure 15. Crack-tip element and local loading.

Classical plate theory is used to predict the overall deformations and strain energies of the element (Davidson *et al.*, 1995; Schapery and Davidson, 1990; Hu, 1995). It has been shown (Davidson *et al.*, 1995; Schapery and Davidson, 1990) that the loading on the crack-tip element, which produces the stress singularity can be fully characterized in terms of a concentrated crack tip force, N_c, and moment, M_c. The concentrated crack-tip force and moment are found by enforcing the condition that the displacements of the upper and lower plates be compatible along the crack plane over $-b < x < 0$. The ERR of the crack-tip element is obtained through a modified virtual crack closure method and may be expressed in terms of N_c and M_c, rather than the four independent quantities N_1, N_2, M_1, and M_2. This gives

$$G = \frac{1}{2}\left(c_1 N_c^2 + c_2 M_c^2 + 2\sqrt{c_1 c_2}\, N_c M_c \sin\varGamma\right) \tag{2.31}$$

where

$$\sin\varGamma = \frac{c_{12}}{\sqrt{c_1 c_2}} \tag{2.32}$$

$$c_1 = A_1' + A_2' + B_1' t_1 - B_2' t_2 + \frac{D_1' t_1^2}{4} + \frac{D_2' t_2^2}{4}$$

$$c_2 = D_1' + D_2' \tag{2.33}$$

$$c_{12} = \frac{D_2' t_2^2}{2} - \frac{D_1' t_1^2}{2} - B_1' - B_2'$$

The concentrated crack-tip force and moment are given by

$$N_c = -N_1 + a_{11}N + a_{12}M \tag{2.34}$$

and

$$M_c = M_1 - \frac{N_1 t_1}{2} + \left(\frac{a_{11} t_1}{2} - a_{21}\right)N + \left(\frac{a_{12} t_1}{2} - a_{22}\right)M \tag{2.35}$$

21

where

$$a_{11} = A_1 A' + \left(B_1 - \frac{A_1 t_2}{2} \right) B'$$

$$a_{12} = E + \left(B_1 - \frac{A_1 t_2}{2} \right) D'$$

$$a_{21} = B_1 A' + \left(D_1 - \frac{B_1 t_2}{2} \right) E$$

$$a_{22} = B_1 B' + \left(D_1 - \frac{B_1 t_2}{2} \right) D'$$

(2.36)

and t_1 and t_2 are the thicknesses of plates 1 and 2 as shown in Figure 15.

Mode Decomposition – Classical Definition

Mode decomposition is performed to define the ERR in terms of its Mode I and Mode II components. The Mode I and Mode II ERRs are given by

$$G_I = \frac{1}{2} \left[-N_c \sqrt{c_1} \, \sin\hat{\Omega} + M_c \sqrt{c_2} \, \cos\left(\hat{\Omega} + \Gamma \right) \right]^{-2}$$

(2.37)

and

$$G_{II} = \frac{1}{2} \left[N_c \sqrt{c_1} \, \sin\hat{\Omega} + M_c \sqrt{c_2} \, \cos\left(\hat{\Omega} + \Gamma \right) \right]^{-2}$$

(2.38)

where $\hat{\Omega}$ is defined as

$$\hat{\Omega} = \Omega + \varepsilon \ln\left(\hat{L} \big/ L \right)$$

(2.39)

In the above equations, $\hat{L}$ is a fixed dimension, regardless of the body being analyzed, whereas L is a characteristic dimension that scales with the body. Equation (2.39) ensures that the correct mode mix will be predicted for those cases where an oscillatory singularity exists. That is, Ω is determined for a specific crack-tip element geometry and is based on the characteristic dimension L. The scaling of $\hat{\Omega}$ given by Equation (2.39) ensures that the same Ω will predict the correct mode mix for arbitrary loadings of a geometrically similar element with different absolute dimensions (Davidson *et al.*, 1995).

Example Problems in Two Dimensions

Instability-Related Delamination Growth

Davidson presented the prediction of instability-related delamination growth (Davidson, 1998) using a global cylindrical buckling analysis along with a local crack tip element analysis (Davidson and Krafchak, 1993). Figure 16 shows a cross-sectional view of a midplane symmetric laminate containing two through-width delaminations located symmetrically with respect to the laminate's midplane.

22

A cylindrical buckling analysis is performed on the laminate model (Davidson and Krafchak, 1993; Yin, 1988). The post-buckled laminate appears as shown in Figure 17, with all internal force and moment resultants shown in their positive conventions (the actual in-plane forces are compressive in this problem and therefore the reverse of those shown in the figure).
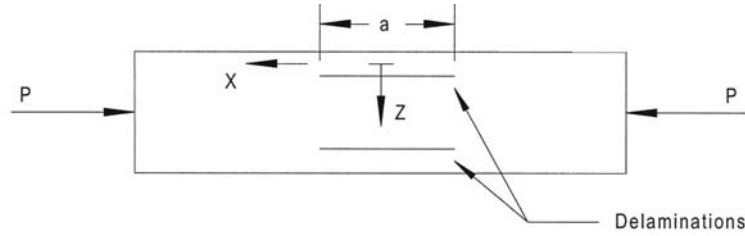
Figure 16. Cross-sectional view of laminate containing two symmetrically located delaminations that is subjected to compressive loading.
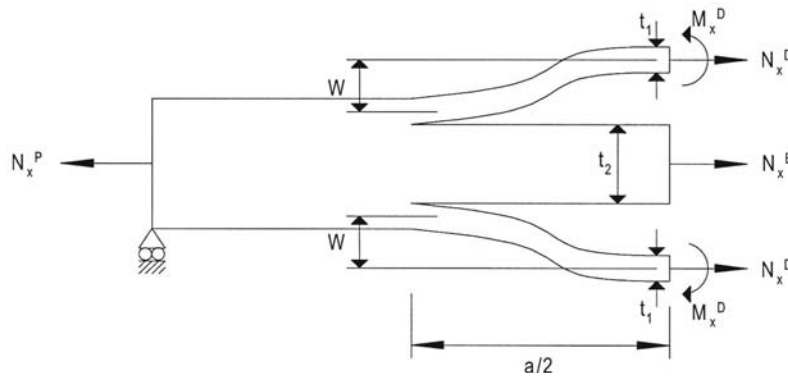
Figure 17. Post-buckled configuration.

Figure 18 shows the crack-tip element and local loading. Minor modifications to the crack-tip element formulation were made to enforce the symmetry constraints. The loads, N, N_1, and N_2, and moment, M_1, acting on the crack-tip element are given by

$$N_1 = N_x^D \quad N_2 = \frac{N_x^B}{2} \quad N = N_1 + N_2 \quad M_1 = M_x^D - N_x^D W \tag{2.40}$$

Substituting these loads into the crack-tip element equations provides an analytical methodology for determining mixed-mode ERRs as a function of the applied far-field loading.

Figure 19 presents a comparison for total ERR between the linear crack-tip element analysis and a geometrically nonlinear finite element analysis (Davidson and Krafchak, 1993). A [02/90/02]$_{3s}$ Gr/Ep laminate with delaminations at the interfaces between the 5th and 6th and 25th and 26th plies was modeled in both cases. The laminate is assumed to be in a state of plane strain. The horizontal axis, denoted as applied compressive strain, is the deformation of one of the loaded ends of the laminate divided by the laminate half-length. The value of $\hat{\Omega}$ used was 14.6º and was found by a linear finite element analysis of the crack-tip element geometry. Because the delamination growth occurs at a 0/0 interface, the stress singularity obeys a classical inverse-square root relation.
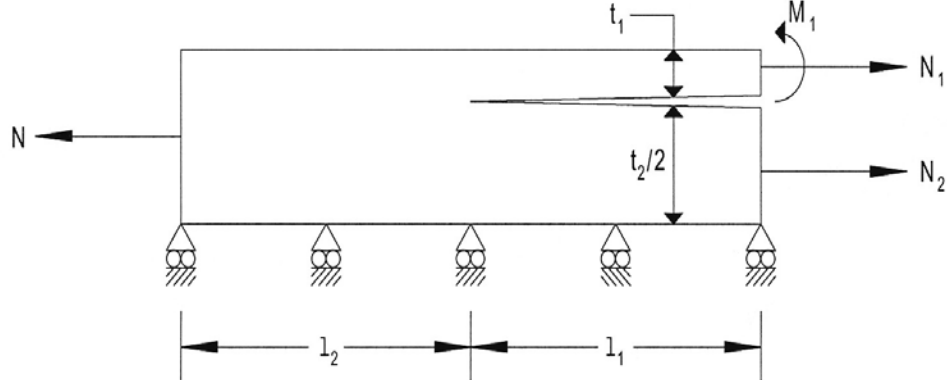
Figure 18. Crack-tip element and loading for delamination buckling problem.
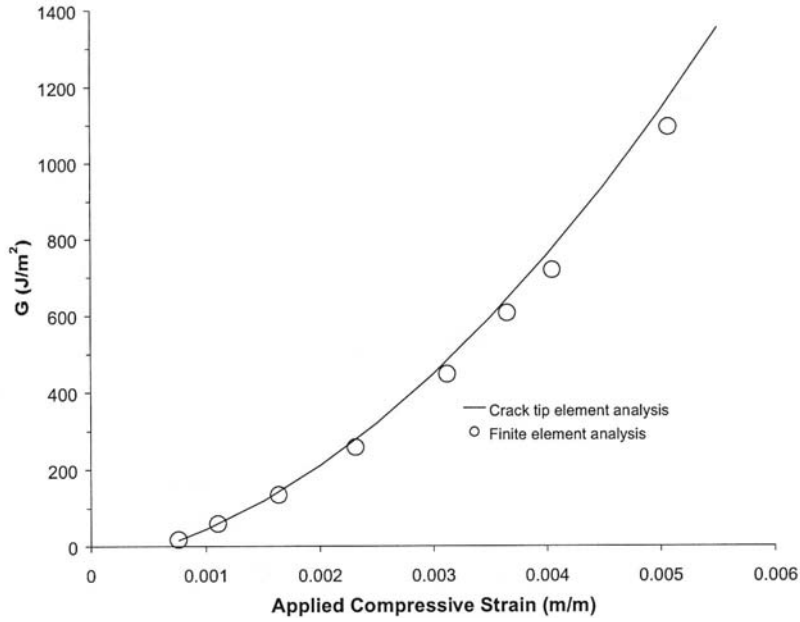
Figure 19. Comparison of total ERR for a $[0_2/90/0_2]_{3s}$ laminate.

Using this method, only a single, linear finite element analysis need be performed to obtain Ω; thereafter, all results are generated analytically. For certain specific problems, no finite element analyses are required, as the value of Ω may be taken directly from Davidson *et al.* (1995).

Edge Delamination

Consider a mid-plane symmetric laminate with a single delamination at its free edge, as shown in Figure 20. The term "sublaminates" will be used to refer to the regions bounded by the delamination and the laminate free surfaces. It is assumed that the delamination length, a, is large compared to the thickness of either of the sublaminates and that the strains and curvatures in the laminate and sublaminates are given by

$$\varepsilon_{1o} = \varepsilon_o \qquad \eta_{6o} = 0 \qquad \chi_1 = \chi_o \qquad \chi_6 = 0 \tag{2.41}$$

First, consider the classical laminated plate theory solution to an uncracked laminate under a specified loading. A transverse stress distribution is obtained for which the resultant transverse force, N_2, and moment, M_2, vanish along those faces of the laminate which are defined by a

24

normal vector in the positive or negative x_2 direction. Assuming a crack is introduced at an arbitrary interface, the resultant transverse forces and moments along the free edge of each of the sublaminates, as well as the shear and normal stresses along the crack plane, must vanish. To achieve this, superpose onto the solution to the uncracked laminate the solution to the problem where the sublaminates are loaded by transverse forces and moments, which are equal and opposite to those which are given by the uncracked solution. This superposition problem is shown in Figure 21 (with all forces and moments shown in their positive conventions).
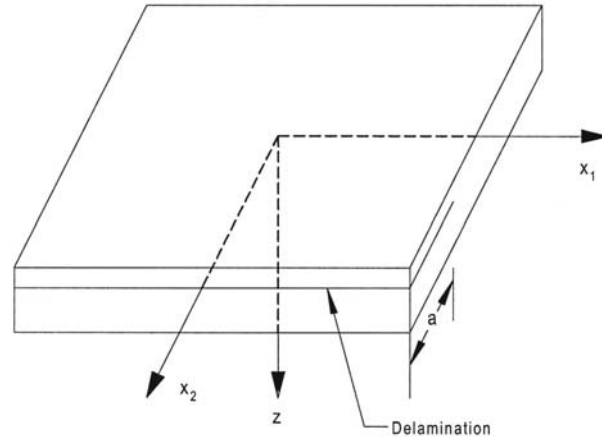
Figure 20. Laminate with a free edge delamination.

(a)

(b)
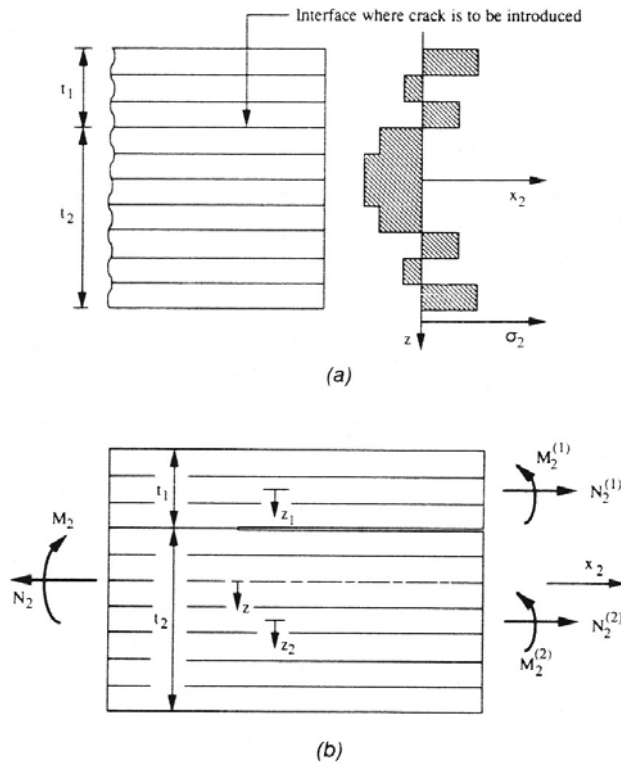
Figure 21. (a)Transverse stress distribution for an uncracked mid-plane symmetric laminate subjected to uniform axial extension in the X_1 direction. (b) Crack-tip element. Superposition of problem (b) onto (a) gives solution to cracked laminate.

Since the ERR for the uncracked laminate (Figure 21(a)) is zero, the ERR for the cracked laminate is simply that from the "crack-tip element" of Figure 21(b). The ERR and fracture mode ratio for this element may be obtained through a modified virtual crack closure method (Davidson, 1995). The equation for G is derived as in Equation (2.31) above. The subscripted quantities A', B', and D' are defined such that, for sublaminate 1 or 2

$$\varepsilon_{2o}^{(i)} = A_i' N_2^{(i)} + B_i' M_2^{(i)}, \quad i = 1, 2 \tag{2.42}$$

$$\chi_2^{(i)} = B_i' N_2^{(i)} + D_i' M_2^{(i)}, \quad i = 1, 2 \tag{2.43}$$

where

$\varepsilon_{2o}^{(1)} =$ is the midplane strain in the x_2 direction in sublaminate 1

$\chi_2^{(1)} =$ is the curvature in the x_2 direction in sublaminate 1, etc.

For those cases where crack growth is between orthotropic layers and the crack tip stress field exhibits an inverse square root singularity, G_I and G_{II} may each be expressed as Equations (2.37) and (2.38) where $\hat{\Omega} = \Omega$.

The value of G_I and G_{II} will never be less than zero. However, when the bracketed portion of G_I is less than zero, a negative Mode I stress intensity factor is predicted and the Mode I ERR component is actually a "closing mode." This implies a crack face interference and the present solution, which does not enforce crack face contact constraints, is invalid for that particular loading case.

The value of Ω is independent of the loading and may be found from numerical or other results of one special loading case. This may be done, for example, by FEA of the crack-tip element or taken from a generalized plane strain FEA of the free edge delamination problem. Also, the value of the total ERR is independent of Ω; that is, the sum of G_I and G_{II} will always give the same result as G, regardless of the value of Ω.

As an example, consider the determination of the ERR in a [45/0/–45/90]ₛ T300/5208 laminate with delaminations at both –45/90 interfaces (Davidson, 1994a and 1995). The laminate is subjected to a uniform strain in the global x_1 direction. The value of the ERR for various hygroscopic loading cases are presented in Figure 22 along with the finite element results from O'Brien *et al.* (1986). The results are found to match almost exactly.
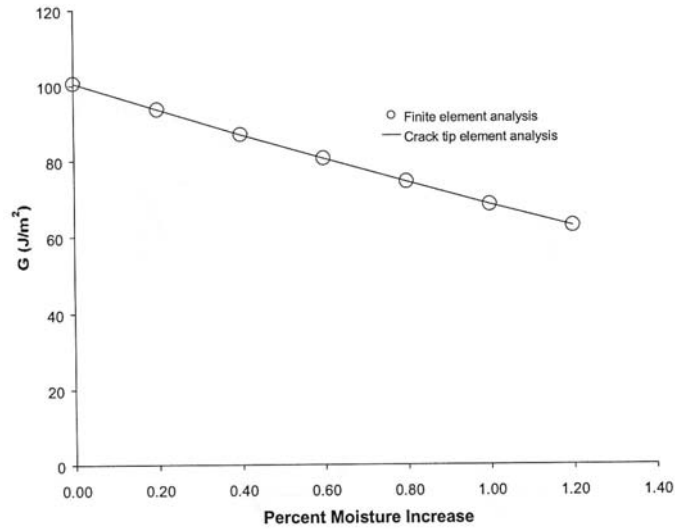
Figure 22. ERR versus hygroscopic loading for a [45/0/–45/90]ₛ T300/5208 laminate with edge delaminations at both (– 45/90).

2.2.2.3   *Progressive Delamination Growth*

A self-contained finite element program developed for progressive delamination growth technique allows non self-similar delamination progression. The approach is demonstrated on the post-buckling delamination growth of a thin composite sublaminate from a thicker sublaminate structure shown in Figure 23. In order to save computational costs, a double shell model is pursued using Mindlin shell theory. Efficiency and accuracy of this approach has been demonstrated in comparison to a 3-D model.
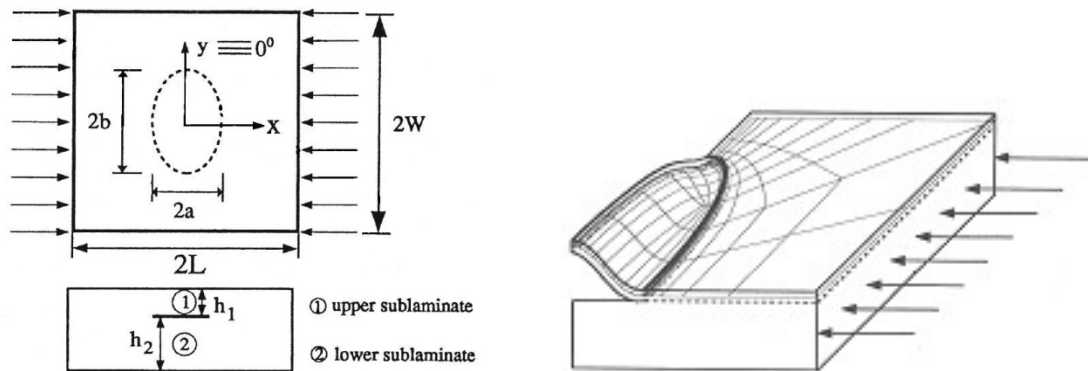
Figure 23. Configuration of embedded delamination.

The conditions for delamination growth are as follows: (1) the delamination exists prior to loading, (2) the growth is along the delamination interface plane, (3) stable growth occurs by increasing the boundary load, and (4) the computed distribution of strain energy release rate will exceed the critical value at the section of the delamination front that is propagating.

The modified crack closure technique (Rybicki and Kanninen, 1977; Jih and Sun, 1990) is used to calculate the strain energy release rate. In this technique, the strain energy released during crack extension is assumed to be equal to the work needed to close the opened surfaces. Generally, if the relationship between the nodal force and relative displacement is nonlinear, the

closure operation must be performed incrementally (Cheong and Sun, 1992). However, it was discovered that even while using large deflection theory, the relations between the nodal force (moment) and relative displacement (rotation) are nearly linear at the delamination front. Thus, one-step closure is adopted in this study. This condition must be verified for each problem as there may be problems where the linear relation does not persist.

In the crack closure method, the virtual crack extension Δa is usually taken to be small compared to the crack length. Thus, the nodal displacements (crack opening displacements) at the original crack tip after the extension can be approximated by the nodal displacements behind the crack tip before the extension. This reduces the analysis to one step instead of two. This procedure is valid if the elements in front of and directly behind the delamination crack front are similar. The conditions for similarity require that the size of each element both in front of and directly behind the crack front must be equal, the length of the elements normal to the delamination front must be Δa, and ideally, the two sides of the elements should be made perpendicular to the delamination front.

A program, FECM209, developed at Purdue University is used to simulate delamination propagation. For simplicity, a total strain-energy release rate, G, is chosen for the approach. The procedure for progressive delamination growth is as follows:
1. Calculate the linear stiffness matrix.
2. Apply the in-plane load incrementally by a specified amount $\Delta\varepsilon_0$ until the final load is reached.
3. Compute the nonlinear stiffness matrix based on the current stress field and displacements.
4. Solve the displacement and stress fields.
5. Find the converged solution or return to Step 3 if the solution is not convergent.
6. Evaluate the strain-energy release rate along the delamination front.
7. Check the distribution of the strain-energy release rate to find the corner nodes that exceed the critical value. If none exists, return to Step 2.
8. Move the nodes in the outward normal direction to the delamination front where the critical strain-energy release rate is exceeded and generate a new mesh.
9. Compute the linear stiffness matrix for the current mesh.
10. Go to Step 3.

In Step 6 the local value of G is computed at every corner node. When the strain-energy release rate at a node exceeds G_{cr}, the node will propagate in the local outward normal directions. The amount of propagation is proportional to the difference in the strain energy release rate and G_{cr}.

During remeshing, the ratios of element sizes along the delamination front remain constant. In addition, the number of elements along the x and y axes remains constant. A large change in element sizing could lead to poor results.

One problem with changing the mesh during loading is that the stiffness matrix must be updated accordingly. In Step 9, the linear stiffness matrix is updated based on the current mesh, but the nonlinear stiffness matrix must be calculated based on current displacements and stress fields. Since the location of the nodes has changed, the displacements and stresses at the new location should be interpolated from those at the previous locations. However, since the movements of

the nodes are very small each time the mesh is updated, the displacements and stresses at the previous location can be used as an approximation for the current location.

Most commonly used commercial codes do not allow the movement of nodes in a mesh during the loading procedure. Consequently, after the mesh is updated, the loading procedure would have to be restarted. In other words, the whole loading process has to be restarted for each movement of the delamination front. This is computationally very time-consuming for simulating delamination growth.

Post-buckling Delamination Growth Predictions

The following are results from simulations of post-buckling embedded and edge delaminations using the above technique. An example of an embedded circular delamination is shown in Figure 24. An initially circular delamination front with a radius of 15 mm (0.6 in.) is embedded in a 100 mm (3.9 in.) square panel. The critical strain-energy release rate $G_{cr} = 200$ J/m^2 (13.7 ft-lb/ft^2)is chosen for the analysis. The panel is loaded in the x-direction under uniform displacement.

Overlapping of the upper and lower sublaminates often occurs over some range at the delamination front. This overlapping can be constrained by contact elements.

The growth contours and corresponding normalized strain-energy release rate distributions for the [(90/0)$_s$] sublaminate are shown in Figures 24 and 25, respectively. The upper sublaminate is four plies while the lower sublaminate is twenty-eight plies. Transverse deflection of the lower sublaminate is constrained. The growth initiates perpendicular to the loading direction and is stable for the first four loading levels ($\varepsilon_1 - \varepsilon_4$). Curves labeled ε_5 and ε_6 have become neutrally stable since the loading level is not increased and the distribution of the strain-energy release rate in the growth-region remains near G_{cr}. The last curve labeled ε_7 is unstable because G has increased to 208 J/m^2 (13.8 ft-lb/ft^2) while the loading level remained constant.
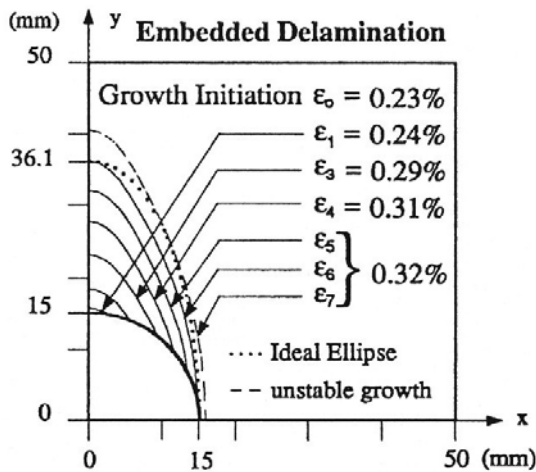
Figure 24. Progressive delamination fronts for the [(90/0)$_s$] laminate.
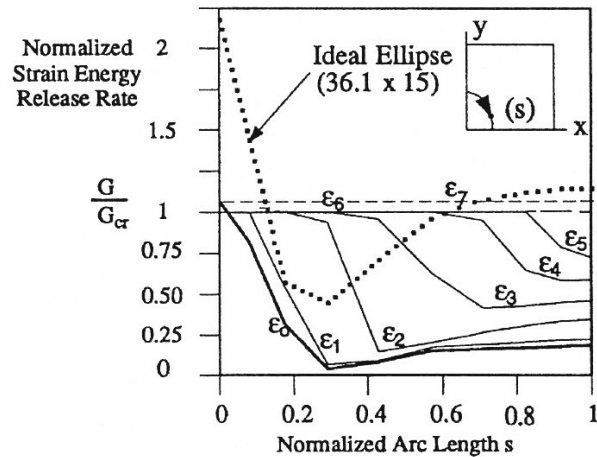
Figure 25. Strain-energy release rate distributions for the [(90/0)$_s$] laminate.

The distribution plot of G for the ideal ellipse (with the aspect ratio of contour ε_6) has a very large oscillation about the G_{cr} line while the distribution at ε_6 is constant. In fact, the maximum

value is more than twice the value of G_{cr}. Thus, the propagating delamination cannot be modeled as an elliptical crack.

It has been found that the initiation and subsequent stable delamination growth is very sensitive to the stacking sequence of the upper sublaminate. Lower bending stiffness parallel to the loading direction leads to higher predictions of strain-energy release rate and delamination growth at lower load levels. Un-symmetric sublaminates may have strong extensional-bending coupling that effectively reduces the bending stiffness leading to higher strain energy release rates.

The analysis neglects matrix cracking that can occur in the post-buckled sublaminate as observed by Whitcomb (1988). Matrix cracking can change the stiffness and may affect the stability of the growth.

A similar approach has been used to simulate the damage at the tip of a notch in cross-ply laminates. A schematic of the failure mode is shown in Figures 26 and 27. An axial split forms in the 0°-ply from a matrix crack and a delamination forms between the 0° and 90° layers. The fractures at the split and along the delamination front are modeled independently. This model has been used to investigate the size of the damage zone under various degrees of ply clustering or repeated plies. Larger damage zones are predicted and observed for increased ply clustering. Laminate strength approaches the laminate net section strength in the with large-ply clustering and damage zones.

See "Efficient Modeling of Postbuckling Delamination Growth in Composite Laminates Using Plate Elements" by Klug *et al*. (1996) for more detailed descriptions of the analysis results.
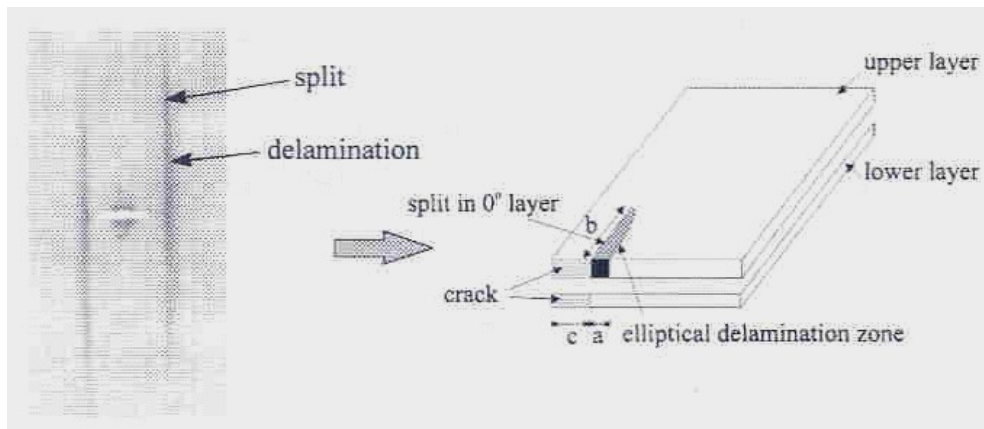
Figure 26. Schematic of axial splitting and delamination in a [(90/0)]ₛ laminate.
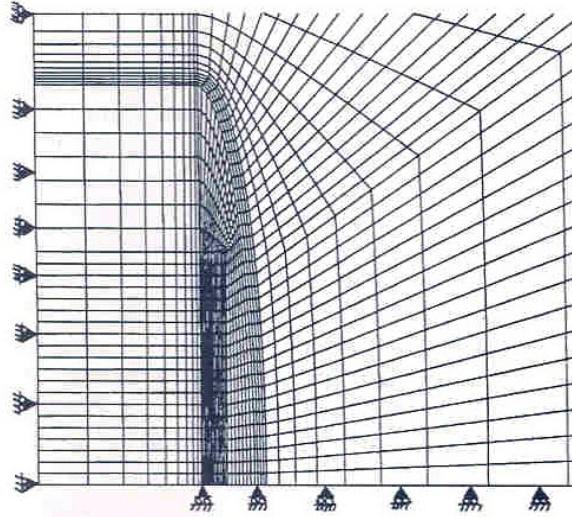
Figure 27. Local finite element mesh.

2.3   Impact Damage

2.3.1   *Prediction of Burst Strength After Impact (BAI) for Composite Overwrapped Pressure Vessel (COPV)*

The prediction of BAI for COPVs is one of most challenging tasks in COPV fracture control. Chen *et al.* (1998 and 1999) developed a procedure that can be used in the BAI predictions for COPVs under impact. A 3-D FEM was constructed with multi-layered, laminated, composite shell elements for the cylindrical COPV and the analysis was performed with ABAQUS™ (Vaidya *et al.*, 1998). The model consisted of two portions. In the cylindrical portion, where the low energy impact occurs, the liner thickness and the composite overwrap lay-up were used to obtain individual ply stress/strain responses. In the hemispherical ends, where the laminate material thickness and fiber orientation change continuously, integrated properties for the overwrap were used for simplicity. Due to symmetry, only half of the vessel was modeled, as shown in Figure 28. The vessel was fully constrained on one end while the other end was constrained only in the radial and tangential directions to simulate the constraint condition in the tests.
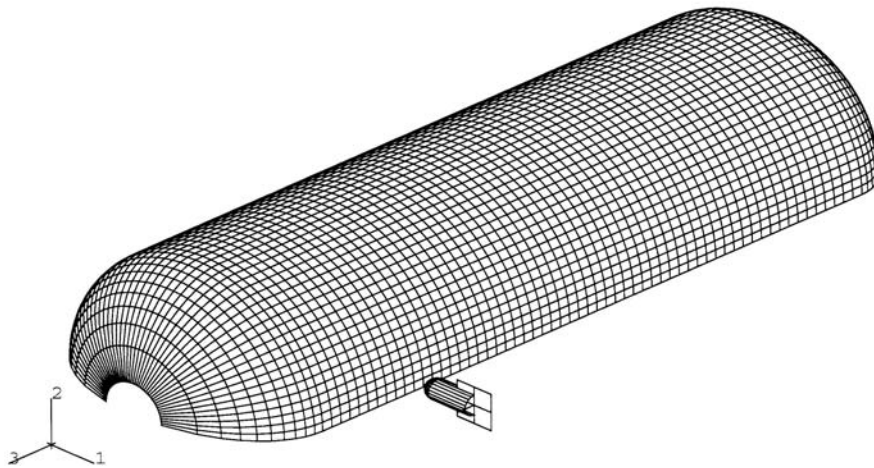
Figure 28. FEM of cylindrical COPV under impact.

The impactor mass was specified through the use of a point mass element, and the impactor geometry was specified using a rigid surface element. Surface definitions were specified for both the impactor and the COPV to ensure proper surface interaction during impact. The analysis was carried out in two steps. In the first step, an internal pressure was applied to the shell structure, and its static response was determined. In the second step, the impactor was assigned an initial velocity, and the resulting transient dynamic response of the COPV to the impact was evaluated using the implicit time integration procedure provided in ABAQUS™.

2.3.1.1   Impact Damage Prediction

Since fiber breakage is more detrimental to the tensile fracture strength of composite laminates than either delamination or transverse matrix cracking, different modes of impact damage must be distinguished in order to accurately predict the BAI of an impact damaged COPV. A modified maximum strain failure theory was used to predict both the extent and the mode of composite damage. The ply normal strains, in the fiber and transverse directions, and shear strains at each integration point were calculated and compared with their respective ultimate strains to determine whether any damage occurred in each ply. The three distinctive damage modes were: damage in the fiber direction (Mode I), damage in the transverse direction (Mode II), and damage in shear (Mode S). The extent of damage was determined by examining the strains in all the finite elements adjacent to the impact location.

A FEM of the cylindrical COPV is shown in Figure 28. The predicted damage mode and extent of damage obtained from the FEA results are summarized in Table 1, where the inner ply is shown at the top of the table and outer ply is shown at the bottom. The damage modes for the two elements adjacent to the impact location are separated by a dash, and a "0" indicates that there is no damage. A blank space in the table indicates that neither element was damaged and a "2s" means that both Mode II and Mode S damages were predicted. It is observed that the damage concentrates on the 72.5º plies and the 27.7º plies. For the 15 and 20 ft-lb (20 and 27 joules) impacts, the inner 19.2º ply was also damaged.

Table 1. Predicted Damage Modes for Each Ply

Laminate Ply	Impact Energy			
	5 ft-lb (7 joule)	10 ft-lb (14 joule)	15 ft-lb (20 joule)	20 ft-lb (27 joule)
19.2º			0-S	0-S
-19.2º				
85.7º				
-85.7º				
27.7º			1-0	1-S
-27.7º		S-0	S-1	S-1
72.5º		S-2	2S-2	2S-2
-72.5º	2-0	2-2S	2-2S	2-2S
85.8º				
-85.8º				

To account for the effect of damage on laminate strength, empirical material degradation factors (DF) were used to reduce the stiffness of damaged plies in the subsequent strength calculations.

The selection of the DF was based on the following empirical rules. For undamaged plies, the DF was zero. For plies with damage, the DF is as follows:

DF = 1.0 if damaged in Mode I
DF = 0.8 if damaged in Mode I or IIS
DF = 0.6 if damaged in Mode S

Mode IIS is considered to be no worse than Mode II and therefore the same DF was assigned to these two modes. In this way, the material effectiveness can be obtained for each ply by considering the damage mode and the damage extent, as

$$EF = 1.0 - \sum \frac{DF}{2} \tag{2.44}$$

where EF is the ply material effectiveness factor and summation is performed over the two elements surrounding the impact location.

For the COPV studied, the results of the material effectiveness calculation of each ply are presented in Table 2. It is observed that the material effectiveness in one of the 72.5° plies was reduced to 60 percent under the 5 ft-lb (7 joule) impact. Similarly, the 72.5° plies and the 27.7° plies were all reduced to 20 percent effective, and the inner 19.2° ply was reduced to 70 percent effective under the 20 ft-lb (27 joule) impact.

Table 2. Calculated Ply Material Effectiveness Factors

Laminate Ply	Impact Energy			
	5 ft-lb (7 joule)	10 ft-lb (14 joule)	15 ft-lb (20 joule)	20 ft-lb (27 joule)
19.2°	-	-	0.7	0.7
-19.2°	-	-	-	-
85.7°	-	-	-	-
-85.7°	-	-	-	-
27.7°	-	-	0.5	0.2
-27.7°	-	0.7	0.2	0.2
72.5°	-	0.3	0.2	0.2
-72.5°	0.6	0.2	0.2	0.2
85.8°	-	-	-	-
-85.8°	-	-	-	-

2.3.1.2   Post Impact Burst Strength Predictions

It was observed in the impact-testing program that debonding between the aluminum liner and the composite laminate occurred upon impact. Therefore, the aluminum liner and composite laminate were assumed to be un-bonded in the analysis and their contributions to the BAI of the COPV were calculated separately. The BAI of the COPV is the sum of the two component strengths. Once the impact damage was determined, the BAI of the COPV laminate was determined by a progressive failure analysis procedure. As the aluminum liner has yielded long before the laminate fails, the burst strength contribution by the aluminum liner, p, was conservatively estimated with a closed-form formula

$$p = \frac{s_y t}{r} \tag{2.45}$$

33

where r is the radius of the pressure vessel; s_y and t are the aluminum liner's yield strength and thickness, respectively. The yield strength of the aluminum liner was assumed to be 42,000 psi (290 MPa).

The burst strength contributed by the undamaged laminate was predicted to be 10,170 psi (70 MPa). The contribution of the aluminum liner was approximately 510 psi (3.5 MPa). The total predicted burst strength was therefore 10,680 psi (73.6 MPa), which was in close agreement with the average test value of 10,700 psi (73.8 MPa). Table 3 compares the predicted burst strengths with test data for the cylindrical COPV with damage caused by impact at various energy levels. The degradation in the burst strength was predicted to range from 7 percent to 29 percent for impact energies of 5 to 20 ft-lb (7 to 27 joules), respectively. One of the 15 ft-lb (20 joule) BAls does not appear to be reasonable because it indicates a greater residual burst strength than that of the 10 ft-lb test (14 joule). Ignoring that particular test data, one can see that the predicted degradation in burst strength was a little larger than the test data for the 10 ft-lb (14 joule) case and fairly close to the test data for all other cases. (See "Impact Damage Effects on Gr/Ep Composite Overwrapped Pressure Vessels" by Chen *et al.* (1999) for more detailed descriptions of the test results.)

Table 3. Comparison of Burst Strengths for Cylindrical COPV

Impact Energy	Test Results		Analytical Results	
	Burst Pressure	Degradation	Burst Pressure	Degradation
0 ft-lb (0 joule)	10,700 psi (73.7 MPa)	-	10,680 psi (73.6 MPa)	-
5 ft-lb (7 joule)	9,800 psi (67.6 MPa)	8.4%	9,920 psi (68.4 MPa)	7.1%
10 ft-lb (14 joule)	8,884 psi (61.2 MPa)	17.0%	8,220 psi (56.7 MPa)	23.0%
15 ft-lb (20 joule)	8,246 psi (56.9 MPa)	22.9%	7,960 psi (54.9 MPa)	25.5%
15 ft-lb (20 joule)	8,377 psi (57.8 MPa)	21.7%	7,960 psi (54.9 MPa)	25.5%
15 ft-lb (20 joule)	9,257 psi (63.8 MPa)	13.5%	7,960 psi (54.9 MPa)	25.5%
20 ft-lb (27 joule)	7,681 psi (53.0 MPa)	28.2%	7,590 psi (52.3 MPa)	28.9%

2.3.2 *Predicting Damage after Low-Velocity Impact*

Choi and Chang developed a method for predicting the impact damage of laminated composite plates resulting from both line-nose and point-nose impacts (ABAQUS™ User's Manual, 1992). The method consists of a stress analysis for determining the stress distributions inside the laminates during impact and a failure analysis for predicting the initiation and extent of the impact damage. The authors used a transient dynamic stress analysis code developed by Wu and Chang (Choi and Chang, 1992). The stress analysis was based on a 3-D linear elastic theory that assumes the materials in each layer to be homogeneous and orthotropic. Eight-node brick elements incorporating incompatible modes were used in the FEA. Elements with incompatible modes were chosen because of the improved accuracy in calculating bending stiffnesses and interlaminar shear stresses. The method was found to correspond well with experiments in predicting the location and extent of impact damage.

The procedure for determining the extent of the impact damage was as follows:
1. Calculate the transient dynamic stresses within each layer as a function of time.
2. Apply the matrix failure criterion for predicting the critical matrix cracks in each layer for determination of the extent of delaminations.
3. If matrix cracking is predicted in a layer of the laminate, then apply the delamination criterion subsequently in the upper and lower layer of the interface during the entire period of impact.

The procedure should be repeated at the other layers during impact for determining any additional matrix cracking and delaminations. The final size of each delamination is determined by the area within which the stress components satisfy the delamination failure criterion during the entire duration of the impact. No material degradation was considered in the model, and the model does not take into account delamination interaction during impact.

Two failure criteria were proposed in the study to predict the initiation of critical matrix cracks and estimate the extent of delamination.

2.3.2.1 Critical Matrix Cracking Criterion

The failure criterion proposed for matrix cracking can be expressed as (Wu and Chang, 1989)

$$\left(\frac{{}^n\bar{\sigma}_{yy}}{{}^n Y}\right)^2 + \left(\frac{{}^n\bar{\sigma}_{yz}}{{}^n S_i}\right)^2 = e_M^2 \qquad \begin{cases} e_M \geq 1 \ \ \text{Failure} \\ e_M < 1 \ \ \text{No Failure} \\ {}^n Y = {}^n Y_t \ \ \text{if} \ \bar{\sigma}_{yy} \geq 0 \\ {}^n Y = {}^n Y_c \ \ \text{if} \ \bar{\sigma}_{yy} < 0 \end{cases} \qquad (2.46)$$

where x and y are local coordinates of the nth layer parallel and normal to the fiber directions, respectively, and z is the out-of-plane direction. S_i is the *in situ* interlaminar shear strength within the laminate under consideration and Y_t and Y_c are the *in situ* ply transverse tensile and compressive strengths, respectively, as defined by Choi and Chang (ABAQUS™ user's manual, 1992).

Whenever the calculated average stresses in any one of the plies in the laminate first satisfy the criterion (i.e., $e_M = 1$) during impact, the initial impact damage is predicted. It was assumed that the matrix crack would propagate throughout the thickness of the ply group that contained the cracked ply. A delamination can be immediately induced from the location of the matrix crack along the interfaces of the ply group. Because additional matrix cracking can occur in other layers as time increases, the criterion should be continuously applied to the neighboring layers.

2.3.2.2 Impact-Induced Delamination Criterion

Once the crack matrix criterion is applied and a critical matrix crack is predicted within a laminate, a delamination is initiated from the crack. A semi-empirical model was developed to estimate the extent of delaminations in the composites. The model includes the following two types of critical cracks initiating delaminations resulting from the impact: the shear crack generated within the laminates, and the bending crack produced from the bottom surface of the laminates as shown in Figures 29 and 30.

It was reasoned that delamination growth due to low-velocity impact could occur only when two sequential conditions were met by the following:

1. One of the ply groups directly above or below the concerned interface failed due to matrix cracking.
2. The combined stresses governing the delamination growth mechanisms through the thicknesses of the upper and lower ply groups of the interface reaches a critical value. This is the impact-induced delamination growth criterion.
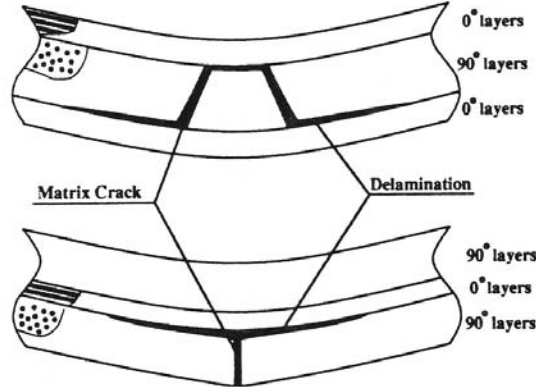
Figure 29. Basic impact damage mechanism of laminates subjected to 2-D line-loading impact. Top: delamination induced by inner shear cracks. Bottom: delamination induced by surface bending crack.
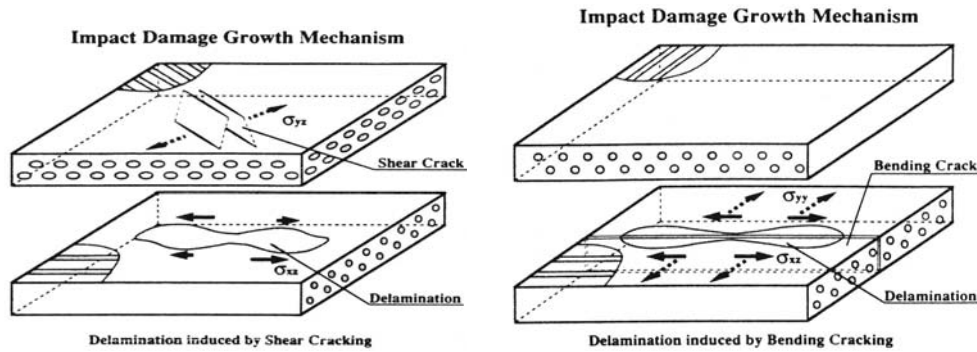
Figure 30. Schematics of the delamination growth mechanism due to a shear crack and a bending crack, respectively, in a laminated composite subjected to point-nose impact.

The second condition can be written in equation form as

$$D_a \left[\left(\frac{^n\bar{\sigma}_{yz}}{^nS_i} \right)^2 + \left(\frac{^{n+1}\bar{\sigma}_{xz}}{^{n+1}S_i} \right)^2 + \left(\frac{^{n+1}\bar{\sigma}_{yy}}{^{n+1}Y} \right)^2 \right] = e_D^2 \quad \begin{cases} e_D \geq 1 \ \text{ Failure} \\ e_D < 1 \ \text{ No Failure} \\ {}^{n+1}Y = {}^{n+1}Y_t \ \text{if} \ \bar{\sigma}_{yy} \geq 0 \\ {}^{n+1}Y = {}^{n+1}Y_c \ \text{if} \ \bar{\sigma}_{yy} < 0 \end{cases} \tag{2.47}$$

where D_a is an empirical constant which must be determined experimentally. The constant has been found to be insensitive to ply orientation and thickness of the laminate, and primarily dependent on the material system used. The superscripts n and n + 1 correspond to the upper and lower plies of the nth interface, respectively. $\bar{\sigma}_{yz}$ and $\bar{\sigma}_{yy}$ are the averaged interlaminar and in-

36

plane transverse stresses within the nth and n + 1th ply, respectively. $\bar{\sigma}_{xz}$ is the averaged interlaminar longitudinal stress within the n + 1th ply.

3.0   Damage Tolerance Life Prediction Methodologies

This section presents life prediction methods for damage growth under fatigue-type loading.

3.1   Delamination Growth in Cyclic Loading

3.1.1   Closed Form Solution for Delamination Growth

A delamination growth criteria that incorporates Mode II was investigated (dL/dN = f(G_{II})). A different delamination growth-rate criterion has been proposed that includes the effects of both ΔG_{II} and G_{IImax}. The following expression was found to provide best fit of the experimental data for a wide range of stress ratios:

$$\frac{dL}{dN} = m_2 \left(\frac{\Delta G_{II} \left(\dfrac{\Delta G_{II}}{G_{max}} \right)}{G_{IIc}} \right)^{n_2} \tag{3.1}$$

This equation is similar to the approaches used to characterize crack growth rates in metals for different stress ratios (Broek, 1986), and for R = ∞ it reduces to Equation (3.1) since $G_{IImax} = \Delta G_{II}$. A comparison of the analytical and experimental cyclic growth rates for three different R values is shown in Figure 31. Again, good agreement in the cyclic growth rates is observed for larger delaminations for which Mode II drives damage growth.
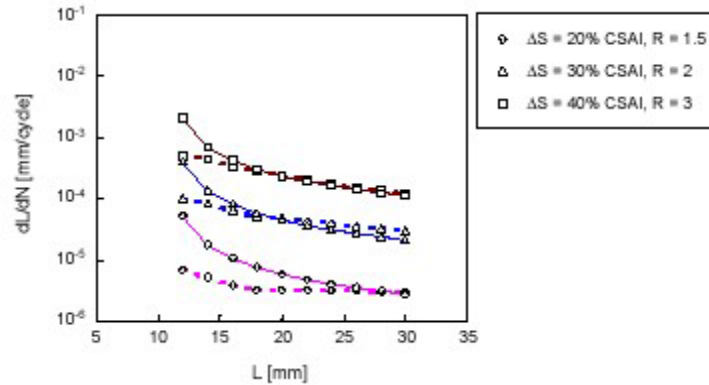
Figure 31. Cyclic growth rates (dL/dN) in constant-amplitude compression-compression loading as a function of L (solid lines – experimental data, dashed lines – analytical prediction).

A 3-D FEM would be required for a full understanding of parameters that influence delamination growth. However, the simplified modeling approach given by Han *et al*. (1999) can provide useful information about the major forces that drive delamination growth. For a delamination that spans only a few surface plies the results suggest that Mode II is the dominant factor that governs delamination growth with minor contributions from Mode I for smaller delamination lengths. If the delamination is nested deep in the thickness of the laminate, the influence of Mode I component becomes dominant and cannot be neglected (see Figure 32). However, the

maximum value of G_I (Whitcomb, 1981). Furthermore, large scatter in reported critical strain ERRs (Shyprykevich, 1997) and uncertainties in loading spectrum and damage characteristics could lead to substantially different delamination growth predictions.

Figure 32. Strain ERRs (G_I and G_{II}) as a function of applied load (ε_x in percent) and delamination length (L) for delamination located between plies 3 and 4.

3.1.2 Delamination Growth Using FEA

While a number of researchers have investigated delamination growth using the concepts of LEFM (Whitcomb, 1989; 1990; 1992; O'Brien *et al*., 1986; Davidson, 1994b; Kardomateas *et al*., 1994; Russell and Street, 1989; and Tratt, 1991), the question of characterizing delamination growth under fatigue is still not well understood. Typically, delamination growth is governed by strain ERRs GI, GII, and GIII, which in the Han et al. study were determined by FEA (Han *et al*., 1999).

Initial impact damage usually has a circular shape with multiple delaminations throughout the thickness. However Han argued that damage growth in fatigue more closely resembles a single delamination propagation front, rather than the growth of embedded multiple delaminations, as shown in Figure 33. Thus, an idealized plane-strain FEM was used to determine Mode I and Mode II components of the strain ERR.
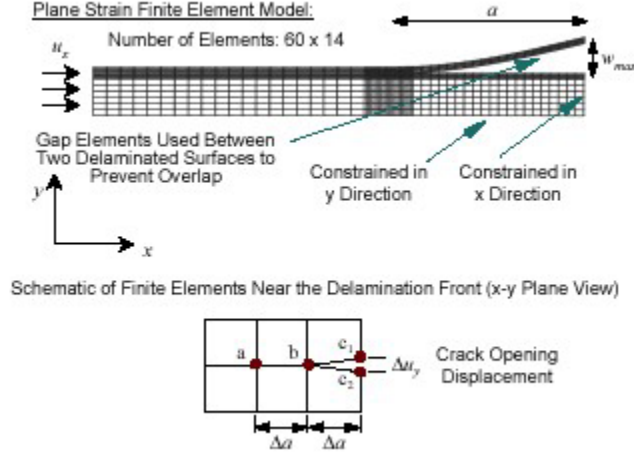
Figure 33. FEM procedure.

When subjected to a compressive load, the thin sublaminate buckles causing high interlaminar stresses at the delamination tip causing delamination growth. Hence, the influence of buckling and postbuckling of the sublaminate on delamination growth can be studied using a geometrically nonlinear static analysis. To initiate out-of-plane displacements an initial imperfection was assumed

$$w_{max} = \cos\left(\frac{\pi \cdot x}{2a}\right) \tag{3.2}$$

where the maximum initial imperfection (w_{max}) is chosen to be 10 percent of the delaminated ply thickness. Strain ERRs along the delamination front were determined using a modified crack closure technique (Rybicki and Kanninen 1977), and the individual strain ERRs, associated with the two modes of fracture, were (Mukherjee *et al.*, 1994).

$$G_I = \lim_{\Delta a \to 0} \frac{1}{2\Delta a} \int_0^{\Delta a} \sigma_{yy}(x) \Delta u_y (x + \Delta a)$$

$$G_{II} = \lim_{\Delta a \to 0} \frac{1}{2\Delta a} \int_0^{\Delta a} \sigma_{xy}(x) \Delta u_x (x + \Delta a)$$
$$\tag{3.3}$$

3.1.2.1   *Comparison with Experimental Results*

Experimental results indicate that once the damage propagated, it resembled a single delamination growth located one or two plies below the laminate surface. To gain a physical understanding of the mechanisms contributing to the delamination propagation, the correlation between the cyclic growth rates and the strain ERRs (*G*) was investigated. The G_I and G_{II} values of Figures 34 and 35 were calculated at different strain levels for delaminations located at one ply and two plies beneath the surface, respectively.

In Figure 34, for a through width delamination, G_I values of a single ply are very small due to the low bending stiffness of the delaminated ply. As the thickness of the delaminated ply increases, G_I also increases (Whitcomb, 1981)as shown in Figure 35. However, the influence of Mode I

39

decreases rapidly as crack length increases, and it does not contribute to the delamination growth once the delamination reaches ~18 mm (0.7 inches). On the other hand, values of G_{II} remain relatively constant over the range of delamination lengths investigated; therefore, a constant value of G_{II} can be assumed for a specific value of applied strain. However, after the initial buckling of the delaminated plies, the crack tip actually closes due to the compressive forces that develop near the crack tip. These compressive forces might decrease the calculated values for G_{II}, thus leading to the decay of cyclic growth rate.
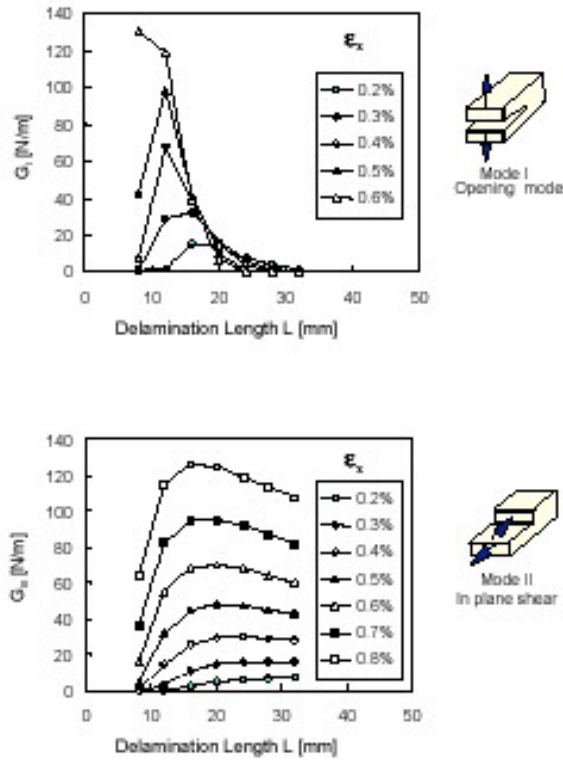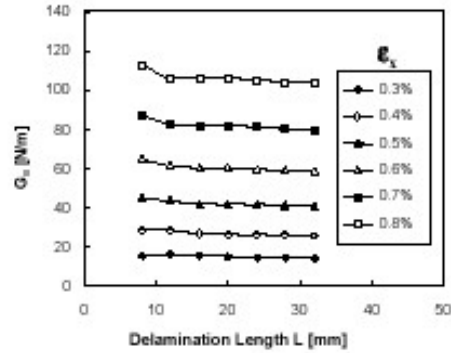

Figure 34. Strain ERRs (G_{II}) as a function of applied load (ε_x in %) and delamination length (L) for delamination located between plies 1 and 2.

a) Mode I.   b) Mode II.
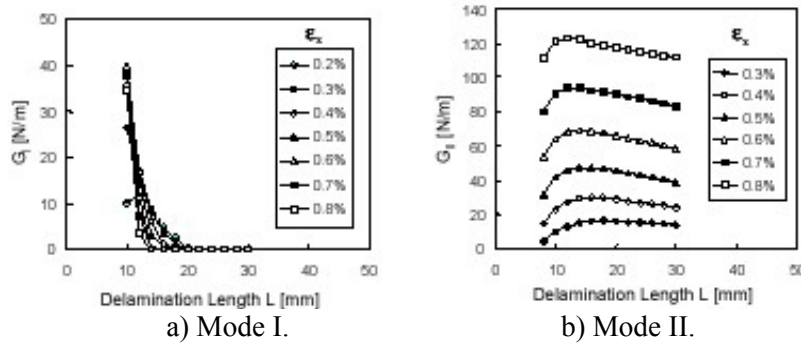
Figure 35. Strain ERRs as a function of applied load (ε_x in percent) and delamination length (L) for delamination between plies 2 and 3.

3.2   Damage Growth at Notch Tip

In a study to predict damage growth at a notch tip of a center-notched carbon fiber/epoxy laminates, Spearing *et al.* modeled the damage as a series of interacting matrix cracks in various forms: splitting, delamination and transverse play cracking (Spearing *et al.*, 1992). The basis of the growth model is the fatigue crack growth law known as Paris' law (Hertzberg and Manson, 1980).

$$\frac{da}{dN} = \lambda_1 (\Delta K)^m \tag{3.4}$$

where da/dN is the crack growth rate, ΔK is the stress intensity factor range and λ_1 and m are empirical constants.

Fatigue damage at notches can be characterized by the split length, l, at the notch tip. It has been observed that splits and delaminations grow in combination at the notch tip. As the split length increases, the associated delamination area grows with a dependence on the square of the split length (Figure 36) which implies an increasing resistance to further crack advance. Because of this, Equation (3.5) can be written as

$$\frac{dl}{dN} = \lambda_3 \left[\frac{\Delta G}{G_c} \right]^{m/2}$$
(3.5)

where l is the split length at the notch tip, ΔG is the driving force, G_c the current toughness (as measured in monotonic loading), and λ_3 is a constant.
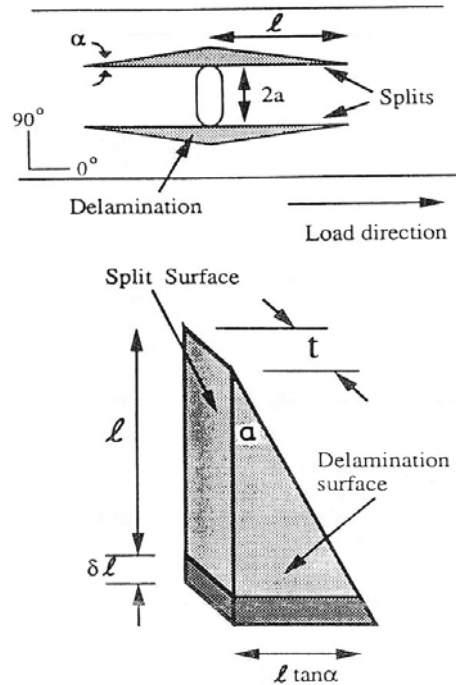
Figure 36. Schematic of the notch tip damage pattern in a cross-ply specimen.

3.2.1 *Damage Growth in Monotonic Loading*

The model that Spearing *et al*. (1992) apply to damage is based on a damage growth model for matrix cracks in monotonic loading. Ignoring transverse ply cracking and the effect of residual stresses, damage at the notch in a [90/0]ₛ laminate will grow by the simultaneous formation of splits in the 0° plies and triangular-shaped delamination zones at the [90/0] interfaces.

Spearing *et al*. used a modified FEM developed by Kortschot and Beaumont in order to calculate ∂C/∂l, the ratio of specimen compliance to an increment of split growth (Kortschot and Beaumont, 1991). The Kortschot and Beaumont model consists of two superimposed identical layers of 2-D plane stress elements. The two layers share the same nodes everywhere except in the delaminated region, where separate nodes are generated in the 90° ply. This model was further discussed in section 2.1.2.1. The model was first developed for edge-notched specimens. In order to use this model for center-notched specimens, some modifications were made. The

relationship between the value of $\partial C/\partial l$ obtained from the FEM ($\partial C/\partial l|_{FE}$) and those for the actual $[90/0]_s$ specimen is given by the scaling equation

$$\frac{\partial C}{\partial l} = \frac{(W/2)_{FE}\,(2t)_{FE}}{(W/2)(2t)}\,\frac{\partial C}{\partial l}\bigg|_{FE} \tag{3.6}$$

where W is width and t is the thickness of the split.

This can be extended to all laminates of the form $[90i/0i]_{ns}$ in which there is an equal total thickness of 90° and 0° plies. The scaling equation, in this case, becomes

$$\frac{\partial C}{\partial l} = \frac{(W/2)_{FE}\,(\text{int})_{FE}}{(W/2)(2\text{int})}\,\frac{\partial C}{\partial l}\bigg|_{FE} \tag{3.7}$$

The method can be extended to laminates with unequal thicknesses of 0° and 90° plies by altering the relative ply thicknesses of the layers of the finite element mesh.

3.2.2 Damage Growth Model Applied to [90/0]ₛ Laminates

For an initial length, l_0, the split length after N cycles of constant load amplitude is given by

$$l = \frac{1}{G_d\tan\alpha}\left[\lambda(\Delta G)^{m/2}\left[\frac{m+2}{2}\right]\times(G_d\tan\alpha)\,N + \left(G_s t + G_d l_0 \tan\alpha\right)^{(m+2)/2}\right]^{2/(m+2)} \tag{3.8}$$

where G_s and G_d are the energies absorbed per unit area of split and delamination, respectively, and ΔG is given by

$$\Delta G = \frac{(\Delta P)^2}{2t}\,\frac{\partial C}{\partial l} \tag{3.9}$$

where P is the range of applied load.

Figure 37 shows a comparison of experimental data with the results from Equation (3.9) for a $[90/0]_s$ laminate cycled at three different peak stresses. Good agreement is shown with the experimental data.
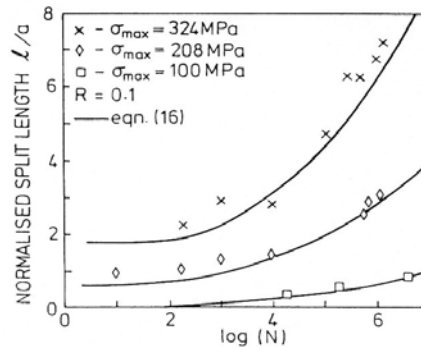
Figure 37. Normalized split length for a $[90/0]_S$ laminate as a function of load cycles showing the effect of varying peak stress. The solid lines represent the prediction of Equation (6.9).

3.2.3 Damage Growth in [90i/0i]ₛ Laminates

For laminates containing plies of equal thicknesses, ΔG increases linearly with ply thickness; $i \times t$. For the $[90/0]_s$ case, there are only two interfaces at which delaminations can grow. In this case, the ratio $\Delta G/G_c$ increases as i increases; so the fatigue law becomes

$$\frac{dl}{dN} = \left[\frac{\frac{1}{2}(\Delta\sigma_\infty)^2 (W/2)(2it)(W/2)_{FE}(2t)_{FE} \left.\frac{\partial C}{\partial l}\right|_{FE}}{G_s it + G_d lt\tan\alpha} \right]^{m/2} \tag{3.10}$$

Good agreement has also been found with experimental data for this case as is shown in Figure 38.

Figure 38. Normalized split length as a function of load cycles for $[90_i/0_i]_{ns}$ laminates. The solid lines represent Equation (3.11).

3.2.4 Fatigue Damage Growth in [90i/0j]ₛ Laminates

Laminates with plies of unequal thicknesses can be modeled in a similar way. The relative ply thicknesses of the layers in the finite element meshes were adjusted and the resulting values of $\partial C/\partial l|_{FE}$ were scaled appropriately. In this case, the fatigue law is

$$\frac{dl}{dN} = \left[\frac{\frac{1}{2}(\Delta\sigma_\infty)^2 (W/2)((i+j)t)(W/2)_{FE}(i+j)t_{FE} \left.\frac{\partial C}{\partial l}\right|_{FE}}{G_s it + G_d lt\tan\alpha} \right]^{m/2} \tag{3.11}$$

From this law, it is shown that for laminates with $j > i$ more rapid damage progression occurs than in $[90/0]_s$ laminates.

3.2.5 Damage Growth in [90/0]ₙₛ Laminates

In the case of $[90/0]_{ns}$ laminates, ply thickness is constant and equal for the 90° and $0G_{II}$ laminae; only the number of 90/0 interfaces varies. Through half the laminate thickness, $2n - 1$ interfaces

43

exist at which delaminations can propagate. Since the split area is n × t × l, and ∂C/∂l scales with the number of plies as shown in Equation (3.8), the fatigue law becomes

$$\frac{dl}{dN} = \lambda \left[\frac{\frac{1}{2}(\Delta\sigma_\infty)^2 (W/2)(2nt)(W/2)_{FE}(2t)_{FE} \left.\frac{\partial C}{\partial l}\right|_{FE}}{G_s nt + G_d (2n-1) l \tan\alpha} \right]^{m/2} \tag{3.12}$$

As the number of plies increases, the model predicts that the rate of damage propagation decreases slightly which causes the model to underestimate the damage growth (Figure 39). This effect was theorized to be due to unequal damage growth through the thickness of the laminate.
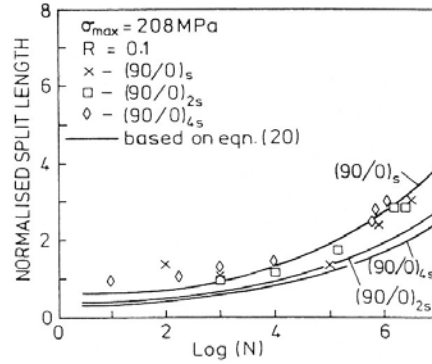
Figure 39. Normalized split length as a function of load cycles for [90/0]$_{ns}$ laminates. The solid lines represent Equation (3.13).

3.2.6   *Damage Growth in [90/+45/-45/0]$_s$ Laminates*

For these laminates, it was assumed that damage is controlled by splitting in the 0° plies and by delamination at the interface between the 0° ply and the innermost –45° plies. In this case, the finite element representation provides values for ∂C/∂l that are independent of the split length, which is different from the cross-ply laminates discussed previously. The fatigue law was derived for this configuration in a similar manner to that of the [90/0]$_s$ laminate, yielding

$$\frac{dl}{dN} = \lambda \left[\frac{1/2(\Delta P)^2 \left(\frac{\partial C}{\partial l}\right)}{G_s t + G_d \left(\frac{1+k}{2}\right)} \right]^{m/2} \tag{3.13}$$

where k is the dimension defining the intersection of the delamination with the center line of the notch.

A good correlation between the experimental data and the fatigue law were also found in this case, as shown in Figure 40.
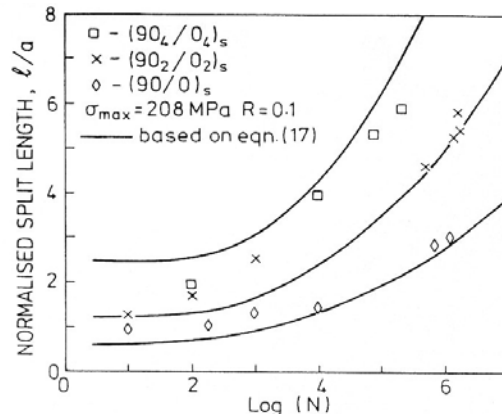
44
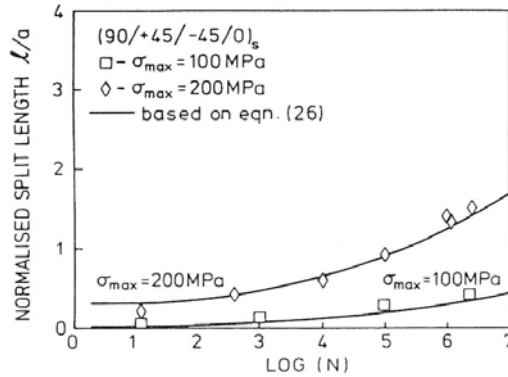
Figure 40. Normalized split length as a function of load cycles in [90/+45/–45/0]$_s$ laminates. The solid lines represent Equation (3.14) in an integrated form.

4.0   Damage Tolerance Analysis Codes

Two computer codes have been developed at The Aerospace Corporation (Aerospace) for predicting residual strength of composite structures containing defects. The first such code is Aerospace Damage Analysis Methodology for Composites (ADAM-C). The other code is Progressive Failure Analysis (PFA). The following sections briefly introduce these two codes. Detailed discussions are presented in Appendices A and B.

4.1   ADAM-C

In a research and development project conducted by Aerospace in the 1980s, a few analytical models were selected for inclusion in a static residual strength prediction software code, ADAM-C (Chang *et al.*, 1985); see Figure 41 for program flow. Refer to Appendix A for a more detailed explanation of the study. Table 4 contains a summary of some of the analytical models reviewed.
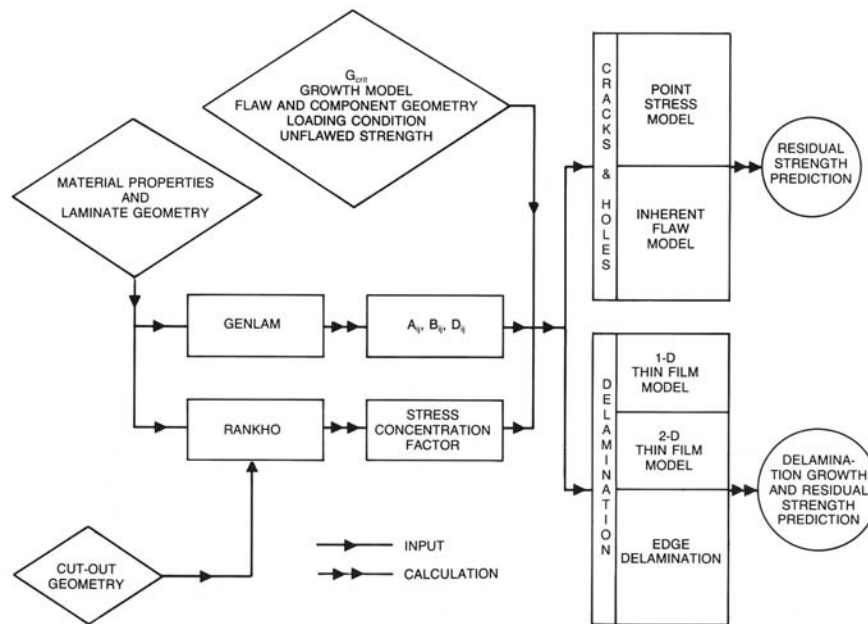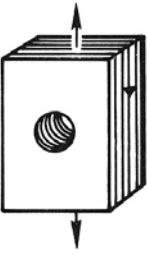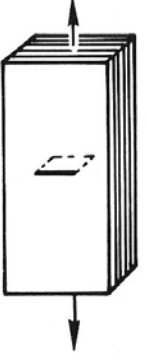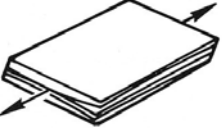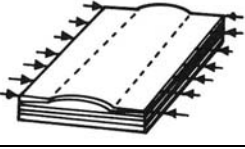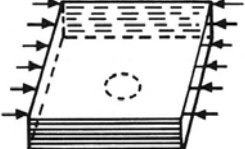
Figure 41. ADAM-C program flow chart.

Table 4. Assessment of Analytical Methods

Loading and Damage Type	Analytical Method	Advantages	Disadvantages
	Point stress failure model	Simple calculation, adequate database	Stress intensity zone size is independent of hole sizes
	Notched fracture stress model	Simple calculation	Extensive testing, limited database
	Damage zone model	Provides more accurate predictions	Lengthy calculation, not enough database
	Inherent flaw model	Simple calculation, adequate database	Characteristic zone size is independent of crack sizes
	Strain energy density factor method	Provides more accurate predictions	Very limited database
	Finite element approach	Provides adequate accuracy for complex geometries	Length calculation
	Damage zone model	Provides more accurate predictions	Length calculation
	Finite element method	Provides adequate accuracy for complex geometries	Length calculation
	Edge delamination model	Simple calculation	Limited application
	Finite element method	Provides adequate accuracy for complex geometries	Length calculation
			Limited application
	Thin-film 1-D model	Simple calculation	
	Finite element method	Provides adequate accuracy for complex geometries	Length calculation
	Thin-film 2-D delamination model	Simple calculation	Prediction accuracy needs to be improved

The IFM developed by Waddoups *et al.* was selected for use in predicting the residual strength of cracked composite laminates (Waddoups *et al.*, 1971). The PSM developed by Whitney and Nuismer was selected for use with laminates containing holes and cutouts (Whitney and Nuismer, 1974). These models require simple calculations and have the advantage of an extensive test database for the more common composite systems such as graphite/epoxy (Gr/Ep). Details of these methods can be found in section 5.1.1.1 of Whitney and Nuismer, 1974.

For composites with delaminations at free edges, the edge delamination model (O'Brien, 1982) of O'Brien was selected. Through-the-width or embedded delaminations are characterized by Chai's thin film model (Chai *et al.* 1981). These two models have two common features in that they avoid lengthy finite element calculations, and use the strain ERR *G* to characterize delamination growth.

4.2   PFA for Composites

In recent years, the research and development for the PFA of composites at Aerospace has integrated and extended the PFA developed at NASA Langley Research Center (LaRC) in the late 1990s and early 2000s. The PFA is implemented in a software tool that integrates with existing commercial FEM software. The tool simulates the growth and propagation of failure modes in a composite and it is constantly adapted for new classes of problems and extended to incorporate new physics. The key features of the PFA code include: (1) delamination simulation by using interface elements; (2) Prediction of in-plane and out-of-plane nonlinear shear damage; (3) Prediction of matrix-cracks based on a modified version of Puck's criterion (Puck and Schurmann, 1998); and (4) A fiber failure criterion based on the work of Chang and Chang (Chang, and Chang, 1987).

The PFA code utilizes concepts from damage mechanics to degrade the material properties of the composite appropriately. The code also handles contact in the event of delamination closure following growth. Similar to ADAM-C, the code was developed to be as generic as possible and applicable to a large range of problems with adequate accuracy and conservatism. The accuracy of the code, however, relies on developing a complete mechanical, strength, and fracture database that can be used directly as input to the code. Appendix B discusses the progressive failure philosophy, the damage models in the PFA code, the characterization testing that is required to define the damage model, and validation of the PFA code. The PFA code is also demonstrated for few examples pertaining to pressure vessels.

5.0   References

5.1   Government Documents

NASA-STD-5003   *Fracture Control Requirements for Payloads Using the Space Shuttle*, 1996.

NASA-STD-5007   *General Fracture Control Requirements for Manned Spaceflight Systems*, 2000.

NASA-STD-5019   *Fracture Control Requirements for Spaceflight Hardware*, 2008.

MSFC-RQMT-3479   *Fracture Control Requirements for Composite and Bonded Vehicle and Payload Structures*, 2006.

JSC-22267B   *Fatigue Crack Growth Computer Program NASGRO®*, Version 3.0, November, 2001.

SSP 30558B   *Fracture Control Requirements for Space Station*, 1994.

CMH-17 (aka MIL-HDBK-17)   *Composite Materials Handbook, Polymer Matrix*, Vol. I-V.

5.2   Government References

The references listed below are in alphabetical order by author.

Byers, B. A. (1980): *Behavior of Damaged Graphite/Epoxy Laminates Under Compression Loading.* NASA-CR-159293, August 1980.

Davidson, B. D. (1998): *A Predictive Methodology for Delamination Growth in Laminated Composites, Part I: Theoretical Development and Preliminary Experimental Results*. FAA Report No. DOT/FAA/AR-97/87, April 1998.

Dopker, B.; *et al*. (1995): "Composite Structural Analysis Supporting Affordable Manufacturing and Maintenance." *Paper presented at the Sixth NASA/DOD/ARPA Advanced Composite Technology Conference*, Anaheim, California; August 1995. Also published in conference publication NASA CP-3326, 1996.

Han, H. T.; Mitrovic, M.; and Turkgenc, O. (1999): *The Effect of Loading Parameters on Fatigue of Composite Laminates: Part III*. FAA Report No. DOT/FAA/AR-99/22, June 1999.

Konno, K.; Woytach, J; and Tyburski, T. E. (2001): *Flywheel Energy Storage System (FESS) Rotor Certification Plan*. NASA Report No. 69011-PLAN-311, Rev. A.

Madan, R. C. (1988): *Composite Transport Wing Technology Development*. NASA-CR-178409, February 1988.

Poe, C. C., Jr.; and Sova, J. A. (1980): *Fracture Toughness of Boron/Aluminum Laminates with Various Proportions of 0° and ±45° Plies*. NASA-TP-1707.

Scholz, D.; *et al*. (1997): *Advanced Technology Composite Fuselage – Materials and Processes*. NASA-CR-4731, April 1997.

Smith, P. J.; and Wilson, R. D. (1985): *Damage Tolerant Composite Wing Panels for Transport Aircraft*. NASA CR-3951, December 1985.

Sollars, T. A. (1987): "Shuttle/Centaur G-Prime Composite Adapters Damage Tolerance/Repair Test Program." AIAA Paper 87-0792, *28th Structures, Structural Dynamics and Materials Conference*, Monterey, California, April 6–8, 1987.

Whitcomb, J. D. (1988): *Instability-Related Delamination Growth of Embedded and Edge Delaminations*. NASA TM-100655, August 1988.

5.3 Non-Government References

The references listed below are in alphabetical order by author.

ABAQUS User's Manual (1992): Pawtucket, Rhode Island: Hibbitt, Karlson and Sorensen, Inc.

Agarwal, B. D.; and Giare, G. S. (1982): "Influence of the Properties of a Matrix Material on the Fracture Toughness of Short-Fiber Composites." *Materials Science and Engineering*, Vol. 52, pp. 139-145.

Anderson, T. L. (1991): *Fracture Mechanics: Fundamentals and Applications*. Boca Raton, Florida, CRC Press.

Aronsson, C-G. (1986): "Tensile Fracture of Laminates With Cracks." *Journal of Composite Materials*, Vol. 20, No. 3, pp. 287-307, May 1986.

Ashton, J. E.; and Whitney, J. M. (1970): *Theory of Laminate Plates*. Stamford, Technomic Publishing Co.

Basham, K. D.; Chong, K. P.; and Boresi, A. P. (1993): "A New Method to Compute Size Independent Fracture Toughness Values for Brittle Materials," *Engineering Fracture Mechanics*, Vol. 46, No. 3, pp. 357-363.

Broek, D. (1986): *Elementary Engineering Fracture Mechanics*. M. Nijhoff Publishers.

Brown, W. F. (1970): "Tentative Method of Test for Plane Strain Fracture Toughness of Metallic Materials." *Review of Developments in Plane Strain Fracture Toughness Testing, American Society for Testing and Materials*, *ASTM STP 463*, American Society for Testing and Materials, 1970, pp. 249-269.

Chai, H.; Babcock, C. D. (1985): "Two-Dimensional Modeling of Compressive Failure in Delami-nated Laminates." *Journal of Composite Materials*, Vol. 19, No. 1, pp. 67-98.

Chai, H.; Babcock, C. A.; and Knauss, W. G. (1981b). "One Dimensional Modeling of Failure in Laminated Plates by Delamination Buckling." *International Journal of Solids and Structures*, Vol. 17, No. 11, pp. 1069-1083.

Chai, H. (1982): *The Growth of Impact Damage in Compressively Loaded Laminates*. Unpublished Ph.D. Thesis, March 1982. Pasadena: California Institute of Technology (Caltech).

Chang, F. K.; and Chang, K. Y. (1987): "A Progressive Damage Model for Laminated Composites Containing Stress Concentrations." *Journal of Composite Materials*, Vol. 32, pp. 834-855.

Chang, J. B. (1981): "Round-Robin Crack Growth Prediction on Center-Cracked Tension Specimens under Random Spectrum Loading." *Methods and Models for Predicting Fatige Crack Growth under Random Loading, ASTM-STP-748*, J. B. Chang and C. M. Hudson, Eds., American Society for Testing and Materials, pp. 3-40

Chang, J. B.; Rogers, J. C.; and Kamrath, A. R. (1985): *Damage Tolerance Analysis Methodology for Composite Structures*. From Aerospace Sponsored Research (ASR) Summary Report, Aero-space Report No. ATR-85(8498)-2, The Aerospace Corporation.

Chang, J. B.; Szamossi, M.; and Liu, K. W. (1981): *A User's Manual for a Detailed Level Fatigue Crack-Growth Analysis Commuter Code – The CRKGRO Program*. AFWAL-TR-81-3093.

Chen, H. C.; Chiu, S. T.; and Chang, J. B. (1999): "Impact Damage Effects on Gr/Ep Composite Over-wrapped Pressure Vessels." *Paper presented at the Proceedings of the 40th AIAA/ASME/ASCE/AHS/ASC Structures, Structural Dynamics, Materials Conference and Exhibit*, AIAA Paper No. 99-1321. Vol. 2, April 12–15, St. Louis, Missouri.

Chen, H. C.; Chiu, S. T.; and Chang, J. B. (1998): Residual Burst Strength Evaluation of Composite Overwrapped Pressure Vessels After Impact. *JANNAF NDES/RNTS/S & MBS Joint Meeting*, Salt Lake City, Utah, March 1998.

Cheong, S. K.; and Sun, C. T. (1992): "Analysis of Postbuckled Delaminations Using Incremental Crack Closure Integral." *Proceedings of the Second International Symposium on Composite Structures and Materials*, Peking Press, Beijing: PRC, pp. 519-524.

Choi, H. Y.; and Chang, F. K. (1992): "A Model for Predicting Damage in Graphite/Epoxy Laminated Composites Resulting From Low-Velocity Point Impact." *Journal of Composite Materials*, Vol. 26, No. 14, pp. 2134-2169.

Davidson, B. D.; and Krafchak, T. M. (1993): "Analysis of Instability-Related Delamination Growth Using a Crack Tip Element," *AIAA Journal*, Vol. 31, No. 11, pp. 2130-2136.

Davidson, B. D. (1994a): "Energy Release Rate Determination for Edge Delamination Under Combined In-Plane, Bending and Hygrothermal Loading. Part I – Delamination at a Single Inter-face." *Journal of Composite Materials*, Vol. 28, No. 11, pp. 1009-1031.

Davidson, B. D. (1994b): Prediction of Delamination Growth in Laminated Structures. *Paper presented at the Proceedings of the 1994 International Mechanical Engineering Congress and Exposition: Failure Mechanics in Advanced Polymeric Composites*. Chicago, Illinois, USA, AMD-Vol. 196, pp. 43-65.

Davidson, B. D. (1995): "Prediction of Energy Release Rate for Edge Delamination Using a Crack Tip Element Approach." *Composite materials: Fatigue and Fracture—Fifth Volume*, *ASTM STP 1230*, R. H. Martin, Ed., American Society for Testing and Materials, Philadelphia, 1995, pp. 155-175.

Davidson, B. D.; Hu, H.; and Schapery, R. A. (1995): "An Analytical Crack Tip Element for Layered Elastic Structures." *Journal of Applied Mechanics*, Vol. 62, pp. 294-35.

Davila, C. G.; Camanho, P. P.; and de Moura, M. F. (2001): "Mixed-Mode Decohesion Elements for Analyses of Progressive Delamination." *Paper presented at 42nd AIAA/ASME/ASCE/ AHS/ASC Structures, Structural Dynamics, and Materials Conference and Exhibit*, April 15–19, 2001. Paper No. AIAA-01-1486. Seattle, Washington.

de Moura, M. F. S. F.; Goncalves, J. P. M.; Marques, A. T.; and de Castro, P. M. S. T. (2000): "Prediction of Compressive Strength of Carbon-Epoxy Laminates Containing Delamination by Using a Mixed-Mode Damage Model." *Composite Structures*, Vol. 50, pp. 151-157.

de Moura, M. F. S. F.; Goncalves, J. P. M.; Marques, A. T.; and de Castro, P. M. S. T. (1997): "Modeling Compression Failure After Low Velocity Impact on Laminated Composites Using Inter-face Elements." *Journal of Composite Materials*, Vol. 31, pp. 1462-1479.

Dodds, R. H., Jr.; and Vargas, P. M. (1988): *Numerical Evaluation of Domain and Contour Integrals for Nonlinear Fracture Mechanics*. Report UILU-ENG-88-2006, August 1988, Urbana: University of Illinois.

Dopker, B.; Murphy, D.; Ilcewicz, L. B.; and Walker, T.(1994): "Damage Tolerance Analysis of Composite Transport Fuselage Structure." *Paper presented at 35th AIAA/ASME/ ASCE/AHS/ASC Structures, Structural Dynamics, & Materials Conference*, AIAA Paper 94-1406.

Eringen, A. C. (1968): *Theory of Micropolar Elasticity*. Fracture, H. Liebowitz, Ed. New York, Academic Press, Vol. 2, pp. 662-729.

Hertzberg, R. W.; and Manson, J. A. (1980): *Fatigue of Engineering Plastics*. Bethlehem, Pennsylvania, Academic Press.

Horton, R.; *et al*. (1988): *Damage Tolerance of Composites – Final Report*. Report No. AF-WAL-TR-87-3030.

Hu, H. (1995): *Analytical Determination of Energy Release Rate and Mode Mix for Interfacial Cracks*. Unpublished Ph. D. dissertation, December 1995. Department of Mechanical, Aerospace and Manufacturing Engineering, New York, Syracuse University.

Hu, T. (1980*): Advanced Crack Propagation Predicative Analysis Computer Program*. FLAGRO 4, Rockwell International, SOD 79-0280.

Irwin, G. R. (1958): *Fracture*. Handbuch der Physik, Vol. 6, No. 551.

Jih, C. J.; and Sun, C. T. (1990): "Evaluation of a Finite Element Based Crack-Closure Method for Calculating Static and Dynamic Energy Release Rates." *Engineering Fracture Mechanics*, Vol. 37, No. 2, pp. 313-322.

Kardomateas, G. A.; Pelegri, A. A.; and Malik, B. (1994): "Growth of Internal Delaminations Under Cyclic Compression in Composite Plates." *Paper presented at the Proceedings of the 1994 International Mechanical Engineering Congress and Exposition; Failure Mechanics in Advanced Polymeric Composites*. Chicago, Illinois, AMD. Vol. 196, pp. 13-29.

Kennedy, T. C. (1999): "Modeling Failure in Notched Plates with Micropolar Strain Softening." *Composite Structures*, Vol. 44, pp. 71-79.

Klug, J.; Wu, X. X.; and Sun, C. T. (1996): "Efficient Modeling of Postbuckling Delamination Growth in Composite Laminates Using Plate Elements." *AIAA Journal*, Vol. 34, No. 1, January 1996.

Kongshavn, I.; and Poursartip, A. (1999): "Experimental Investigation of a Strain-Softening Approach to Predicting Failure in Notched Fibre-Reinforced Composite Laminates." *Composites Science and Technology*, Vol. 59, pp. 29-40.

Kortschot, M. T.; and Beaumont, P. W. R. (1991): "Damage-Based Notched Strength Modeling: A Summary." *Composite Materials, Fatigue and Fracture (Third Volume)*, *ASTM STP 1110*; T. K. O'Brien, Ed., American Society for Testing and Materials, Philadelphia, 1991, pp. 596-616.

Lin, K. Y.; and Mar, J. W. (1977): "Finite Element Analysis of Stress Intensity Factors for Cracks at a Bi-Material Interface." *International Journal of Fracture*, Vol. 12, No. 2, pp. 521-531.

Llorca, J.; and Elices, M. (1992): "A Cohesive Crack Model to Study the Fracture Behavior of Fiber Reinforced Brittle-Matrix Composites." *International Journal of Fracture*, Vol. 54, pp. 251-267.

Mar, J. W.; and Lin, K. Y. (1977): "Fracture Mechanics Correlation for Tensile Failure of Filamentary Composites with Holes." *Journal of Aircraft*, Vol. 14, No. 7, pp. 703-704.

Mazars, J.; and Bazant, Z. P., Eds. (1988): "Strain Localization and Size Effects due to Cracking and Damage." *Paper presented at the Proceedings of France-U.S. Workshop* held at E. N. S de Cachan, University of Paris, Elsevier, London, U.K., September 1988.

Mi, Y.; and Crisfield, M. A. (1996): *Analytical Derivation of Load/Displacement Relationships for Mixed-Mode Delamination Comparison with Finite Element Results*. Department of Aeronautics, London, Imperial College.

Moran, B.; and Shih, C. F. (1987): "A General Treatment of Crack Tip Contour Integrals." *International Journal of Fracture*, Vol. 35, pp. 295-310.

Mukherjee, Y. X.; Gulrajani, S. N.; Mukherjee, S.; and Netravali, A. N. (1994): "A Numerical and Experimental Study of Delaminated Layered Composites." *Journal of Composite Materials*, Vol. 28, No. 9, pp. 837-870.

Nahan, M.; and Kennedy, T. (2000): "A Nonlocal Damage Theory for Laminated Plat with Application to Aircraft Damage Tolerance." *Journal of Reinforced Plastics and Composites*, Vol. 19, No. 5, pp. 354-363.

Nuismer, R. J.; and Whitney, J. M. (1975): "Uniaxial Failure of Composite Laminate Containing Stress Concentrations." *Fracture Mechanics of Composites, ASTM STP 593*, American Society for Testing and Materials, 1975, pp. 117-142.

O'Brien, T. K. (1982): "Characterization of Delamination Onset and Growth in a Composite Laminate." *Damage in Composite Materials, ASTM STP 775*, K. L. Reifsnider, Ed., American Society for Testing and Materials, 1982, pp. 140-167.

O'Brien, T. K.; Raju, I. S.; and Garber, D. P. (1986): "Residual Thermal and Moisture Influences on the Strain Energy Release Rate Analysis of Edge Delamination." *Journal of Composite Technology and Research*, pp. 37-47.

Poe, C. C., Jr. (1983): "A Unifying Strain Criterion for Fracture of Fibrous Composite Laminates." *Engineering Fracture Mechanics*, Vol. 17, No. 2, pp. 153-171.

Puck, A.; and Schürmann, H. (1998): "Failure Analysis of FRP Laminates by Means of Physically Based Phenomenological Models." *Composite Science and Technology*, Vol. 58, Issue 7, July 1998, pp. 1045–1067.

Rhoades, M. D.; Williams, J. G.; and Starnes, J. H., Jr. (1978): "Effect of Impact Damage on the Compression Strength of Filamentary-Composite Hat-Stiffened Panels." *Society for the Advancement of Material and Process Engineering*, Vol. 23, May 1978.

Rybicki, E. F.; Kanninen, M. F. (1977): "A Finite Element Calculation of Stress Intensity Factors by a Modified Crack Closure Integral." *Engineering Fracture Mechanics*, Vol. 9, No. 4, pp. 931-938.

Riks, E. (1979): "An Incremental Approach to the Solution of Snapping and Buckling Problems." *International Journal of Solid Structures*, Vol. 15, pp. 529-551.

Russell, A. J.; and Street, K. N. (1989): "Predicting Interlaminar Crack Growth Rates in Compressively Loaded Laminates." *Composite Materials: Fatigue and Fracture (Second Volume), ASTM STP 1012*, P. A. Lagace, Ed., American Society for Testing and Materials, Philadelphia, pp. 162-178.

Schapery, R. A.; and Davidson, B. D. (1990): "Prediction of Energy Release Rate for Mixed-Mode Delamination Using Classical Plate Theory." *Applied Mechanics Reviews*, Vol. 43, No. 5, pp. S281-S287.

Shih, C. F.; Moran, B.; and Nakamura, T. (1986): "Energy Release Rate Along a Three-Dimensional Crack Front in a Thermally Stressed Body." *International Journal of Fracture*, Vol. 30, pp. 79-102.

Shyprykevich, P. (1997): "Damage Tolerance of Composite Aircraft Structures: Analysis and Certification." *Paper presented at the Proceedings of ICCM-11*, July 1997, Australia. Vol. 1, pp. 552-561.

Spearing, S. M.; Beaumont, P. W. R.; and Ashby, M. F. (1992): "Fatigue Damage Mechanics of Composite Materials. II: A Damage Growth Model." *Composites Science and Technology*, Vol. 44, pp. 169-177.

Tratt, M. D. (1991): "Analysis of Delamination Growth in Compressively Loaded Composite Laminates." *Composite Materials: Fatigue and Fracture (Third Volume), ASTM STP 1110*, T. K. O'Brien, Ed., American Society for Testing and Materials, Philadelphia, 1991, pp. 359-372.

Vaidya, R. S.; Klug, J. C.; and Sun, C. T. (1998): "Effect of Ply Thickness on Fracture of Notched Composite Laminates." *AIAA Journal*, Vol. 36, No. 1, pp. 81-93.

Waddoups, M. E.; Eisenmann, J. R.; and Kaminski, B. E. (1971): "Macroscopic Fracture Mechanics of Advanced Composite Materials." *Journal of Composite Materials*, Vol. 5, October 1971, pp. 446-455.

Whitcomb, J. D. (1992): "Analysis of a Laminate with a Postbuckled Embedded Delamination, Including Contact Effects." *Journal of Composite Materials*, Vol. 26, No. 10, pp. 1523-1535.

Whitcomb, J. D. (1981): "Finite Element Analysis of Instability Related Delamination Growth." *Journal of Composite Materials*, Vol. 15, No. 9, pp. 403-426.

Whitcomb, J. D. (1990): "Mechanics of Instability-Related Delamination Growth," *Composite Materials: Testing and Design (Ninth Volume), ASTM STP 1059*, S. P. Garbo, Ed., American Society for Testing and Materials, Philadelphia, 1990, pp. 215-230.

Whitcomb, J. D. (1989): "Predicted and Observed Effects of Stacking Sequence and Delamination Size on Instability Related Delamination Growth." *Journal of Composites Technology and Research*, Vol. 11, No. 3, pp. 94-98.

Whitcomb, J. D. (1989): "Three-Dimensional Analysis of a Postbuckled Embedded Delamination." *Journal of Composite Materials*, Vol. 23, No. 9, pp. 862-889.

Whitcomb, J. D. (1989): "Comparison of Full 3-D, Thin-Film 3-D, and Thin-Film Plate Analyses of a Postbuckled Embedded Delamination." *Journal of Composite Technology and Research*, Vol. 11, No. 4, pp. 154-157.

Whitehead, R. S.; and Dee, R. B. (1983): "A Building Block Approach to Design Verification Testing of Primary Composite Structures." *Paper presented at the Proceedings of the 24th AIAA/ASME/AHS SDM Conference*.

Whitney, J. M.; and Nuismer, R. J. (1974): "Stress Fracture Criteria for Laminated Composites Containing Stress Concentrations." *Journal of Composite Materials*, Vol. 8, pp. 253-265.

Wu, H. T.; and Chang, F. K. (1989): "Transient Dynamic Analysis of Laminated Composite Plates Subjected to Transverse Impact." *Journal of Computers and Structures*, Vol. 31, pp. 453-466.

Yin, W. L. (1988): "The Effects of Laminated Structure on Delamination Buckling and Growth." *Journal of Composite Materials*, Vol. 22, pp. 502-517.

Zweben, C. (1973): "Fracture Mechanics and Composite Materials: A Critical Analysis." *Analysis of Test Methods for High Modulus Fibers and Composites, ASTM STP 521*, American Society for Testing and Materials, 1973, pp. 65-97.

Appendix A: ADAM-C Computer Code

A-1   ADAM-C Methodology

Aerospace developed a computer software, ADAM-C, in the mid-1980s (Ref. A.1) with the intention to predict residual strength for composite structures containing defects such as cuts, holes and delaminations. A detailed discussions of the models incorporated in ADAM-C are presented as follows:

Four basic failure modes determine the damage tolerance of composite materials: matrix cracking, fiber breakage, interfacial debonding, and interply delamination. All failure modes may be traced to localized flaws and defects that are introduced into the material through many potential sources, e.g., manufacturing and assembly procedures, impact damage, and hygrothermal environment.

The literature survey results indicate that the growth behavior and failure modes of all flaws are strongly dependent on such parameters as laminate strength, stiffness, ply orientation, stacking sequence, fiber volume fractions, load application, and environmental conditions. These parameters must be integrated into a consistent methodology before full exploitation of composite materials can be achieved with confidence.

A survey of aircraft industry practices revealed that the damage tolerance capability of critical composite hardware is often demonstrated by conducting safe-life tests on coupons, or small structural components, with preconceived and prefabricated flaws. This approach, however, may require an extensive test program when several potential laminates with different layups are being considered. Inasmuch as each laminate has unique properties, the test results for one layup are not directly applicable to the other candidate laminates.

Several investigators have developed analytical models that predict laminate response to a variety of damage types common to aircraft structures. The environmental and structural requirements of aircraft and spacecraft, however, are quite different. Spacecraft components generally tend to be more highly stressed than their aircraft counterparts; hence, the applicability of these models to space hardware needs further evaluation.

It is common practice in the spacecraft industry to perform acceptance proof tests on all primary composite structures, an approach that is both costly and time consuming. In some cases, such as the cryogenic temperature environment, only limited testing is possible because of the difficulty in simulating environmental conditions. Thus, the need for a reliable damage tolerance methodology that could minimize the number of these expensive tests is apparent.

As shown in Table A-1 survey results have yielded two broad categories that encompass most combinations of flaw type and loading condition. The category I models concentrate on through-the-thickness flaws such as holes, cutouts, and cracks, whereas the category II models are restricted to delamination, which is the predominant failure mode unique to composite structures.

Table A-1. Summary of Literature Survey Results

Category	Method/Model	Description	Developer	Ref. No.
I	Inherent flaw model	Uses linear fracture mechanics parameter for predicting residual strength of cracked body.	Waddoup *et al.*, 1971	A. 2
	Point stress failure model	Uses laminate theory to calculate stress concentration factor for predicting residual strength of holes and cutouts.	Whitney and Nuismer, 1974	A. 3
	Finite element method	Uses finite element analysis for predicting residual strength of laminate containing cracks.	Wang, 1974	A. 4
	Notched fracture stress model	Relates fracture stress to composite fracture toughness; for cracked body residual strength calculation.	Lin, 1977	A. 5
	Strain energy density factor method	Uses strain energy density factor to predict residual strength of cracked composite structures.	Sih, 1978	A. 6
	Strain failure criterion	Relates critical fiber strain to a general fracture toughness parameter; for cracked body residual strength prediction.	Poe and Sova, 1980	A. 7
	Damage zone model	Uses Dugdale approach to represent damage; for predicting strength of holes, cutouts, and cracks.	Backlund, 1981	A. 8
II	Finite element method	Uses 3-D finite element to determine interlaminar stresses; for delamination growth prediction.	Ratwani, *et al.*, 1979	A. 9
	1-D thin-film model	Uses laminate buckling theory for through-the-thickness delamination prediction.	Chai *et al.*, 1981	A.10
	Edge-delamination model	Uses rule-of-mixture for onset of edge delamination prediction.	O'Brien, 1982	A.11
	2-D thin-film model	Uses laminate buckling theory for embedded delamination prediction.	Shyprykevich *et al.*, 1984	A.12

The analytical methods in each category of Table A-1 have been evaluated. The advantages and disadvantages of each approach are summarized in Table A-2. In general, none of the existing models provides reliable results at reasonable cost. This is particularly true for category II models. The finite element approach is ideally suited for analyzing composite structures that contain delaminations, but computer costs are often prohibitive.

The following selection criteria were established to distinguish which of the available models should form the basis of the required methodology:

Models shall be generic in nature.

- Lengthy calculations shall be avoided.
- Models shall provide predictions with adequate accuracy and conservatism for space hardware application.
- Models shall use the existing composite material database.
- Methodology shall be readily adaptable to existing Aerospace computer systems.

On the basis of these criteria, the IFM developed by Waddoups *et al*. (Ref. A.2) was selected for use in predicting the residual strength of cracked composite laminates. The PSM developed by Whitney and Nuismer (Ref. A.3) was selected for use with laminates containing holes and cutouts. These models require simple calculations and have the advantage of an extensive test database for the more common material systems such as fiberglass/epoxy and Gr/Ep.

For composites with through-the-width or embedded delaminations are characterized by the thin film model of Chai *et al*.(Ref. A.10). For delaminations at free edges, the edge delamination model of O'Brien (Ref. A.11) was selected. These two models have two common features: they avoid lengthy finite element calculations, and they use the strain-energy release rate *G* to characterize delamination growth.

The previously mentioned models form the basis for an Aerospace-developed damage tolerance software package called ADAM-C, which was the primary product of the Aerospace Sponsored R program. ADAM-C architecture is illustrated in Figure A-1. Material properties, laminate, and flaw geometries are input into preprocessor modules (GENLAM and RANKHO), which generate the laminate constitutive relations and the stress concentration factors for certain flaw shapes. These codes were acquired from the Air Force Materials Laboratory and linked to the remaining modules such that unnecessary programming effort was avoided.
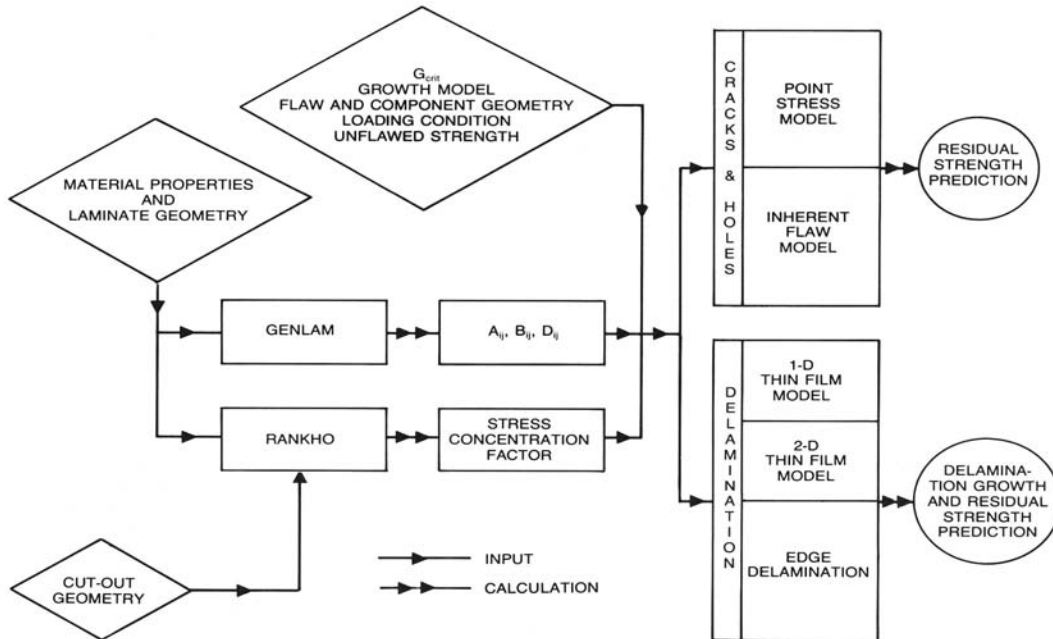

Figure A-1. ADAM-C methodology.

Once the stiffness matrices and stress concentration factors have been calculated, control is transferred to the appropriate module, depending on the type of flaw selected. The program addresses holes, cracks, and elliptical cutouts. In each case, a residual strength prediction is the final product. The safe-life and residual buckling strength of a composite laminate that has a delamination may also be obtained by running ADAM-C.
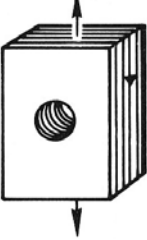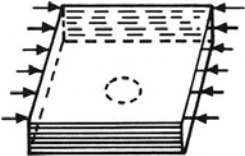
ADAM-C is available on both the VAX and IBM-PC systems. Each model is independent and modular, thus facilitating any future enhancements. The program is menu-driven and user-friendly. The material database contains many commonly used graphite and glass/epoxy systems, but this list can be updated by users at any time by simply running an interactive program called MATRPR (Ref. A.13). Thus, any new material systems can be quickly accommodated.

The following list summarizes the current ADAM-C output:

Laminated plate theory stiffness matrices

- Stress concentration factors due to holes or cutouts at arbitrary angles of inclination;
- Static residual strength of cracked panels;
- Static residual strength of panels with holes and cutouts;
- 1-D and 2-D delamination growth with residual buckling strength;
- Edge delamination growth and residual strength.

Table A-2. Assessment of Analytical Methods

Loading and Damage Type	Analytical Method	Advantages	Disadvantages
	Point stress failure model	Simple calculation, adequate database	Stress intensity zone size is independent of hole sizes
	Notched fracture stress model	Simple calculation	Extensive testing, limited database
	Damage zone model	Provides more accurate predictions	Length calculation, not enough database
	Inherent flaw model	Simple calculation, adequate database	Characteristic zone size is independent of crack sizes
	Strain energy density factor method	Provides more accurate predictions	Very limited database
	Finite element approach	Provides adequate accuracy for complex geometries	Length calculation
	Damage zone model	Provides more accurate predictions	Length calculation
	Finite element method	Provides adequate accuracy for complex geometries	Length calculation involved
	Edge delamination model	Simple calculation	Limited application
	Finite element method	Provides adequate accuracy for complex geometries	Length calculation involved
	Thin-film 1-D model	Simple calculation	Limited application
	Finite element method	Provides adequate accuracy for complex geometries	Length calculation involved
	Thin-film 2-D delamination model	Simple calculation	Prediction accuracy needs to be improved

Certain refinements were incorporated into the selected ADAM-C modules. In the PSM, for example, a finite width correction factor that accounts for the interaction between the hole and the free edge of the plate was added. The importance of the correction function is illustrated in Figure A-2. Experimental residual strengths for a Gr/Ep laminate are compared with theoretical values obtained for different combinations of damage zone sizes and finite width correction factors. It is apparent that only the curve that represents the combined effect of the damage zone and the finite width correction factor correlates most closely with the experimental data. Thus, the incorporation of an appropriate correction function is vital to the residual strength prediction of the model.
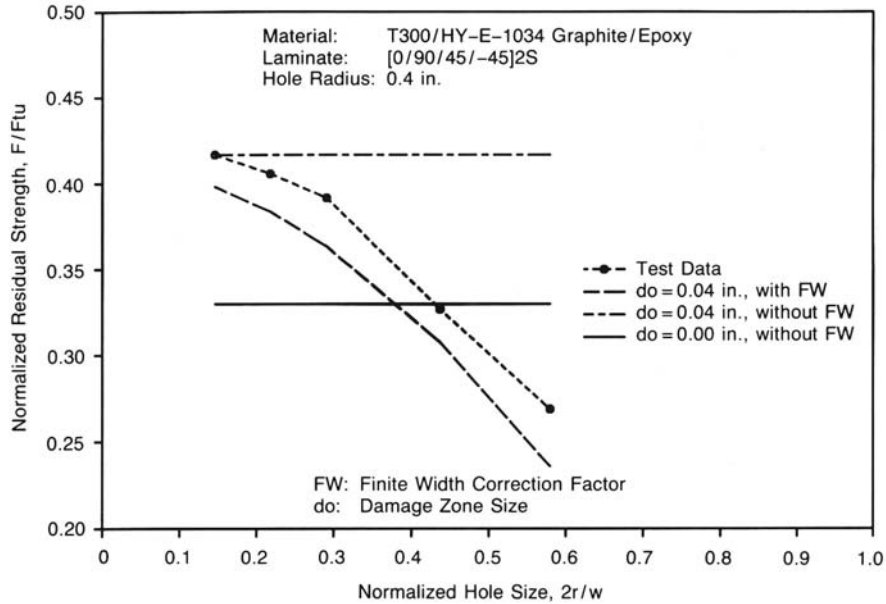
Figure A-2. Point stress model parametric study. From Reference A.8.

The IFM is based on the linear elastic fracture mechanics model for metals containing cracks, but was modified to include the damage zone size. This expression depends on such parameters as the crack length, damage zone size, unnotched laminate tensile strength, finite width correction function, and most importantly, the laminate fracture toughness K_q.

Unlike metals, there are no standards for the definition and experimental determination of K_q for composite materials, i.e., the fracture toughness is open to interpretation. Therefore, the calculation of K_q by analytical techniques is an important topic, as we have already established that experimental determination of the important parameters of all candidate laminates in a given structure is not economically feasible. At the present time, our methodology uses two approaches to calculate the fracture toughness because no single model adequately covers the wide range of laminate behavior. The first approach assumes a simple relationship between the fracture toughness and the unnotched tensile property of a laminate, i.e., K_q, is one-half of the unnotched strength (in English units). The second approach uses an analytical prediction of K_q proposed by Poe (Ref. A.14), who attempted to develop a general fracture toughness parameter that depends on the lamination constants as well as certain assumptions about the importance of load carrying plies. For conciseness, the first K_q approximation is abbreviated as IFM-A and the second as IFM-B.

Results of the delamination studies indicate that the strain-energy release rate G is a preferred parameter from the standpoint of delamination growth. An approach based on G avoids the necessity and expense of calculating stress distributions near flaw boundaries. Often, these stresses become singular and thus of no practical use in predicting stable delamination growth.

Delamination growth requires work that may be supplied by external forces during delamination or by the decrease in the strain energy of the system or both. For thin film models, energy is supplied by the change in strain energy resulting from delamination extension. If the energy loss is greater than the work required to create a unit area of delaminated composite, growth will occur. The delamination growth is assumed to follow a power law based on the strain-energy release rate raised to some exponent. This approach has been incorporated into ADAM-C.

58

In order to substantiate the predictive capabilities of the ADAM-C program, an extensive correlation study was performed. Test data found in the open literature were correlated with predictions by means of the PSM and IFM modules. Although appreciable data are available on laminates with holes, cutouts, and cracks, information about delamination growth under cyclic loads is very sparse. Our future experimental work will seek to fill this data gap, and correlations will be made with the ADAM-C delamination growth modules.

In Figures A-3 and A-4, the predictive accuracy of the PSM and IFM is correlated with some typical experimental data found in the literature. All of the data, both holes and cracks, are compared with three models: PSM, IFM-A, and IFM-B. The purpose of this approach is to investigate the extent to which the hole and crack models are interchangeable and thus develop some insight into the nature of these flaws in composite structures. Briefly, the results indicate that, for cracked structures, the IFM-B approach is preferred, whereas for composites with holes, the PSM provides the desired conservatism. Laminated structures have such a wide range of behavior that no single model can be completely endorsed, but it is believed that these models have the potential to be extended to more general types of loading conditions.
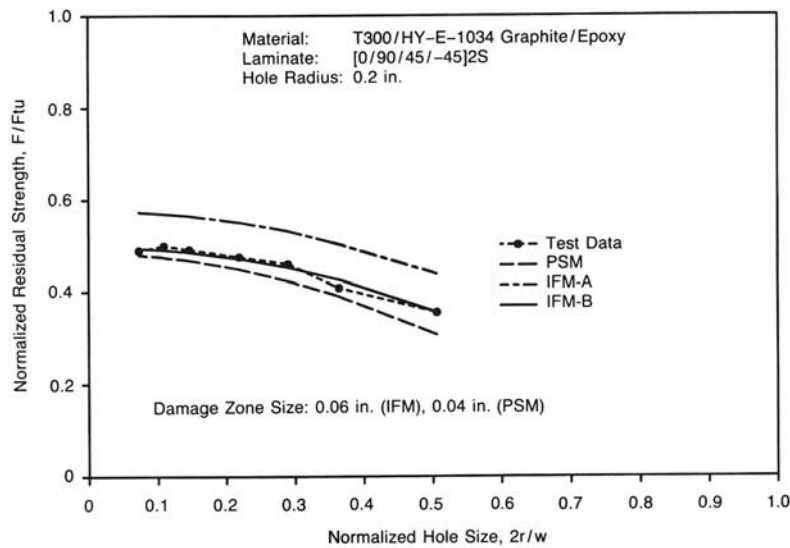

Figure A-3. Hole data correlation. From Reference A.8.

The correlation between the PSM and typical data for laminates with holes is shown in Figure A-3. The selected database represents a wide range of laminate configurations and sources within the open literature. It should be noted that both axes have been normalized with respect to unflawed laminate strengths such that all data can be plotted as percentages of unity. Perfect correlation between theory and experiment is achieved along the darkened line with a slope of 1. The data points below the curve indicated conservative predictions. In general, the PSM provides adequately conservative predictions over most hole sizes of practical interest.

In Figure A-4, IFM-A and B are correlated to some of the existing cracked laminate data. Again, the data have been normalized and the six symbols represent the three data sources and their comparisons with the two approaches for determining K. The scatter in the residual strength predictions is greater for cracks than for holes.
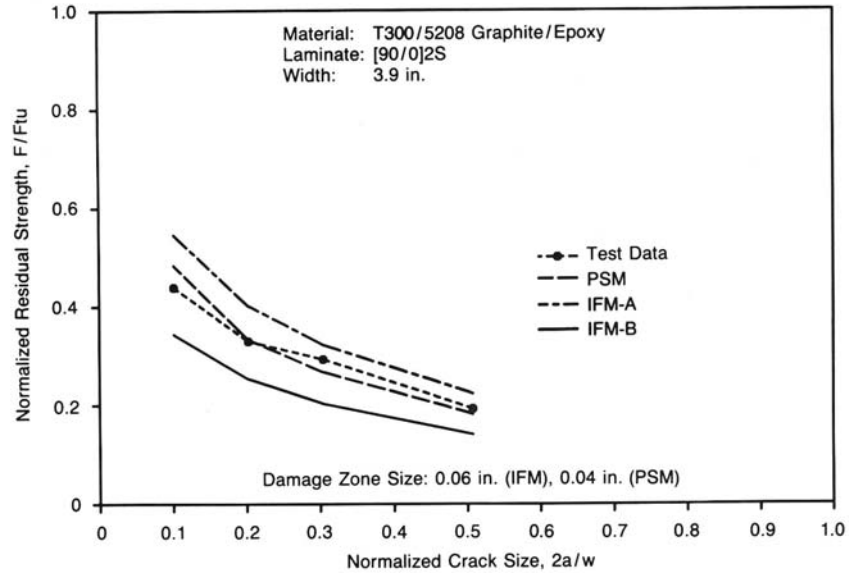
Figure A-4. Crack data correlation. From Reference A.13.

Further insight into each model is provided in Figures A-5 and A-6, where frequency of occurrence is plotted versus the ratio of the predicted-to-experimental residual strength values for the PSM and IFM calculations. A perfect model would always duplicate an experimental result, and hence the strength ratio (X-axis) would always be 1; there would be no distribution. Theoretical models are seldom perfect, however, and a reasonable basis for comparison is to cross-plot all distributions on the same figure. A good model should peak near X = 1 and should have a low-frequency response in the unconservative regime, i.e., X > 1.
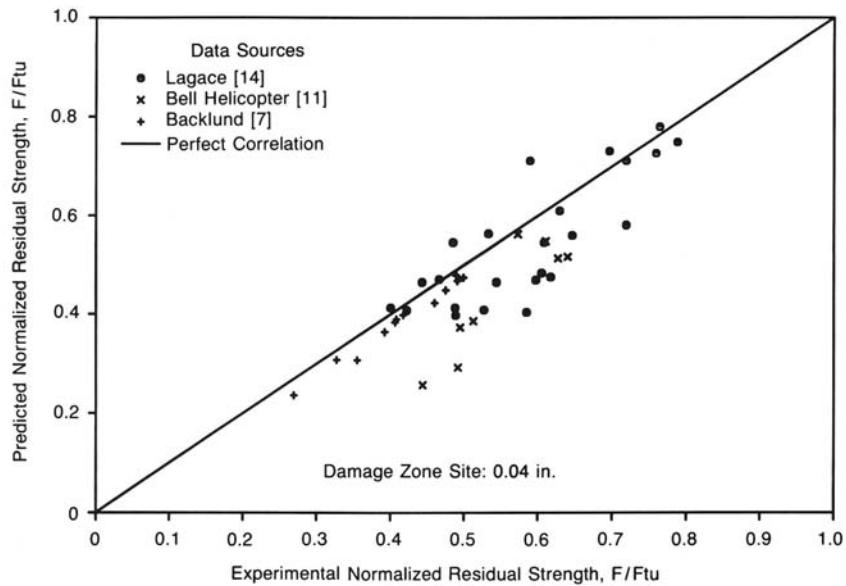

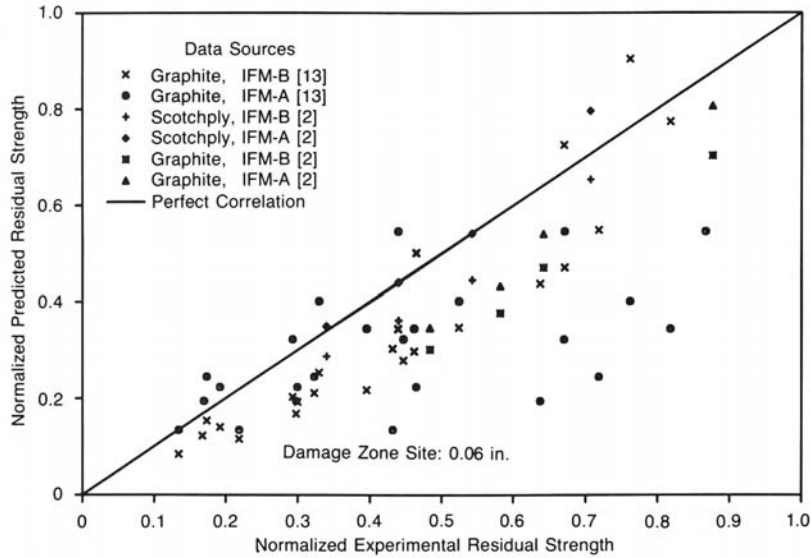Figure A-5. Point stress model correlation for plates with holes.

Figure A-6. IFM correlation for plates with cracks. The data points below the curve indicate conservative prediction.

In Figure A-7, the peak PSM response is in the range of 0.9 to 1.1. The IFM models also perform well, but are more frequently unconservative than is the PSM. Therefore, these findings indicate that the PSM is the preferred ADAM-C module for analyzing laminated structures containing holes.
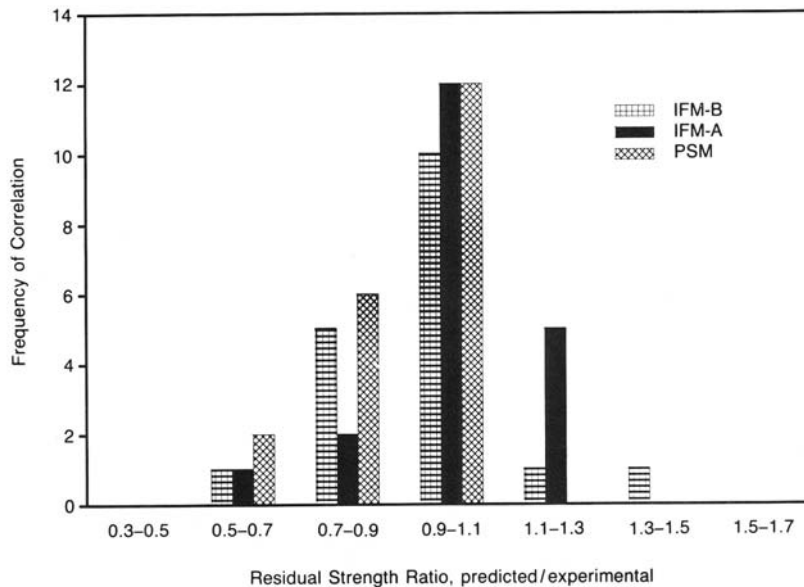

Figure A-7. Frequency correlation (hole data). Less than 1.0 indicates conservative prediction.

In Figure A-8, the three models are cross-plotted with respect to the cracked laminate data. The PSM is slightly unconservative. IFM-A yields a relatively flat response with both very conservative and unconservative answers. IFM-B results are sometimes too conservative but seldom unconservative. The broad scatter indicated in Figure A-8 suggests that it is difficult for a single approach to cover the residual strength variations of cracked laminate data.
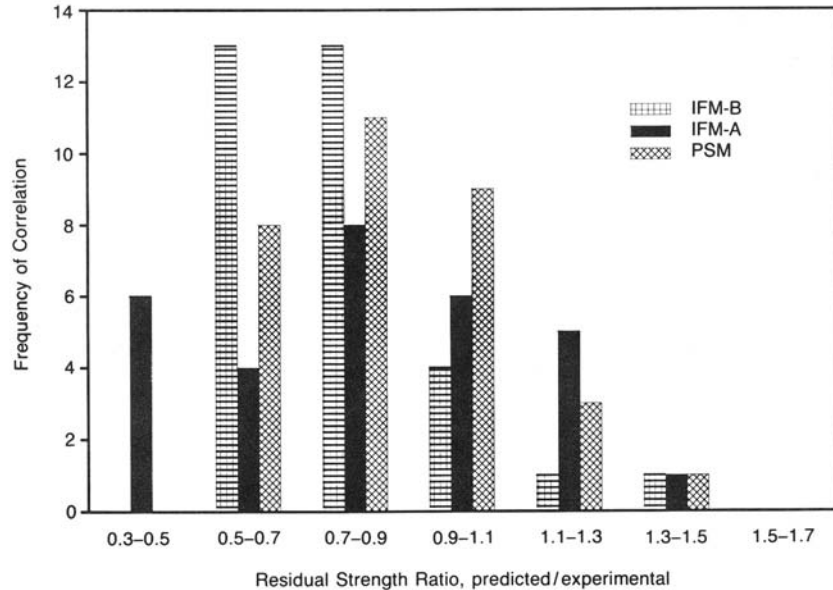
61

Figure A-8. Frequency correlation (crack data). Less than 1.0 indicates conservative prediction.

In summary, this project addresses the need for a reliable and cost-effective damage tolerance methodology for composite spacecraft structures. During the project, a literature survey was conducted, model selection and enhancements were made, software was developed, and comparisons were made between experimental and analytical results. These tasks resulted in the development and implementation of the ADAM-C code. This work is the first step in an effort to characterize the damage tolerance capabilities of composite structures in space environment.

Now that the basic methodology is in place, the process of final refinement begins. As stated earlier, the aircraft and aerospace structural requirements can be quite different. Generally speaking, aircraft structures operate in a low-stress, high-cycle environment, whereas the reverse is often true for spacecraft components. The latter condition is more severe, but the existing test data were generated for aircraft applications in the low-cycle, high-stress regime. Therefore, an accurate correlation and refinement of ADAM-C will require further experimental testing under conditions relevant to spacecraft structures.

A damage tolerance testing program is planned with specimens to be constructed from commonly used composite material systems. Flaws and defects will be prefabricated in the specimens to represent a variety of damage conditions. The results of these tests will be correlated with ADAM-C, and appropriate refinements to the methodology will be incorporated. With this approach, the goal of developing reliable damage tolerance analysis techniques with respect to spacecraft structures will be achieved.

A-2   References

A.1   Chang, J. B.; Rogers, J. C.; and Kamrath, A. R. (1985): *Damage Tolerance Analysis Methodology for Composite Structures*. From Aerospace Sponsored Research (ASR) Summary Report, Aerospace Report No. ATR-85(8498)-2, The Aerospace Corporation.

A.2   Waddoups, M. E.; Eisenmann, J. R.; and Kaminski, B. E. (1971): "Macroscopic Fracture Mechanics of Advanced Composite Materials." *Journal of Composite Materials*, Vol. 5, October 1971, pp. 446-455.

A.3   Whitney, J. M.; and Nuismer, R. J. (1974): "Stress Fracture Criteria for Laminated Composites Containing Stress Concentrations." *Journal of Composite Materials*, Vol. 8, pp. 253-265.

A.4   Wang, S. S. (1974): *Fracture of Graphite Fiber Reinforced Composites*. Unpublished Sc. D. Thesis, 1974, Boston: Massachusetts Institute of Technology.

A.5   Lin, K. Y. (1977): *Fracture of Filamentary Composite Materials*, Ph. D. Thesis, 1977, Massachusetts Institute of Technology.

A.6   Sih, G. C. (1978): "Mechanics of Fracture: Linear Response." *Paper presented at the Proceedings of the First International Conference on Numerical Methods in Fracture Mechanics*, Swansea, United Kingdom.

A.7   Poe, C. C.; and Sova, J. A. (1980): *Fracture Toughness of Boron/Aluminum Laminates with Various Proportions of 0 and +/-45 Degree Plies*. NASA TP-1707, November 1980.

A.8   Backlund, J. (1981): "Fracture Analysis of Notched Composites." *Computational Structures.* Vol. 13.

A.9   Ratwani, M. M.; and Kan. H. P. (1979): *Compression Fatigue Analysis of Fiber Composites.* Report No. NADC-78049-60, Warminster, Pennsylvania: Naval Air Development Center.

A.10   Chai, H.; Babcock, C. D.; and Knause, W. G. (1981): "One Dimensional Modeling of Failure in Laminated Plates by Delamination Buckling." *International Journal of Solids and Structures*, Vol. 17, No. 1069.

A.11   O'Brien, T. K. (1982): "Characterization of Delamination Onset and Growth in a Composite Laminate." Damage in Composite materials, ASTM STP 775, K. L. Reifsnider, Ed., American Society for Testing and Materials, 1982, pp. 140-167.

A.12   Shyprykevich, P.; Flanagan, G.; and Sharp, D. (1984): *Damage Tolerance of Composites, Bell Helicopter Report* No. 699-089-088. Ft. Worth, Texas.

A.13   Tsai, S. (1985): *Composites Design – 1985*. Think Composites, Dayton, Ohio.

A.14   Poe, C. C. (1984): *Fracture Toughness of Fibrous Composite Materials*. NASA TP-2370, November 1984.

Appendix B: PFA Code for Composites

The research and development for the PFA of composites at Aerospace has integrated and extended the PFA developed at NASA LaRC in the late 1990s and early 2000s (Ref. B-1). The PFA is implemented in a software tool that integrates with existing commercial FEM software. The tool simulates the growth and propagation of failure modes in a composite and it is constantly adapted for new classes of problems and extended to incorporate new physics. The key features of the PFA code include: (1) Delamination simulation by using interface elements; (2) Prediction of in-plane and out-of-plane nonlinear shear damage; (3) Prediction of matrix-cracks based on a modified version of Puck's criterion (Ref. B-2, B-3); and (4) A fiber failure criterion based on the work of Chang (Ref. B-4). The PFA code utilizes concepts from damage mechanics to degrade the material properties of the composite appropriately. The code also handles contact in the event of delamination closure following growth. Similar to ADAM-C, the code was developed to be as generic as possible and applicable to a large range of problems with adequate accuracy and conservatism. The accuracy of the code, however, relies on developing a complete mechanical, strength, and fracture database that can be used directly as input to the code. The next subsections will discuss the progressive failure philosophy, the damage models in the PFA code, the characterization testing that is required to define the damage model, and validation of the PFA code. The PFA code is also demonstrated for few examples pertaining pressure vessels.

B-1   Progressive Failure Philosophy

Refer to Figure B-1 for the following discussion on progressive damage philosophy and its relation to validation. The goal is to develop a reliable and practical analytical tool capable of simulating the response of composite joints and predicting their structural margins. This effort can be broadly divided into three sections: coupon testing, component testing and analysis. Coupon testing is essential in the damage modeling of composites since it is used to determine material properties, fracture properties and failure criteria. Coupon tests can also give insight into the progression of damage and response of the structure based upon observations and measurements. From component testing, the second leg in the model development, the structure can be evaluated on a macro-scale to evaluate margins.

However, insight into the progression of failure is more difficult since failure may be unstable and the testing cost is considerably higher for flight components than it is for coupons. Finally, analysis is conducted to validate the material model. Since the coupon tests are simpler than the flight component, it follows that the analytical model will first be used to predict the response of the coupon tests. A FEM is created to reflect the experimental set-up; material properties are carried over from coupon testing or found in the literature, as appropriate, and care is taken to ensure that the loads and boundary conditions reflect the actual test configuration. The next step in the process is to compare predictions with test observations – including the measured strain, delamination formation and growth, shear damage, matrix cracking or fiber failure – in order to correlate the relevant material parameters. This is especially important in the modeling of damage, whereby friction coefficients and even strength the finite element results and the test data, the model can be used to analyze a subscale structural component and compared to experimental results. If large differences exist between the finite element results and the test data, then the model needs to be re-examined. Typically, the material, boundary conditions, and

failure criteria would be revised at the coupon level. This refinement continues until the subscale analysis shows good agreement with the subscale test data. The analytical tool is considered to be reliable once the model can accurately predict the response of both the coupon and component tests.

Figure B-1 illustrates the modeling technique and adjust for specific applications. Both coupon and component testing are required, along with corresponding finite element analyses.
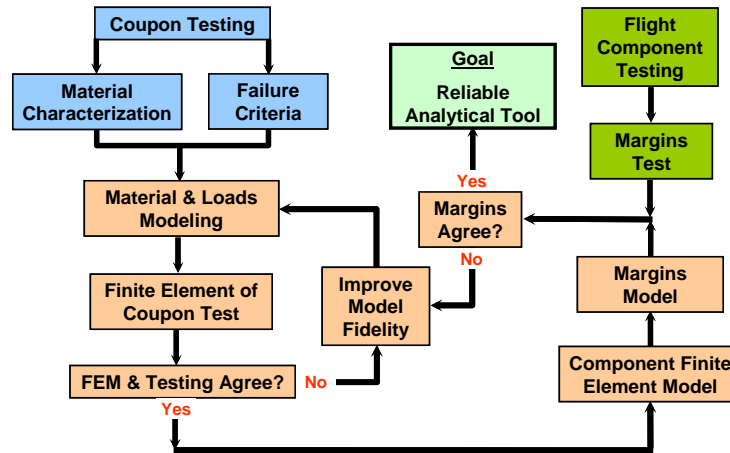

Figure B-1. Modeling flowchart.

B-2   Progressive Failure Methodology

A progressive failure methodology is developed that is an extension of the methodologies found in Pifko and Kushner (Ref. B-5) and Sleight *et al*. (Ref. B-6]). The methodology requires a nonlinear solver to establish equilibrium because both geometric and material nonlinearity are considered. The geometric nonlinearity is due to large strain and large rotation kinematics. The nonlinear material behavior is due to the degradation of the material properties of the plies and the material in between the plies to simulate intralaminar and interlaminar damage mechanisms. An incremental iterative approach is adopted for the nonlinear finite element analysis, and the Newton-Raphson method is used to trace the loading path of the structure with a displacement-control analysis. A line search algorithm is only activated to provide an initial approximation to the Newton-Raphson method, or to minimize a large residual force. The progressive failure methodology complies with two requirements: (i) optimum size load steps to achieve solution convergence while representing accurately local load redistribution, and (ii) a fine mesh in regions that undergo material degradation to represent proper stress gradients at the boundary of the damaged zones.

Damage parameters used in the analysis can be divided in two parts: one relates to the failure prediction at the lamina level, and second relates to the prediction of damage initiation at the laminate level, which can then progress and lead to ultimate failure. The progressive damage implementation is depicted in Figure B-2. The damage evolution equations are solved at the Gaussian integration points within each material ply, thus explicitly accounting for damage variation through the thickness and in the plane of each material ply. The flowchart is color-coded as follows: Green represents the stage at which the user interfaces directly with the finite element software ABAQUS™ (Ref. B-7); Blue represents the user material subroutine UMAT; and Peach represents the ABAQUS™ standard nonlinear incremental procedure. First, the

ABAQUS™ input file needs to be prepared in a typical fashion with additional parameters relating to the strength and fracture of the composite. Then, the analysis is initiated by applying an initial load to the FEM. A converged solution must be obtained because the structure is no longer in equilibrium due to differences between the internal loads and the external loads. The stress, strain, and stiffness matrix (Jacobian) are updated. At each load step, failure criteria are applied at each Gaussian point. If failure occurs, the damage state is obtained and the components of the stiffness matrix are reduced correspondingly. The components are reduced to a small value instead of zero, because a reduction to zero leads to numerical difficulties in the nonlinear procedure. Following the application of the damage tensor, the modified Newton-Raphson nonlinear iterative procedure is conducted to achieve equilibrium prior to the next load step.
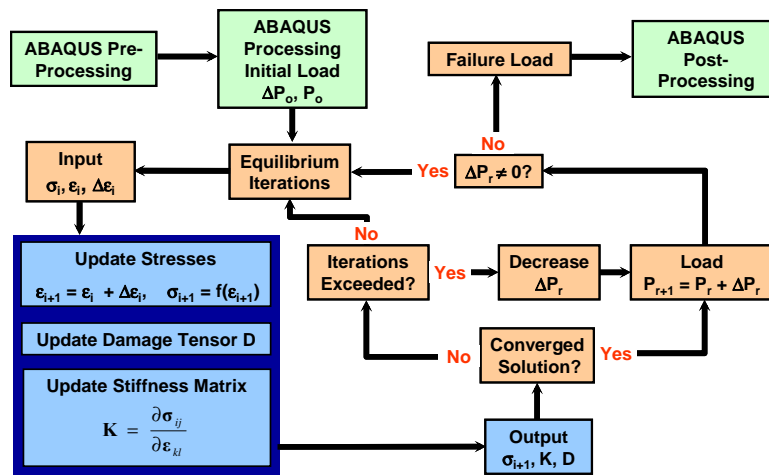
Figure B-2. Flowchart of the progressive damage implementation using ABAQUS™.

The progressive failure methodology was implemented in a user subroutine package compatible with ABAQUS™ finite element code, Figure B-3, because it has the ability to solve large models, has advanced material models and contact definitions, and it has a built-in post processing software.
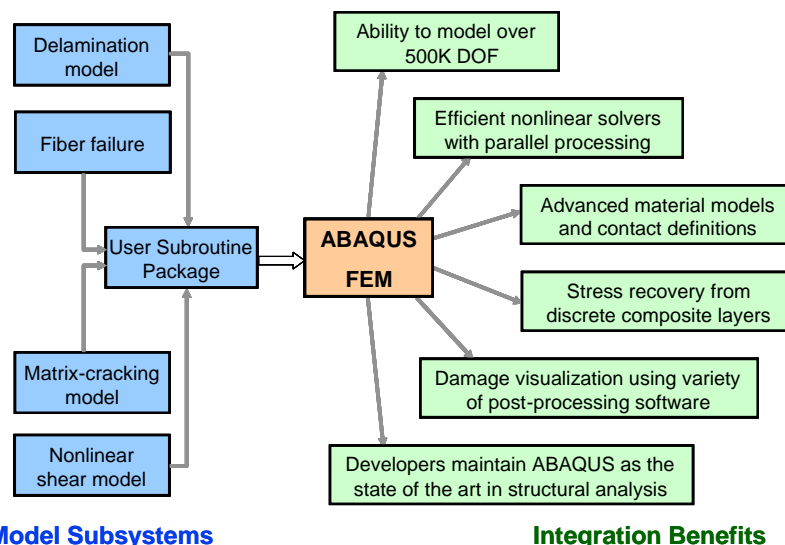
Figure B.3. Failure modes integrated into a user subroutine package.

B-3   Failure Modes and Degradation of Mechanical Properties in PFA

A brief description of following failure modes considered in the progressive failure methodology is presented: (1) Delamination; (2) In-plane and out-of-plane nonlinear shear damage; (3) Matrix-cracking; and (4) Fiber failure.

<u>Delamination</u>

A new computational fracture mechanics technology has been developed in recent years (Refs. B-8 and B-9) for the prediction of discrete delaminations in composite materials via the use of interface elements coupled with cohesive zone models. The interface element formulation consists of a nonlinear distribution of continuous springs, Figure B-4, with a cohesive-decohesion constitutive law that satisfies a strength based failure criterion and a fracture-based criterion. The interfacial constitutive law for the formulation of the interface element governs the deformations of these interface layers and determines whether delamination growth occurs or not. This unified strength-fracture approach allows the prediction of the initiation and growth of delamination. Interface elements are positioned at interfaces where the delamination may potentially grow. The prediction of multiple delaminations and non-self similar delamination growth is then obtained depending upon the natural response of the structure being analyzed.
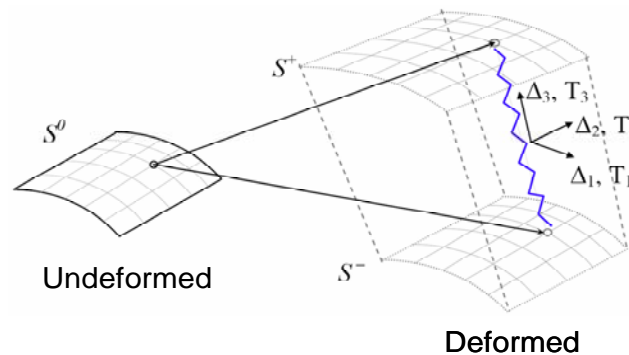

Figure B-4. Interface element consists of a continuous distribution of breakable springs.

Prior versions to ABAQUS™ 6.5-6 did not have the interface finite element formulation to predict delamination, and thus the element was previously developed and implemented in ABAQUS™ using a user element subroutine (UEL). The drawback with the UEL approach is that ABAQUS™ does not support visualization of the damage distribution at the interface element level, so the shape and size of the delamination is not known, except for separations that are visible from the deformation plot. To overcome this visualization difficulty, an effort was undertaken to predict delamination using standard, but very thin, solid brick elements (C3D8I) available in the ABAQUS™ element library. The traction-separation law normally accompanying interface elements was transformed to a stress-strain law for an interphasic element of very small thickness and implemented in ABAQUS™ with a user material subroutine UMAT. Severe convergence issues surfaced occasionally, mainly triggered by excessive element distortion. The element distortion problem occurred more often under the initiation and growth of shear delamination. Moreover, the formulation of the C3D8I element was not meant to be used for the prediction of delamination. The most current version of ABAQUS™ has added the capability to predict delamination using interface elements.

The interface element type used in this paper is the COH3D8, an eight-noded element, three displacement degrees of freedom per node, and linear interpolation. There are two convergence issues with the COH3D8. The first issue is that the convergence has been found to be excessively slow with the built-in bilinear constitutive law that accompanies this element formulation. The source of the slow convergence is the tangent stiffness discontinuity present in the bilinear constitutive law. The Newton-Raphson nonlinear solver enters into nonconvergent oscillating cycles of the residual force while attempting to converge to a solution. The second issue for slow convergence is related to numerical instabilities arising from stiffness matrices with negative eigenvalues and ill-conditioned stiffness matrices that often accompany the type of problems involving softening behavior.

The first convergence issue is addressed by selecting a constitutive law with a smooth slope, Figure B-5. The constitutive law has an exponential form, and it naturally satisfies the following multi-axial quadratic stress criterion for the onset of delamination:

$$\left(\frac{T_3}{S_{3t}}\right)^2 + \left(\frac{T_1}{S_1}\right)^2 + \left(\frac{T_2}{S_2}\right)^2 = 1, \ T_3 \geq 0 \ ,$$

$$\left(\frac{T_3}{S_{3c}}\right)^2 + \left(\frac{T_1}{S_1 - \eta T_3}\right)^2 + \left(\frac{T_2}{S_2 - \eta T_3}\right)^2 = 1, \ T_3 < 0 \ ;$$

where T_1 and T_2 are the interfacial traction components associated with shear and S_1 and S_2 are the interfacial shear strengths. T_3 is the normal interfacial traction component, S_{3t} is the tensile interfacial normal strength, and S_{3c} is the compressive interfacial normal strength. The quadratic failure criterion includes a 'friction coefficient' that incorporates the apparent increase in shear strength due to transverse compression. The constitutive law also naturally satisfies the following mixed-mode fracture criterion for the progression of delamination:

$$\frac{G_{\text{I}}}{G_{\text{Ic}}} + \frac{G_{\text{II}}}{G_{\text{IIc}}} + \frac{G_{\text{III}}}{G_{\text{IIIc}}} = 1;$$

where the Mode I, II, and III energy release rates are G_{I}, G_{II}, and G_{III}, respectively; and the critical Mode I, II, and III energy release rates are G_{Ic}, G_{IIc}, and G_{IIIc}, respectively. *Naturally* means that the criteria do not need to be evaluated in the numerical algorithm, because the criteria and its corresponding failure degradation rule is built-in in the constitutive law. These constitutive equations are also thermo-mechanically consistent, and this is achieved by including a damage parameter to prevent the restoration of the previous cohesive state between the interfacial surfaces. The second convergence issue is resolved by setting negative diagonal terms in the material tangent stiffness matrix to zero. This modification does not affect the solution, but it improves convergence efficiency. The constitutive law implementation is conducted with a user material subroutine UMAT. The constitutive law requires definition of the critical energy release rate for Mode I, II, and III; and the shear and normal interlaminar strengths.
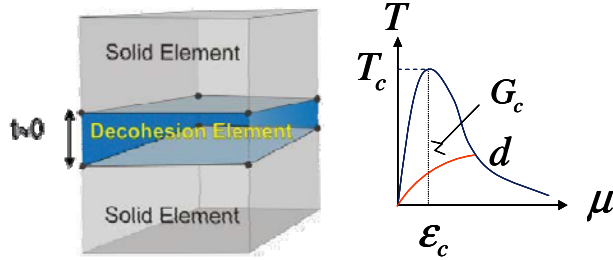
Figure B-5. Interface element coupled with a cohesive zone model.

In-Plane and Out-of-Plane Nonlinear Shear

Composite laminates typically exhibit a nonlinear response when subjected to shear loads either in the plane of the composite or transverse to the plane of a thick composite. Material nonlinearity in the plane of the composite can be replicated during off-axis testing or Iosipescu testing. A typical nonlinear curve is shown in Figure B-6. Testing is generally used to extract the initial shear modulus and the shear strength. Hahn and Tsai (Ref. B-10) have proposed a cubic polynomial to represent the nonlinear in-plane shear stress-strain relationship.
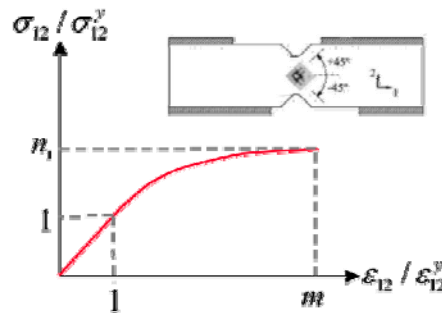
Figure B-6. Typical nonlinear shear constitutive law.

The work at Aerospace has been extended to account for nonlinear shear through-the-thickness of the composite. The extension was conducted because there is extensive evidence presented in the literature indicating that the nonlinear shear model plays an important role in accurate predictions of the failure strength. Including this nonlinearity is of paramount importance to find the appropriate stress distribution and concentration at the bolt hole. Otherwise, premature predictions of in-plane matrix-cracks are predicted and may result on a gross underprediction of strength. Including the nonlinear shear behavior of the composite in the failure modeling relieves the in-plane shear stress concentration at the hole boundary and delays the prediction of matrix-cracks. Although complex polynomial forms and sophisticated nonlinear models have been proposed, at Aerospace the following exponential constitutive law was developed that requires a minimum number of material parameters:

$$\sigma_i = {}^y\sigma_i \left[1 + (n_i - 1) \left(\frac{e_i - 1}{m_i - 1} \right) \left(\frac{m_i - 1}{n_i - 1} \right)^{\lambda} \right]$$

$$\lambda_i = 1 - \left(\frac{e_i - 1}{m_i - 1} \right)^{\varphi_i}, \quad \varphi_i^{-1} = \ln \left(\frac{m_i - 1}{n_i - 1} \right), \quad i = 12, 13, 23$$

69

$$e_i = \frac{\varepsilon_i}{^y\varepsilon_i}; \; n_i = \frac{^u\sigma_i}{^y\sigma_i}; \; m_i = \frac{^u\varepsilon_i}{^y\varepsilon_i}.$$

The material properties that need to be specified for the nonlinear shear constitutive law are the initial shear modules, ultimate shear strengths, ultimate shear strains, and the yield strengths.

Matrix-cracking

The strength-based failure criteria developed by Hashin (Ref. B-11) based on experimental observations of unidirectional composites subjected to tensile loads, has been extended because it does not always fit experimental data as shown by numerous studies, especially in the case of matrix compression. The World-Wide Failure Exercise (WWFE) was conducted, whereby the leading theories for predicting failure in composite laminates were compared against experimental evidence in order to assess the qualitative and quantitative robustness and accuracy of each failure theory. The comparisons included biaxial strength envelopes for a range of unidirectional and multi-directional composites. The WWFE results indicated that even for simple layups and loadings, many of the failure criteria that have been proposed to-date fall short of predicting the failure strength accurately. Since the numerical predictions with the failure theory by Puck and Schurmann (Ref. B-3) showed good agreement with experimental results for the prediction of biaxial failure envelopes in the WWFE studies, their criterion is extended from in-plane only to a 3-D form that accounts for through-the-thickness failure. The failure theory follows the work of Hashin. Hashin's failure criteria for matrix-cracks consists of a quadratic interaction of stress invariants, whereby the criteria is made independent of the stress parallel to the fiber based on the fact that any possible failure plane is parallel to the fibers. The failure criteria proposed by Puck and Schurmann is essentially an extension of Hashin's postulate.

The fracture plane is unknown and it must be determined. This is accomplished by maximizing the failure index with respect to the fracture plane angle. Since matrix-cracking occurs in a plane parallel to the fibers, the fracture plane oriented at an angle β with respect to the global coordinate system must be obtained. The tractions acting in a potential fracture plane are determined by force equilibrium as follows:

$$\sigma_{nn} = \frac{\sigma_{22} + \sigma_{33}}{2} + \frac{\sigma_{22} - \sigma_{33}}{2} \cos(2\beta) + \sigma_{23} \sin(2\beta)$$

$$\sigma_{nt} = -\frac{\sigma_{22} - \sigma_{33}}{2} \sin(2\beta) + \sigma_{23} \cos(2\beta)$$

$$\sigma_{nl} = \sigma_{12} \cos(\beta) + \sigma_{13} \sin(\beta)$$

where σ_{ij} is the local state of stress that rotates with the lamina orientation. σ_{11} is the stress parallel to the fiber, σ_{33} is the stress in the stacking direction, σ_{12} is the in-plane shear stress, and σ_{13}, σ_{23} are the transverse shear stresses. The matrix-cracking failure criterion for a tensile traction is postulated as

$$\left(\frac{\sigma_{nn}}{Y}\right)^2 + \left(\frac{\sigma_{nl}}{S_l}\right)^2 + \left(\frac{\sigma_{nt}}{S_t}\right)^2 = 1$$

70

and for a compressive traction as follows:

$$\left(\frac{\sigma_{nl}}{S_l - \eta\sigma_{nn}}\right)^2 + \left(\frac{\sigma_{nt}}{S_t - \eta\sigma_{nn}}\right)^2 = 1$$

The contribution of the compression traction has been eliminated but added to increase the shear strength in order to indicate that shear fracture is impeded in compression. In compression there is additional resistance to shear fracture. This effect is incorporated with a 'friction coefficient'. Here, the denominators in this failure index can be regarded as effective shear strengths. The potential fracture plane as shown in Figure B-7 is obtained by maximizing the failure index. Once failure has been established, corresponding mechanical properties are degraded to emulate fracture.
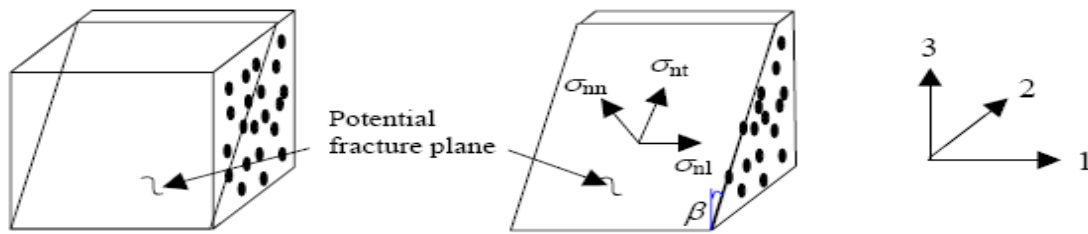
Figure B-7. Potential fracture plane in the 3-D failure criterion for matrix-cracking.

Fiber-breakage

The failure criteria for the prediction of fiber failure utilizes critical strain and it is simply:

$$\varepsilon_{11} < {}^c\varepsilon_{11}, \ \varepsilon_{11} < 0; \ \varepsilon_{11} > {}^t\varepsilon_{11}, \ \varepsilon_{11} > 0$$

where the ${}^c\varepsilon_{11}$ is the strain allowable in compression and ${}^t\varepsilon_{11}$ is the strain allowable in tension. For fibers surrounding a hole, an area satisfying the failure criterion is used as the criteria. The need for a critical fiber area criterion in the case of a hole is made evident by stress concentrations that significantly exceed the fiber strain allowable, thus causing rapid damage growth at load levels that are not realistic. Utilizing the critical fiber area as a criterion delays the failure of the composite with a notch or hole. Otherwise, the strength could be under predicted by more than 50 percent.

Degradation to Mechanical Properties

Now that the failure mechanisms with their respective failure criteria have been defined, the constitutive law for the composite material needs to be modified accordingly to simulate damage initiation and growth. The new constitutive law, as derived from damage mechanics is:

$$\overline{C}_{ij} = C_{ij}(1-d_i)(1-d_j)$$

where i = 1,2,3 correspond to the direction of the fiber, to the direction perpendicular to the fiber in the plane of the laminate, to the direction perpendicular to the fiber transverse to the laminate, respectively.

Fiber breakage corresponds to $d_1 = 1$ and the components of the damage elasticity tensor C_{1j}, C_{j1} become zero. The physical interpretation of the reduction in stiffness $C_{13}, C_{31}, C_{21}, C_{12}$ is that if

the fiber fails, there is no load transfer from the fiber to the matrix. From the engineering standpoint, this reduction represents that the Poisson ratio no longer affects the mechanical behavior of the composite. Similarly, for matrix cracking in the plane of the laminate and transverse to the laminate $d_2 = 1$, and the components of the damage elasticity tensor C_{2j}, C_{j2} become zero. If matrix-cracking occurs, the shear stiffness for each shear plane is also degraded using the damage parameter d_2. For delamination, the energy dissipated by this failure mechanism will be taken into account using interface elements, hence the damage variable d_3 will be held as zero.

B-4 Material Characterization for the PFA

To properly simulate damage initiation and growth of different failure mechanisms and their interaction, the mechanical, strength, and fracture properties must be determined from coupon testing. Table B-1 shows basis material properties determined from coupon testing. The type of tests needed are simple tensile test, Iosipescu testing, and the open-hole strip testing. For fiber failure and matrix-cracking coupon testing can be used to fully characterize failure in large scale structures, Figures B-8 and B-9. From the tensile test, one can determine the Young modulus and the ultimate tensile strength in the fiber direction. The shear stiffness, the yield stress, and the ultimate shear strength in the plane of the laminate can be determined either from $[-45/+45]_{ns}$ off-axis loading test, short-beam shear test, or torsion test. From the open-hole strip testing, one can determine the critical area for which neighboring fibers fail.

The fracture properties to characterize delamination growth are obtained from fracture testing that are either an American Society for Testing and Materials (ASTM) standard or are in the process of being certified. The Mode I critical energy release rate is determined from the double cantilever beam. End loads are applied in opposite directions to peel the composite beam in to two sublaminates. The test is generally performed on unidirectional composites with the fibers oriented such that these are parallel to the length of the initial delamination. The experiment consists of a load that is applied at aluminum end blocks jointed to the DCB specimen by an adhesive. The test is performed under displacement-controlled tensile test machine. The conventional quasi-static tests are generally performed at constant displacement rates that can be chosen between 5 mm/min and 15 mm/min.

Table B-1. Basic Material Properties Determined from Coupon Testing

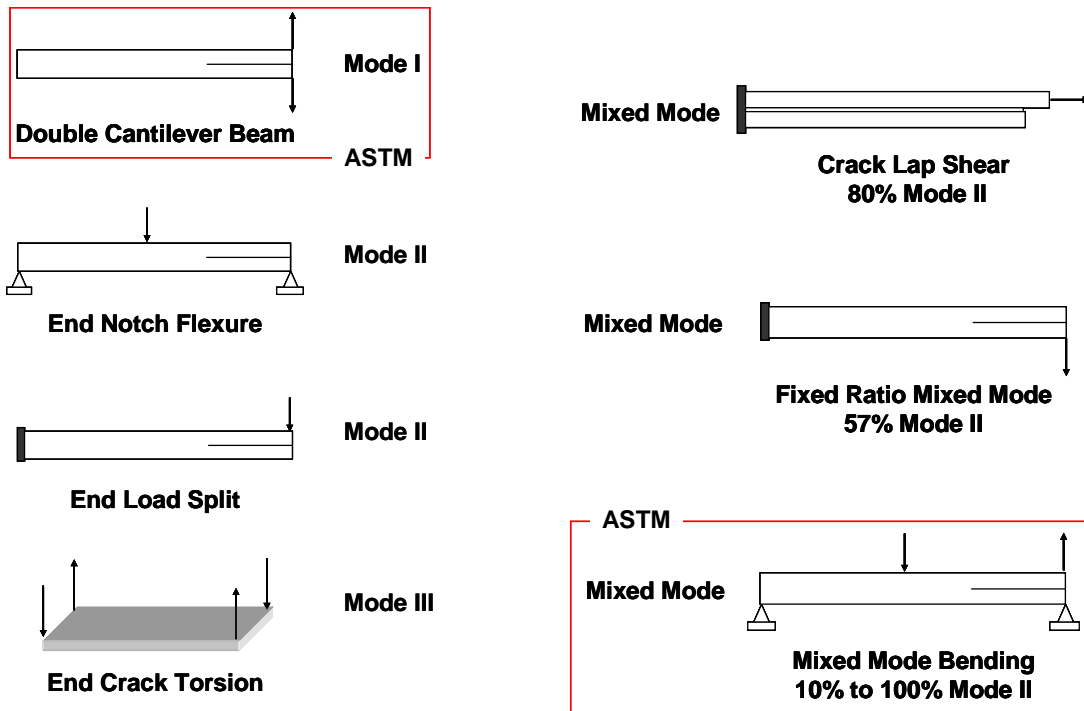| Test Coupon		Stiffness	Strength	ASTM Standard
	Tensile	E_{11}	X	D3039/3039M-95a
	Iosipescu Shear	G_{12}	σ_y, σ_u	D5379/D5379M-98
	Open Hole Strip		A_f	D5766/D5766M-95

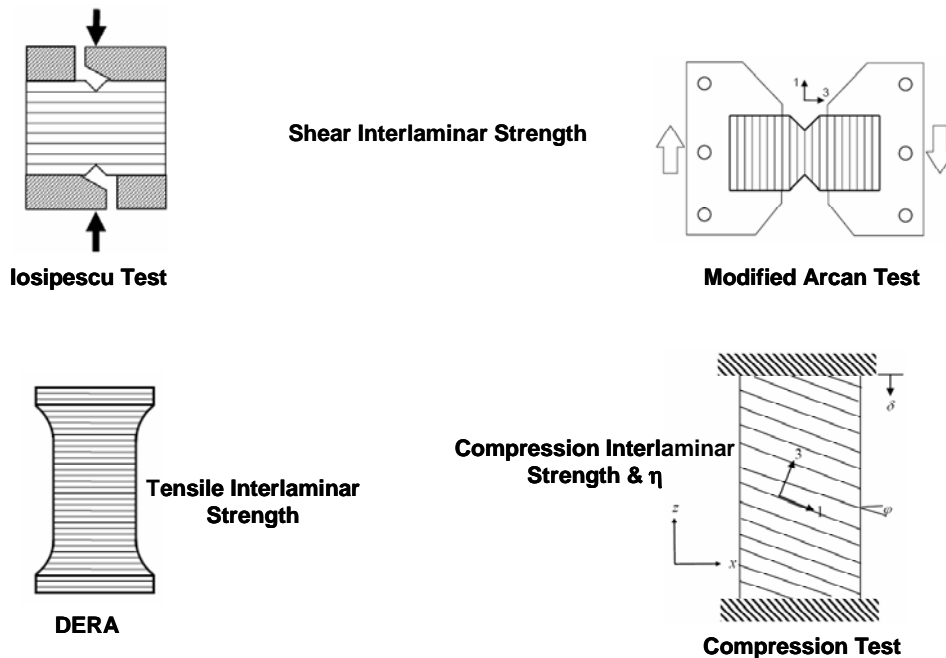Figure B-8. Test configurations for the characterization of fracture properties.

Figure B-9. Test configurations for the characterization of strength properties.

The initial delamination is achieved by incorporating a Teflon film at the midplane of the laminate layup prior to curing. There are issues pertaining the test specimen layup. With these test specimens, the delamination front may not be straight due to uneven distribution of the energy release rate across the width of the beam. This uneven distribution is caused by the anticlastic bending effect. Secondly, the main delamination may branch into multiple cracks that may follow the fiber-matrix interfaces. This situation may lead to Mode II loading. In addition,

the phenomenon of fiber bridging caused by fiber nesting in 0-degree composites can lead to variations of the critical energy release rate.

Table B-2 summaries fracture test configurations. A complex fracture behavior involving fiber breakage, ply jumping, and fiber bridging often occurs when arbitrary orientation in ply angles are considered in the design of DCB test specimen. The delamination branches to interfaces away from the midplane, which leads to larger values of fracture toughness. They developed a DCB test method to suppress crack jumping and fiber bridging effects. To achieve pure Mode I delamination in a layup other than 0-degrees, the arms of the DCB specimen were designed such that these are balanced and symmetric to eliminate the stretching-shearing and stretching coupling effects. In addition, the layup of the angle ply laminate was designed to minimize the bending-twisting effects. The tests were designed to ensure there was no curvature or shear distortion of the laminate due to thermal stresses from curing.

The critical energy release rate for Mode II is determined either from the ENF, end load split (ELS), mixed-mode bending (MMB) apparatus, or the four-point ENF. Only the ENF and the ELS will be discussed because these are the most commonly used in determining the fracture energies under Mode II loading. The ENF is simply supported at the ends with the load applied at the middle of the specimen. If the delamination length is approximately less than 35 percent of the total length, the test specimen undergoes delamination.
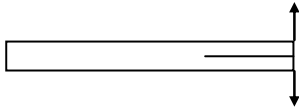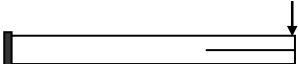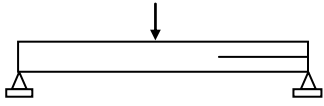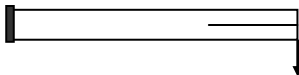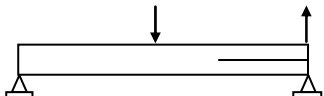
The ELS test configuration is clamped at one end and a load is applied at the other end. For this test configuration, the delamination growth is unstable for short delamination lengths that are less than 55 percent of the length of the specimen. In both test configurations, Mode II loading is promoted by the relative sliding of the upper surface of the lower lamina with respect to the lower surface of the upper lamina. The relative sliding occurs due to the rotation of the upper and lower arms. The practical difficulties in measuring the Mode II fracture toughness with these test configurations is the choice of starter defect, the stability of the test, and frictional effects between the crack faces. Using a film insert as a starter defect leads to a larger fracture toughness than a test specimen with a pre-crack. The main problem encountered with the Mode II tests is that determining the stability of short cracks is complex since these can dynamically propagate.

The critical energy release rate for Mode III can be determined from the end crack torsion (ECT), the split cantilever beam, and the crack rail shear. The split cantilever beam generates a substantial Mode II strain-energy release rate component near the free edges, thus invalidating the test. Extensive efforts undertaken by NASA LaRC to standardize the ECT test to characterize Mode III have been unsuccessful. The edge-crack torsion test configuration consists of a rectangular composite of a $[90/(\pm45)_n/(\pm45)_n/90]_s$ laminate with a rectangular pre-crack introduced by a non-adhesive film inserted at the midplane along one edge during manufacture. The sample is mounted in a special fixture that provides support at three points, and a transverse load is introduced at the fourth point by compressing a loading pin. Usually, the specimen and fixture assembly is loaded in a test machine with a constant stroke rate of 1.5 mm/min. This special fixture creates torsion along the length of the laminate, thus inducing Mode III delamination.

The MMB test, crack lap shear, or fixed ratio mixed mode (FRMM) can be used to determine the failure envelope for a delamination under a mixed-mode condition. From all the tests discussed, the double cantilever beam and the MMB tests are ASTM standards, while the end notch flexure is a European Agency standard. Extensive efforts are underway to develop the other fracture test

configurations into ASTM standards fully. For the full characterization of the transverse strength properties including the nonlinearities required in the PFA, the Iosipescu test, Modified Arcan Test, and the off-axis compression tests can be used to determine the interlaminar shear strength, tensile strength, and the mixed-mode interaction. The benefit of the off-axis compression test is that it provides the means to determine the 'friction coefficient' required for the formulation of the interface elements. Typically, this 'friction coefficient' is 0.28 and it can be confirmed by testing. This 'frictional parameter' is essentially a phenomenological representation of physical events occurring at the microscopic level that are not well understood. Many researchers including Puck have treated this parameter as friction for matrix undergoing brittle fracture under compression.

Table B-2. Summary Table for Fracture Test Configurations Analyzed Using Finite Elements

Test Configuration	Failure Modes	Failure Description
1. DCB Layups: $[0]_2$	Mode I	(1) Delamination front is curved. (2) For short cracks, delamination is dominated by strength, while for long cracks delamination is dominated by fracture energy. Unstable delamination growth occurs under load control.
2a. ELS 2b. ENF	Mode II	(1) Unstable delamination growth occurs either under displacement or load control if the crack length to specimen length ratio is 0.55 for the ELS and 0.35 for the ENF. (2) The energy dissipated due to friction is negligible compared to the fracture dissipation. However, frictional forces can cause temporary crack arrest. (3) For short cracks, a snapback algorithm is required to follow the load-displacement response.
3. ECT Layups: $[90/\pm45_3/\mp45_3/90]_s$	Mode III	(1) Delamination is governed by G_{III}, although a G_{II} component does exist. Thus, delamination growth occurs non-self-similarly. (2) Proper determination of the transverse shear modulus G_{23} is critical for an accurate determination of the anti-plane shear mode. (4) Unstable delamination growth occurs if the initial delamination is sufficiently small.
4a. FRMM Layups: $[0]_2$ 4b. MMB	Mixed-mode failure	(1) Delamination is governed by G_I and G_{II}. (2) The delamination growth is unstable under either load or displacement control if the crack length to specimen length ratio is 0.41 for the FRMM and 0.35 for the MMB. Snapback required to trace the structural response. (3) The Riks algorithm required to follow the loading path of the MMB, since the loads are applied proportionally. (5)

B-5   Validation of PFA for Coupon Test Configurations

To demonstrate the capability to predict delamination and the irreversibility capability of the PFA code, steady-state delamination growth of unidirectional T300/977-2 carbon fiber-reinforced epoxy laminate beams were simulated for quasi-static loading-unloading cycle of various fracture test configurations. The finite element results for Mode I double cantilever beam (Figure B-10), the Mode II ELS (Figures B-11), ENF (Figure B-12), and the mixed-mode tests (Figures B-13, Figure B-14) were in excellent agreement with either experimental data available in the literature or with linear elastic fracture mechanics analytical solutions. The PFA code was also validated with test data available for the ECT, a very unstable test configuration. The ECT test specimen is a G40-800/R6376 graphite epoxy composite laminate with a $[90/(\pm45)_3/(\pm45)_3/90]_s$ stacking sequence. The predicted failure load was within 5 percent of the test, Figure B-15, and the predicted damage distribution was in close agreement to the scans of the failed specimens, Figure B-16. Lastly, the finite element simulations of the DCB and the ELS made of AS4/PEEK were conducted and the numerical response was in close agreement with experiments, Figure B-17.

The effect of through-the-thickness compressive/tensile loads on the strength and response of woven carbon/epoxy composite blocks loaded in an off-axis configuration with respect to the stack direction was investigated using the PFA code. This particular problem tests the ability of the code to consider the apparent increase in shear strength when a composite is subjected to through-the-thickness compressive stress. Published data suggests that the composite blocks fail primarily by delamination. Thus, to predict the strength of the blocks, decohesion elements were placed between adjacent lamina. This is an improvement over previous codes that relied on a simple quadratic strength-based failure criterion, thus, under-predicting the failure load. Compression simulations were conducted for 0-degree, 7.5-degree, 19-degree, 25-degree, and 45-degree off-axis angles test configurations. Simulations were able to capture the catastrophic failure of the blocks, whereby the composite blocks crack into two pieces and the upper and the lower portions instantaneously rotate in opposite directions, Figure B-18. The failure event as observed from testing and predicted by analysis is dynamic and catastrophic. The predicted failure loads were in close agreement with the test data for all compression test configurations. The failure envelopes for the composite blocks were in close agreement with the testing conducted by Schubel and Sun's failure criteria, Figure B-19. The PFA code also includes the nonlinear shear constitutive law, which enabled the prediction of the nonlinear structural response, Figure B-20.
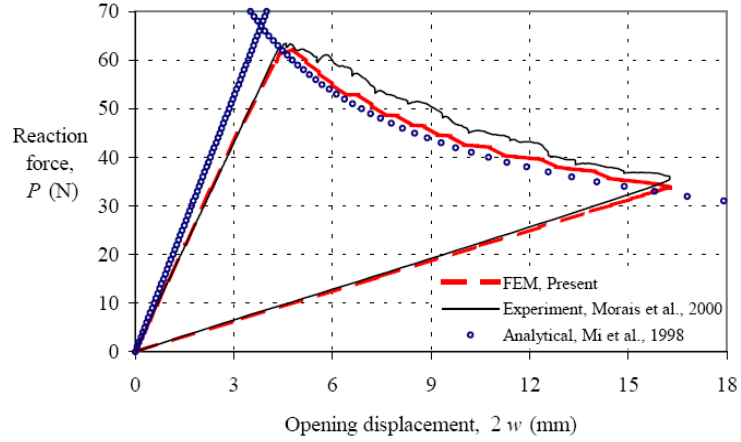
Figure B-10. Predictions by PFA of the DCB compare well to experimental data and analytical solutions.
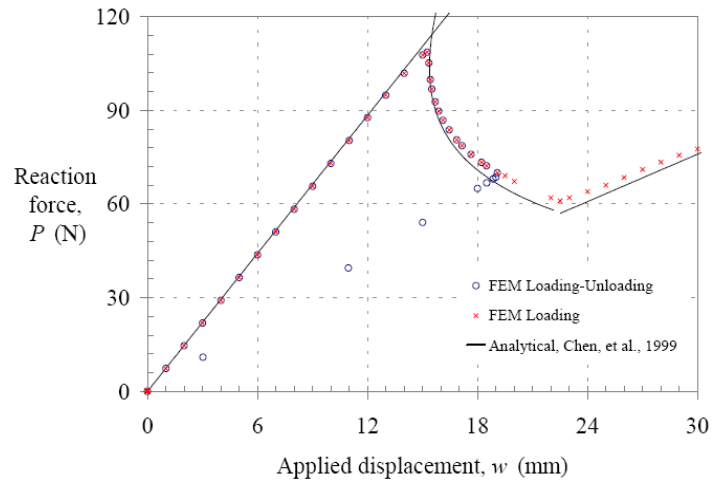

Figure B-11. Predictions by PFA for the ELS compare well to analytical solutions.
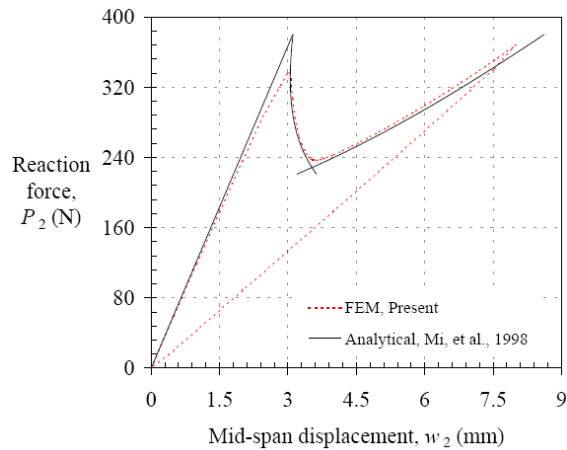

Figure B-12. Predictions by PFA for the ENF compare well to analytical solutions.
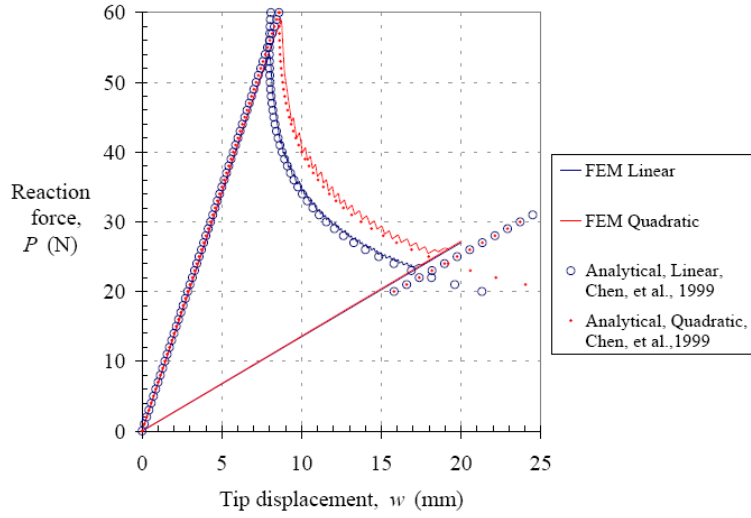
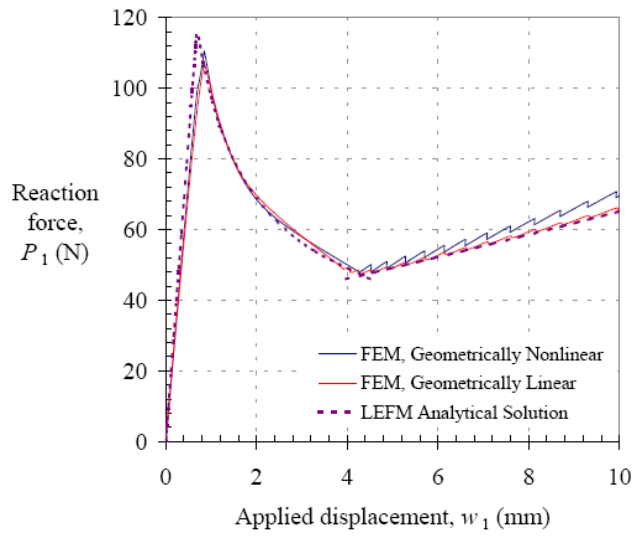Figure B-13. Predictions by PFA for the FRMM compare well to analytical solutions.

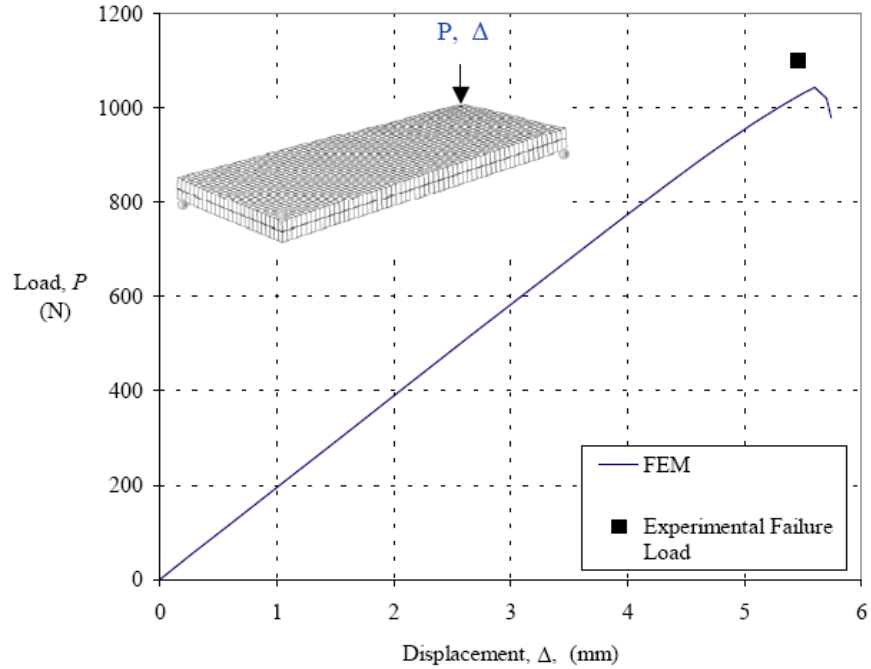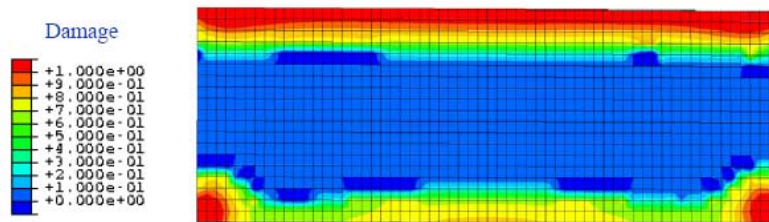Figure B-14. Predictions by PFA for MMB compare well to analytical solutions.

Figure B-15. Predictions by PFA for ECT compare well to testing.

Figure B-16. Damage predicted by PFA compared well by scans of the failed coupon.
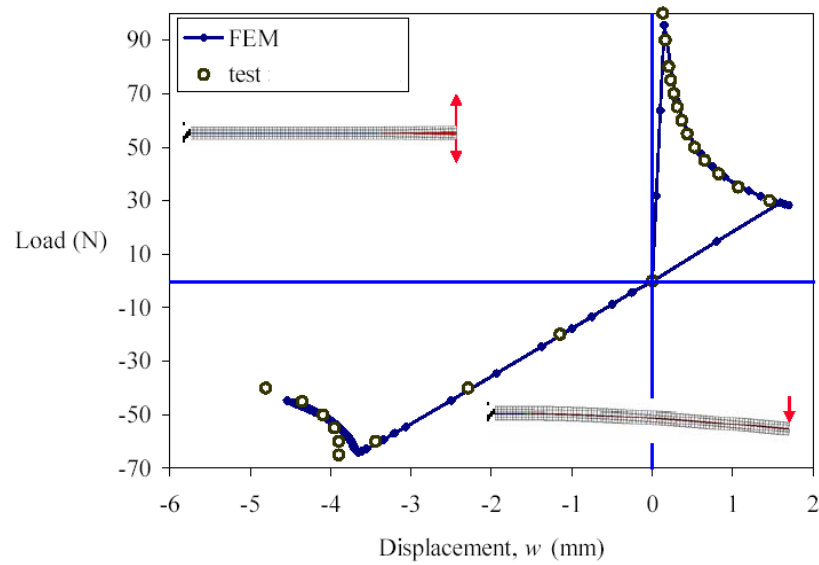
Figure B-17. PFA predicted load-displacement response for DCB and ELS accurately.
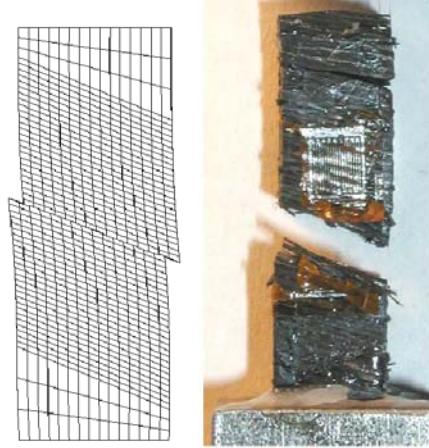
Figure B-18. Predicted catastrophic failure of the off-axis test configurations.
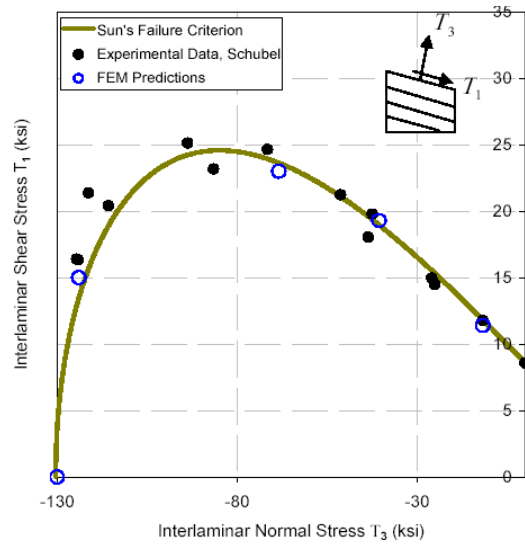
Figure B-19. Failure envelope predictions compared to experimental data for compression tests.
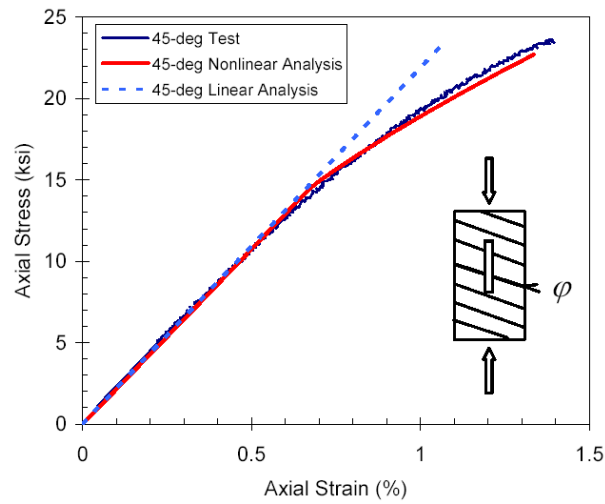
Figure B-20. Failure response compared well with the experimental response.

B-6   Subscale test panels

The PFA code is now demonstrated to simulate the initiation and growth of intralaminar and interlaminar failure modes occurring in AS4-3503 Gr/Ep panels with centrally located circular cutouts when subject to compression or shear loads, Ref. B-1. The testing of these panels was conducted at NASA LaRC. The failure of these panels is of special interest, because buckling, interlaminar, and intralaminar failures interact into the postbuckling regime of the structural response. The flat composite panel, Figure B-21, consisted of 24 plies with a stacking sequence of $[\pm 45/0_2]_{3s}$ and framed by a square fixture made of steel. Three corners of the frame were held by pin joints, while a displacement was specified in the remaining corner at 45 degrees with respect to the edge of the panel.

Two curved composite panels one with diameter to width ratio of 0.4 and the other one with a ratio of 0.2, Figure B-22, were subject to axial compression. Both panels had a laminate stacking sequence of $[\pm 45/0/90]_{3s}$. The PFA code was necessary to predict the structural response of these panels reasonably, Figures B-23 thru B-25. The extent and location of delaminations predicted by the PFA code was confirmed, Figure B-26, by visual inspection of the failed test specimens. The delaminations both as observed from test and analysis occurred at the midplane of the flat panel loaded in shear and the curved panel with d/W = 0.4 loaded in compression. For the curved panel with d/W = 0.2, delamination occurred in multiple locations throughout the thickness of the panel. Specifically, the PFA code predicted delamination initiation and growth perpendicular to the loading direction in regions where large compressive loads were present. As simulations identified the shear panel collapsing, a rapid progression of delamination perpendicular to the loading axis was predicted, while delamination arrest was predicted parallel to the loading axis.
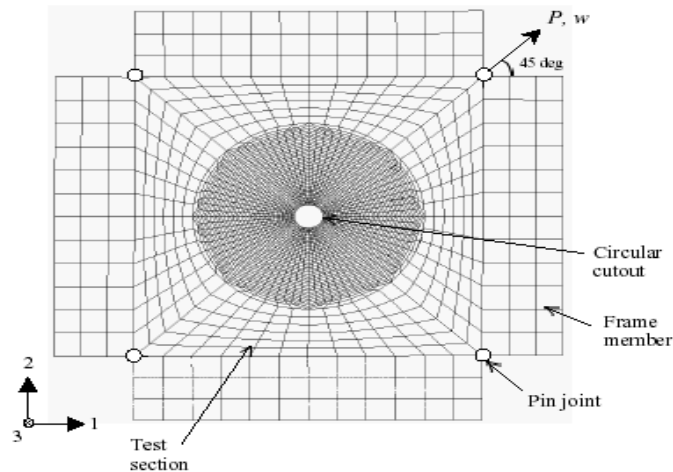

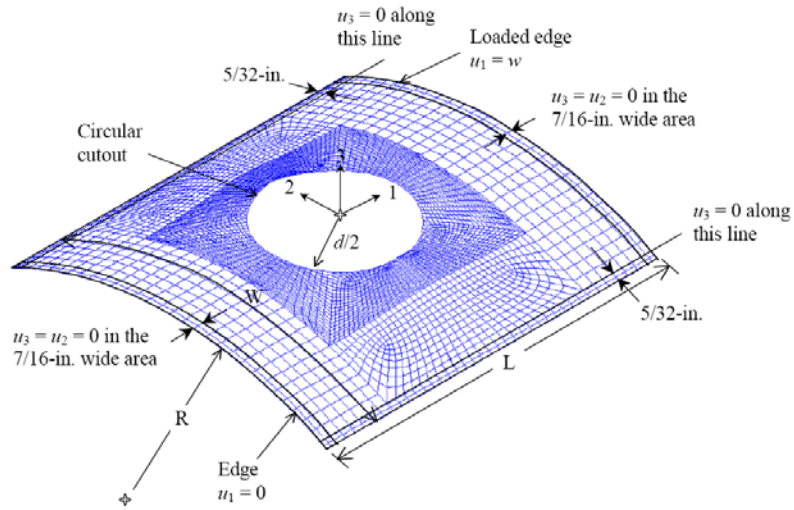Figure B-21. Flat panel loaded in shear.
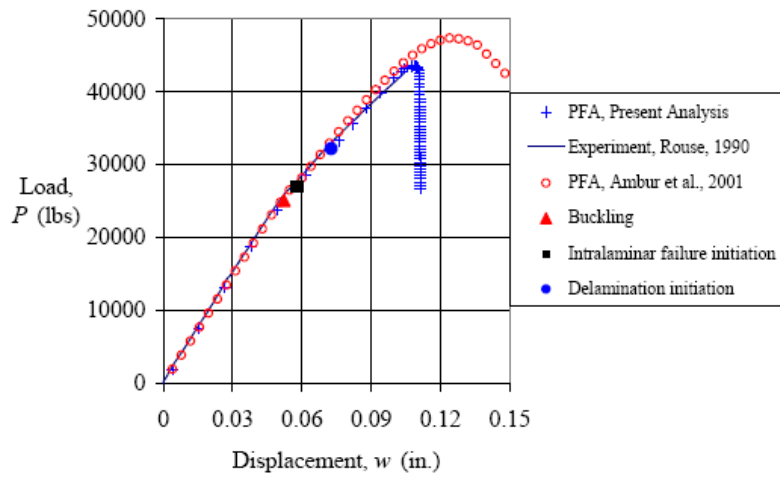
Figure B-22. Curved panel loaded in compression.

Figure B-23. Structural response of the flap panel loaded in shear.
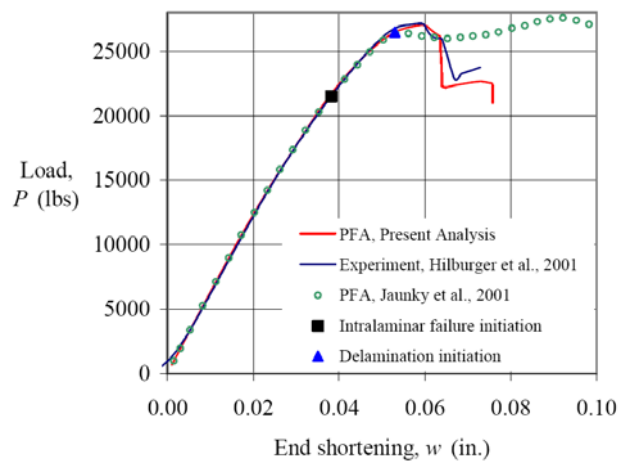

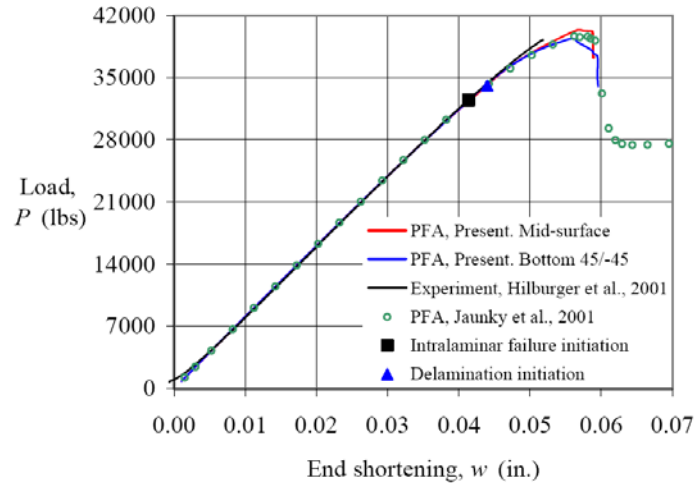Figure B-24. Structural response of the curved panel loaded in compression for d/W = 0.4.

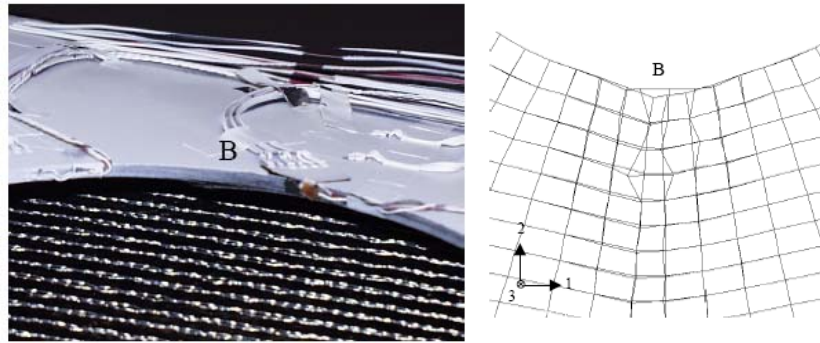Figure B-25. Structural response of the curved panel loaded in compression for d/W = 0.2.

Figure B-26. Visual indications of delaminations correspond to delamination prediction locations.

The PFA code also predicted delamination growth occurring perpendicular to the compressive loads for the two curved panels with different cutout sizes. Simulations indicated that the compression panel with smaller diameter cutout-to-width ratio failed with rapid progression of delamination from the edge of the cutout. For the compression panel with larger diameter cutout-to-width ratio, the predicted delamination growth was followed by delamination arrest. At this point, the numerical response indicates a residual strength, a finding consistent with the experimental data. After further loading, the predicted delamination growth leads to catastrophic failure. Thus, the PFA code was capable of predicting the rapid progression of delamination from the edge of the cutout at a location perpendicular to the loading axis including non-self-similar delamination growth, delamination arrest, and closure of delaminated faces.

B-7   Impact Damage of Structures

The PFA code was also used to determine the extent and shape of delaminations of a square sandwich panel with facesheets made from woven carbon fabric/epoxy laminates (AGP370-5H/3501-6S) and a closed-cell core made of PVC foam (Divinycell H250) subject to a low velocity impact caused by a free-falling blunt impactor, Figure B-27, Ref. B-12. The predicted delaminations were ringed shape, extended outwards from just the circular edge of the impactor, and were located in the midplane of the upper facesheet. The predictions compared well with ultrasonic scanning of the failed test specimen, Figure B-28. The predicted global response of the sandwich structure was in close agreement with the tests, Figure B-29.
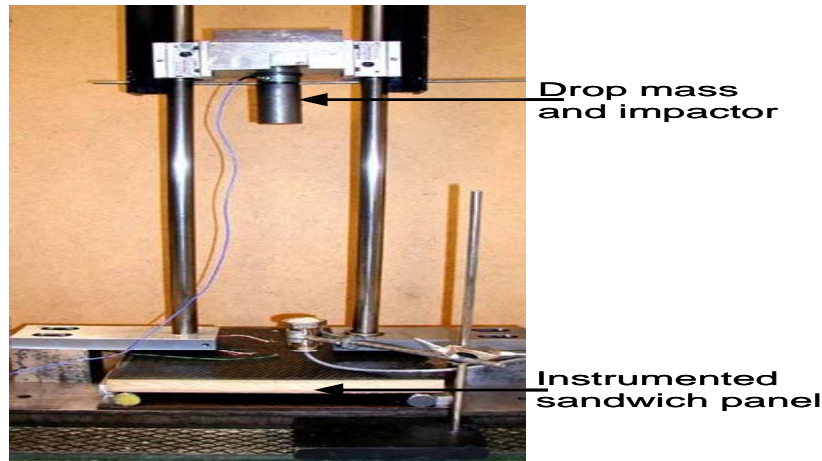
Figure B-27. Sandwich structure impacted by a free-falling mass.
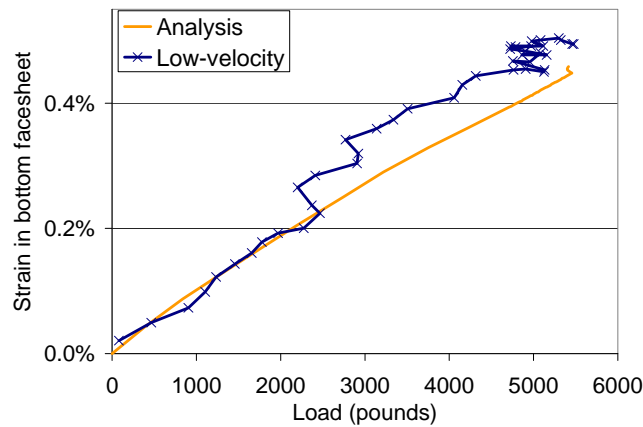

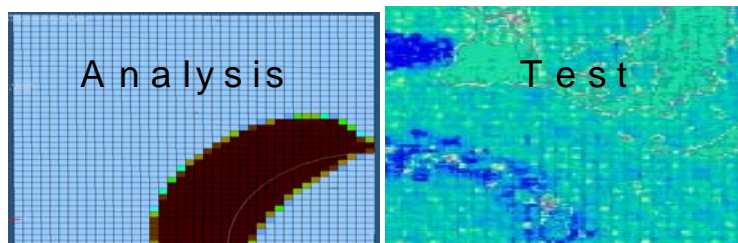Figure B-28. Strain response at bottom facesheet of the sandwich structure.

Figure B-29. Delamination predicted by analysis compared well with the test.

Two characteristics of the PFA code were instrumental in the good correlation that was achieved: it incorporates both the increase in interlaminar shear strength, Ref. B-13, and Mode II fracture toughness when the composite is subject to transverse compression loads. The simulation of this impact event demonstrated that considering other damage modes not included in the PFA code is important. A separate damage model for the foam core was necessary in order to properly simulate the extent and shape of delamination. The PFA code was also able to predict a decrease in load carrying capability caused by delamination growth, which was also observed in testing.

The PFA code was validated with test data generated at NASA LaRC of a J-section circular fuselage frame made of textile perform 3M PR500 epoxy resin subject to radially inward load

representing a crash-type event, Figure B-30. The architecture of the textile composite is a 2×2, 2-D triaxial braid with a yarn layup of [0 degree 18k/±64 degrees 6k] 39.7 percent axial. The PFA of the frame correlated reasonably well with the predicted failure modes of the composite, including the structural response of the structure, Figure B-31. The PFA code was numerically stable enough to predict the load-displacement response through several major failure events interacting with buckling. Since different failure modes, as predicted by analysis, occur simultaneously at different locations of the stiffener, the exact sequence from the model could not be extracted. However, in multiple locations kinking of axial tows led to matrix-crazing and eventually delamination.
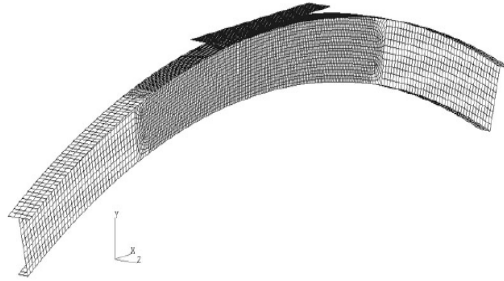

Figure B-30. J-section of a circular fuselage frame subject to a radial load.
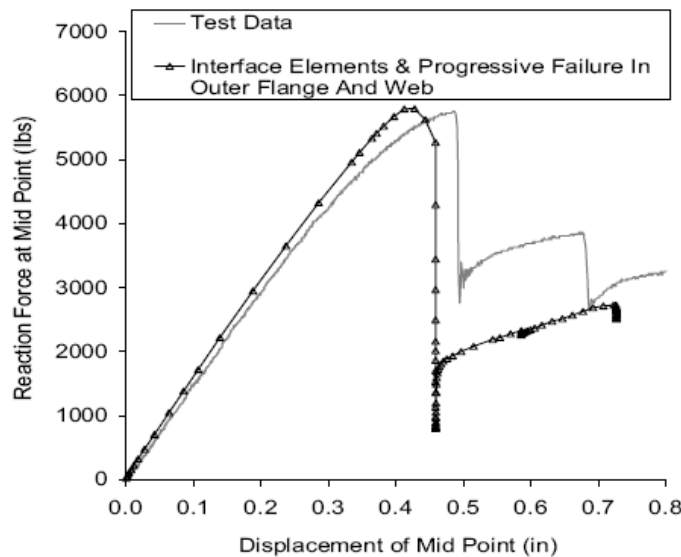

Figure B-31. Structural response of the J-beam subject to radial loads for the prediction and testing.

B-8   Adhesively Bonded Joints

The PFA code was validated against test data for several adhesively bonded joint configurations, Ref. B-14. The first validation was conducted with a single lap joint test configuration. The single lap joint test specimen, Figure B-32, was made of woven carbon epoxy fabric and epoxy-acrylate adhesive. The PFA code predicted two cracks initiating from the reentrant corners and propagated towards the middle of the test specimen. The PFA predictions compared well with the structural response from the experiments.
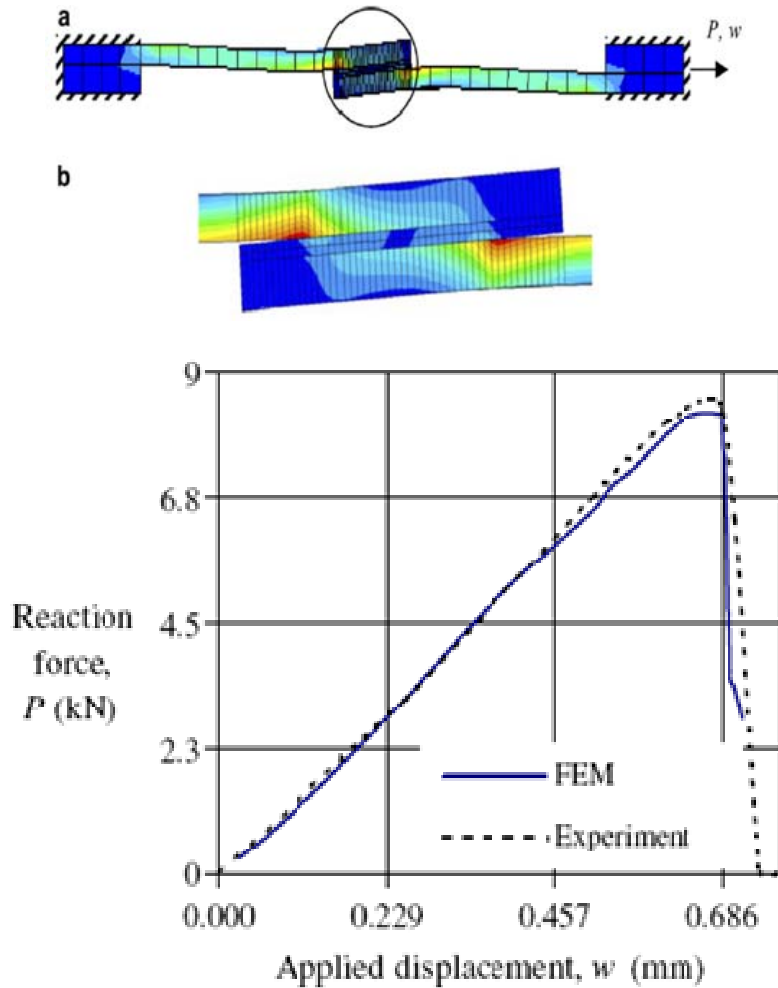
Figure B-32. Failure and response of the single lap joint test configuration.

The second validation example was that of an Aluminum 6061-T6 DCB with a thermoplastic acrylic polymer adhesive, Figure B-33. Interface elements were placed within the adhesive to provide multiple paths for crack propagation and allow for the prediction of hackle crack patterns. The PFA code predicted crack paths similar to those observed with tests and compared well with the structural response from the experiment. Through the PFA it was found that a small component of Mode II fracture turned the crack and contributed to temporary crack arrests also observed in testing.
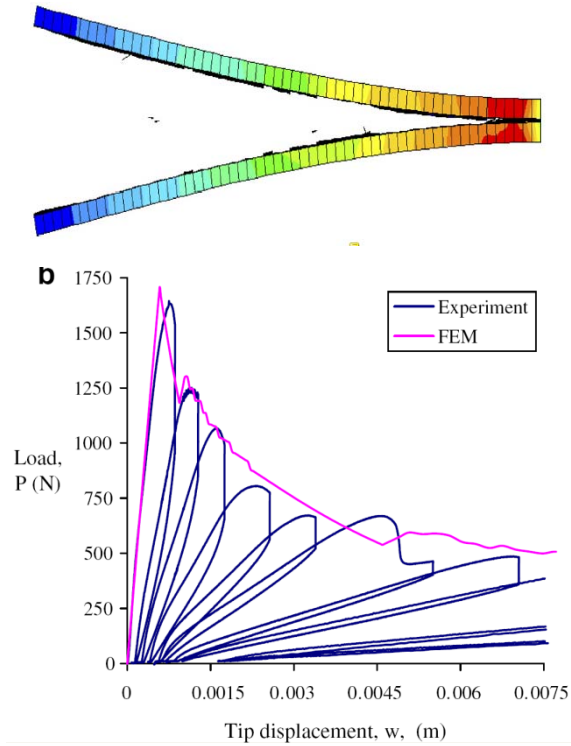
Figure B-33. Failure and response of a double cantilever beam test.

The third validation example was that of a crack lap shear test, Figure B-34. The crack initiates in the vicinity of the reentrantcorner, or, at the material discontinuity as predicted by PFA and observed in testing. The PFA indicates that the crack is mainly dominated by a Mode II loading. The predicted failure and response of the crack lap shear test configuration compared well with the testing, Figure B-35.
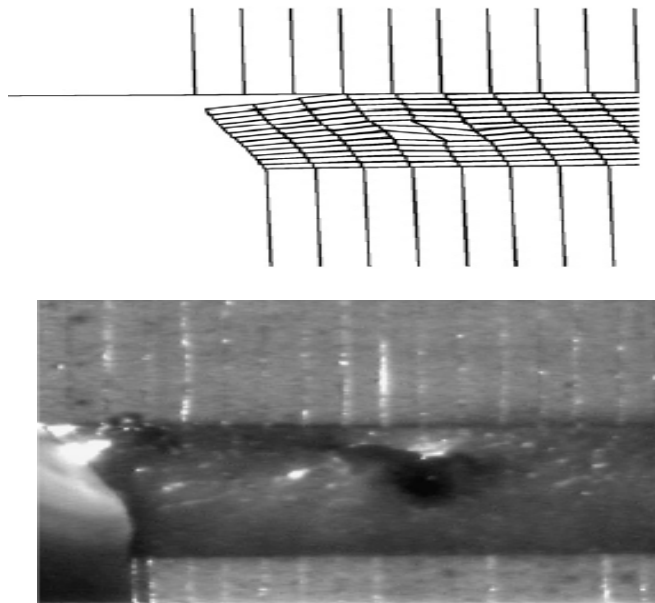

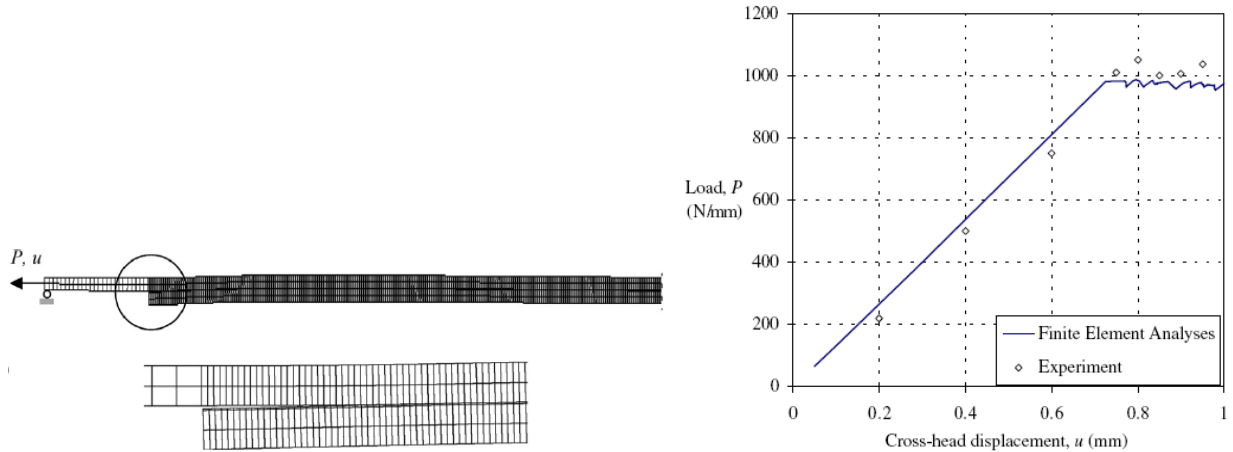Figure B-34. Predicted crack path versus that observed in testing.

Figure B-35. Failure and response of a crack lap shear test**.**

B-9   Mechanically Fastened Joints

The PFA code was further validated for problems involving composite mechanically fastened joints, Ref. B-15 and Ref. B-16. The composites were 128 plies $[0/{-}45/90/45]_{16s}$ quasi-isotropic panels and 0.75 inches thick. The analysis simulated bypass only test, double-sided bearing and bypass load test, and single-sided bearing and bypass load test, Figure B-36. These tests were performed at Aerospace's Space Materials Laboratory. The model incorporated nonlinear material behavior, and progressive damage of composites.
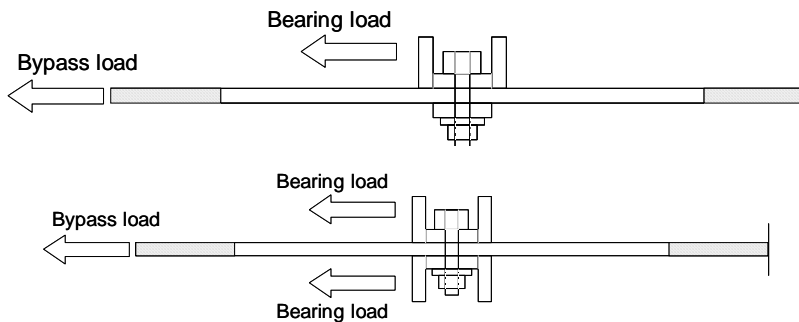

Figure B-36. Single-sided bearing and bypass load (top) and double sided bearing and bypass load (bottom).

The orientation and density of matrix-cracks and fiber damage are represented through a damage tensor, an internal state tensor that is thermodynamically consistent within the framework of continuum damage mechanics. The damage tensor evolves as damage associated with different failure modes accumulates. As described earlier, matrix-cracks are predicted using a 3-D failure criteria, which is based on the stresses acting on a potential fracture plane. For use with the failure criteria, a new anisotropic shear constitutive law is postulated governing the transverse and the in-plane shear nonlinear mechanical behavior.

The prediction of initiation and progression of multiple delaminations through the thickness of the composite is simulated via cohesive-decohesive constitutive law. Numerical simulations were in good agreement using filled hole tension, double sided bypass and bearing load, and single sided bypass and bearing test configurations. The predicted strength and the strain behavior was in good correlation with in-house experimental data, Figures B-37 thru B-39.
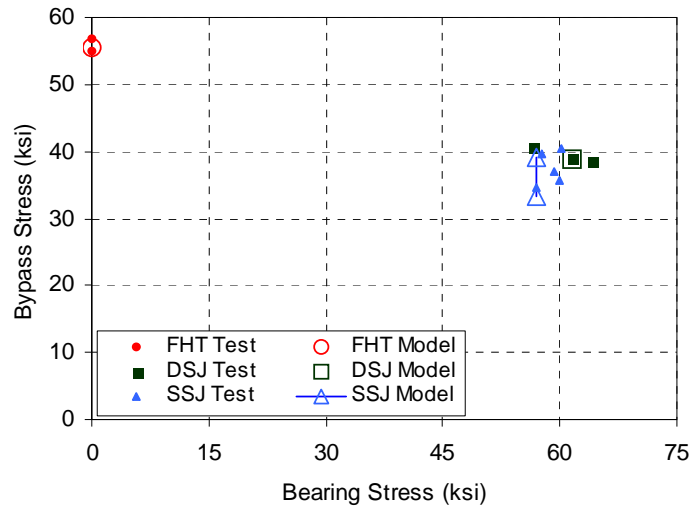
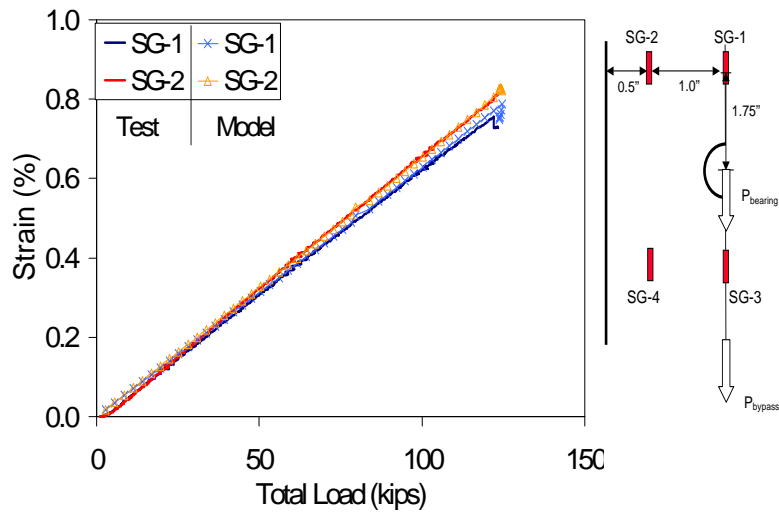Figure B-37. Joint strength failure of various specimen configurations.

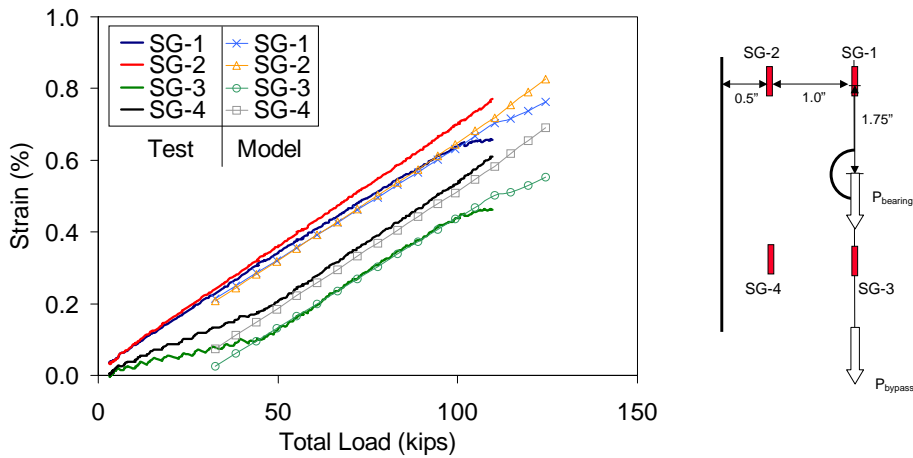Figure B-38. Strain comparison for filled-hole tension test.

Figure B-39. Strain comparison for single-sided bearing testing.

B-10 Modeling Delaminations in COPVs

Delaminations occasionally occur in COPVs. The objective of this section is to describe a method used to evaluate these defects by using a pre-processor in conjunction with progressive failure analysis. An example is used to illustrate this approach for a typical COPV. COPVs store highly pressurized gases in launch vehicles and spacecraft. Typical COPV construction consists of high-strength fiber composites wrapped around a thin metal liner. The purpose of the liner is to act as a leakage barrier while the composite carries the most of the load from pressurization. This combination leads to lighter weight designs for the same pressure capability, which is valuable for space applications.

Structural integrity and conformance to safety requirements demand accurate stress, fatigue and fracture mechanics analyses. Typically, netting analysis has been used as a design tool for COPVs, but is a highly simplified method that cannot always be used to evaluate the structural integrity of a discrepant COPV. Accurate analysis is particularly important since the consequences of a local defect propagating can lead to catastrophic failure and possibly complete mission loss. Aerospace has been on the forefront in the development of high-fidelity analysis of composites, including the specialized tools that are required to evaluate delaminations and debonds in COPVs.

Aerospace continues development of the COPV Stress Analysis Program (COSAP), begun in the 1990s under Air Force and NASA sponsorship. COSAP is primarily comprised of pre-processing code that is designed to work with the commercial finite element code ABAQUS™. COSAP is flexible enough to model various vessel configurations, winding patterns and peculiar situations resulting from manufacturing considerations including delaminations. COSAP has been validated through experiments (Ref B-17). Although COSAP is designed for analysis of COPVs, it may also be used for analysis of other filament-wound vessels, such as composite solid rocket motor cases.

COSAP is designed to handle complicated features, such as the continuously changing local wrap angle and thickness resulting from the filament winding process. COSAP is designed to automatically generate an axisymmetric FEM for a COPV, while calculating the effective 3-D composite material properties. The input file requires major dimensions, basic material properties and definition of the winding pattern. The dome geometry can be specified by the user directly or optimized by the pre-processor. Depending upon the winding method, geodesic or planar, COSAP will automatically determine the local wrap angle and thicknesses of composite layers based on the input data and then generate the finite element mesh. To limit the total number of elements, a group of composite layers, sublaminate, can be incorporated into a row of elements.

COSAP generates a FEM suitable for analysis with ABAQUS™. ABAQUS™ is used to perform a multi-step analysis that may include fabrication, sizing and burst cycles. Sizing, or autofrettage, is part of a typical manufacturing process, whereby the COPV is pressurized in order to yield the metal liner and as a result, the liner retains compressive residual stresses at lower operating pressure. This increases the number of cycles the tank can sustain before leaking. Upon completion of the multi-step analysis, the results are processed to evaluate burst pressure capability, fatigue life and the leak-before-burst failure mode. Prediction of the burst pressure is based upon progressive failure analysis described earlier, wherein for COPVs the ultimate failure

is usually fiber breakage. Preceding the global failure, delaminations may propagate into the boss region or into other regions of criticality, thereby leading to decreased fiber capability.

The objective of this section is to demonstrate how COSAP or equivalent tools can be used to evaluate the burst strength reduction due to the presence of a delamination. A typical COPV with a 20-inch diameter and alternating hoop and helical plies with a total thickness of up to 0.5 inches is analyzed, Figure B-40. In this example, the model development consisted of the following steps:

The liner contour was found by digitizing the available drawings and using software to determine the exact shape;

Ply thickness and initial ply angle at the tangent point were specified in the winding program, which then generated the remaining ply angle and thickness throughout;

The modeling also considered the inclusion of proper ply drop off geometry and location; this data was obtained from a cross section of a constructed component;

Candidate delamination locations were identified in critical ply interfaces, Figure B-41;

With the above geometric information, COSAP was used to generate an axisymmetric FEM with cohesive elements located at candidate locations including the liner-to-overwrap interface.
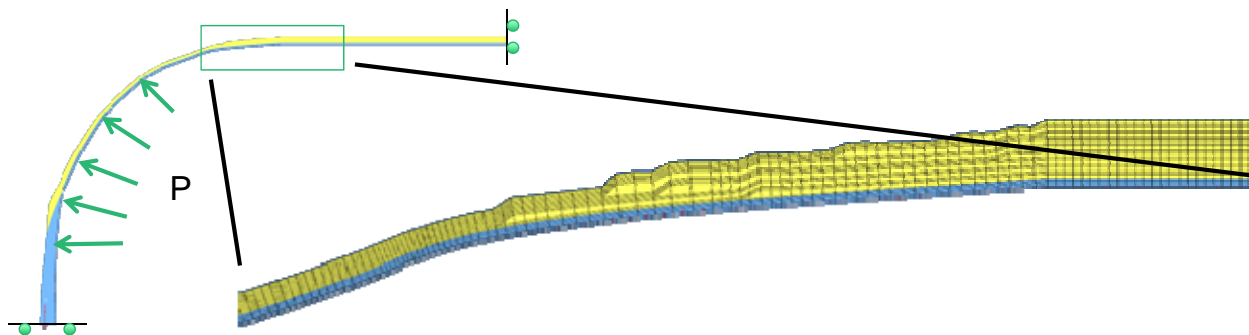

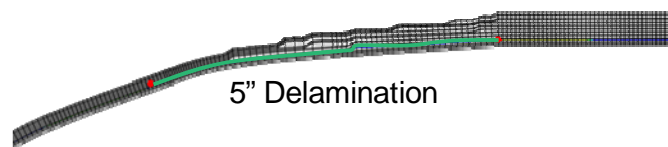Figure B-40. A typical COPV with boundary conditions.

Figure B-41. Delamination location for this example.

The analysis was performed in ABAQUS™ and included elastic-plastic material properties of the metallic liner and contact modeling was enforced to prevent delaminated surfaces from penetrating. Three load steps were required to properly evaluate the COPV: 1) loaded to autofrettage pressure of 4000 psi; 2) unloaded to 0 psi; and 3) loaded to maximum effective operating pressure, 3000 psi. Progressive failure analysis was active during these analysis steps. To build confidence in the model, strain gage data compared well to the predicted strains in the model. This was also true for the COPV axial and radial growth during autofrettage.

Two failure modes that could result from an initial delamination were evaluated. The first failure mode is decreased burst capability due to a hypothetical fiber defect occurring directly above the delamination, Figure 42. The concern was that the delamination growth could amplify the effects

91

of local fiber damage. The fiber defect was modeled by substantially reducing the elastic modulus in the hoop direction. The analysis showed that while the fiber defect itself could substantially reduce the burst capability, the addition of a delamination near this hypothetical fiber damage reduced the strength by less than 5 percent. Based on previous experience the effects of delamination can be much larger than in this example, arising from multiple factors.
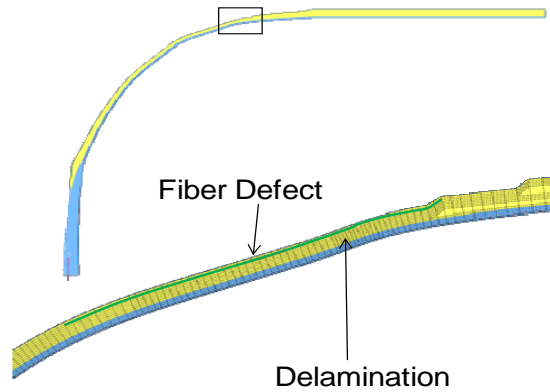

Figure B-42. Hypothetical fiber defect near delamination.

The second failure mode is delamination propagation towards the boss, Figure B-43. A delamination in this region could have uncertain effects due to the large external loads that exist in this region. Progressive failure analysis, as described earlier, was used to predict delamination growth. Fracture toughness properties were not available from test data, so values from 1.0–5.0 lbs/in were assumed. The analysis predicted delamination growth in the region of ply drop-offs, which can be explained by the high transverse shear stresses present in this region. Once the delamination grew outside of the drop-off region, the delamination growth rate slowed substantially. Further, results showed that this growth was insensitive to the fracture toughness chosen, Figure B-44. Again, based on previous experience, delamination growth characteristics are driven by multiple factors and this example should not be used for the assessment of any other structure, especially considering that delamination growth to the boss is plausible.
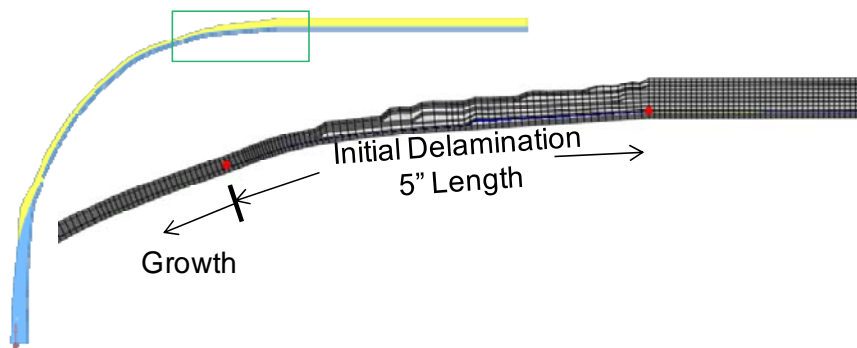

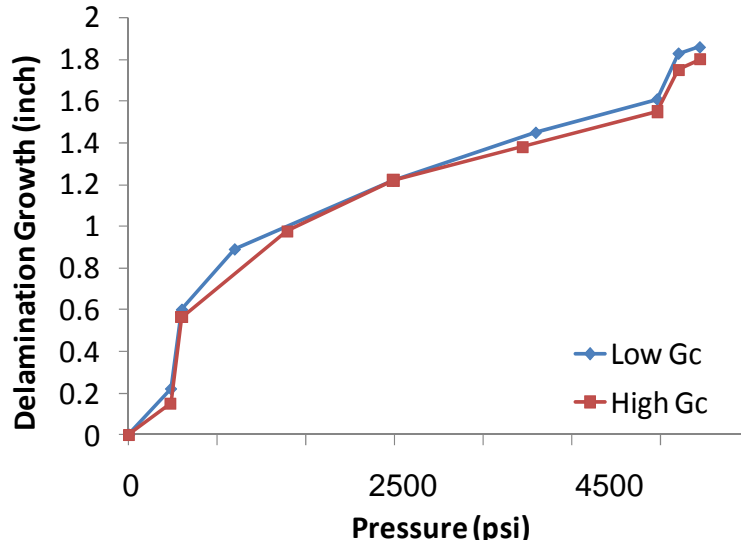Figure B-43. Direction of delamination growth in this example.

Figure B-44. Predicted delamination growth for low and high fracture toughness values.

In summary, an example was used to demonstrate how progressive failure analysis in conjunction with state-of-the-art pre-processing tools can be used to evaluate delaminations in COPVs. A limitation of this example is that not all failure modes were considered. While these tools can be used as part of an assessment of other failure modes, additional sophisticated analysis may be required. Particular to liner buckling, analysis tools need to be improved and validated through a test, non-destructive evaluation and analysis program.

B-11 References

B-1. Goyal, V. K.; Jaunky, N.; Johnson, E.; and Ambur, D.: "Intralaminar and Interlaminar Progressive Failure Analyses of Composite Panels with Circular Cutouts." *Composite Structures*, 64, 2004, pp. 91–105.

B-2. Goyal, V. K.; Rome, J. I.; and Klug, J. C.: "Progressive Failure Analysis for the Prediction of Bearing Strength in Composites." *47th AIAA/ASME/ASCE/AHS/ASC Structures, Structural Dynamics, and Materials Conference*, Newport, Rhode Island, 1–4 May 2006, AIAA-2006-2172.

B-3. Puck, A.; and Schürmann, H. (1998): "Failure Analysis of FRP Laminates by Means of Physically Based Phenomenological Models." *Composite Science and Technology*, Vol. 58, Issue 7, July 1998, pp. 1045-1067.

B-4. Chang, F.; and Chang, K.: "A Progressive Damage Model for Laminate Composites Containing Stress Concentrations." *Journal of Composite Materials*, Vol. 21, 1987, pp. 834-855.

B-5. Pifko, A. B.; and Kushner, A. S.: *Impact Analysis of Composite Aircraft Structures, Computational Methods for Crashworthiness*. Ahmed K. Noor and Huey D. Carden (Compilers), NASA CP-3223, 1993.

B-6. Sleight, D. W.; Knight, N. F., Jr.; and Wang, J. T.: "Evaluation of a Progressive Failure Methodology for Laminate Composite Structures." *In Proceedings of the AIAA/ASME/ASCE/AHS/ASC 38th Structures, Structural Dynamics, and Materials*.

B-7. Anon.: ABAQUS User's Manual, Vol. 1-3, Version 5.6. Hibbitt, Karlsson, and Sorensen, Pawtucket, RI, 1995.

B-8.   Goyal, V. K.; Johnson, E.; Davila, C.; and Jaunky, N.: "An Irreversible Constitutive Law for Modeling the Delamination Process Using Interface Elements." *Proceedings of the AIAA/ASME/ASCE/AHS/ASC 43rd Structures, Structural Dynamics, and Materials Conference*, April 22–25, 2002,Paper AIAA-2002-1576, CD-ROM, 2002.

B-9.   Goyal, V. K.; and Klug, J.: "Interphasic Formulation for the Prediction of Delamination." *45th AIAA/ASME/ASCE/AHS/ASC Structures, Structural Dynamics and Materials Conference*, Palm Springs, California, Apr. 19–22, 2004, AIAA-2004-1845, 2004.

B-10.   Hahn, H.; and Tsai, S.: "Nonlinear Elastic Behaviour of Unidirectional Composite Laminates." *Journal of Composite Materials*, 7, 1973, pp. 102-118.

B-11.   Hashin, Z.: 1980, "Failure Criteria for Unidirectional Fiber Composites." *Journal of Applied Mechanics*, 47, 329-334.

B-12.   Rome, J. I.; Schubel, P. M.; and Goyal, V. K.: "Prediction of Low Velocity Impact Damage in a Composite Sandwich using a Progressive Failure Methodology." *Paper presented at the 22nd ASC Technical Conference*.

B-13.   Goyal, V. K.; Schubel, P. M.; Rome, J. I.; and Keough, M. R.: "Enhancements to the Interfacial Element Formulation for the Prediction of Fracture." *Paper presented at the 48th AIAA Structures, Structural Dynamics, and Materials Conference*.

B-14.   Goyal, V. K.; and Johnson, E. R.: "Predictive Strength-Fracture Model for Composite Bonded Joints." *Composite Structures*, Volume 82, Issue 3, February 2008, Pages 434-446.

B-15.   Goyal, V. K.; Rome, J. I.; Klug, J. C.; Chang, D. J.; Katzman, H. A.; and Ross, F. D.: "Failure Modeling and Simulation of Composites Subjected to Bypass and Bearing Loads." *47th AIAA/ASME/ASCE/AHS/ASC Structures, Structural Dynamics, and Materials Conference*, AIAA 2006-2172, 1–4 May 2006.

B-16.   Rome, J. I.; and Goyal, V. K.: "Effects of Geometric and Material Parameters on the Strength of Composite Joints." *48th AIAA/ASME/ASCE/AHS/ASC Structures, Structural Dynamics, and Materials Conference*, AIAA 2007-2281, 23–26 April 2007.

B-17.   Chiu, S. T.; Shu, J. C.; and Chang, J. B.: "Evaluation of Analysis Methods for Composite Overwrapped Pressure Vessels." *The 1994 JANNAF NDE and Structures & Mechanical Behavior Joint Meeting*, Hill AFB, Utah, 24–28 October, 1994.

REPORT DOCUMENTATION PAGE

Form Approved
OMB No. 0704-0188

1. REPORT DATE *(DD-MM-YYYY)*	2. REPORT TYPE	3. DATES COVERED *(From - To)*
01-03-2012	Contractor Report	

4. TITLE AND SUBTITLE

Composite Structures Damage Tolerance Analysis Methodologies

5a. CONTRACT NUMBER

NNL04AA09B

5b. GRANT NUMBER

5c. PROGRAM ELEMENT NUMBER

6. AUTHOR(S)

Chang, James B.; Goyal, Vinay K.; Klug, John C.; Rome, Jacob I.

5d. PROJECT NUMBER

5e. TASK NUMBER

5f. WORK UNIT NUMBER

869021.05.07.04.11

7. PERFORMING ORGANIZATION NAME(S) AND ADDRESS(ES)

NASA Langley Research Center
Hampton, VA 23681-2199

8. PERFORMING ORGANIZATION REPORT NUMBER

ATR-2011(5175)-2

9. SPONSORING/MONITORING AGENCY NAME(S) AND ADDRESS(ES)

National Aeronautics and Space Administration
Washington, DC 20546-0001

10. SPONSOR/MONITOR'S ACRONYM(S)

NASA

11. SPONSOR/MONITOR'S REPORT NUMBER(S)

NASA/CR-2012-217347 (Corrected Copy)

12. DISTRIBUTION/AVAILABILITY STATEMENT

Unclassified - Unlimited
Subject Category 16-Space Transportation and Safety
Availability: NASA CASI (443) 757-5802

13. SUPPLEMENTARY NOTES

14. ABSTRACT

This report presents the results of a literature review as part of the development of composite hardware fracture control guidelines funded by NASA Engineering and Safety Center (NESC) under contract NNL04AA09B. The objectives of the overall development tasks are to provide a broad information and database to the designers, analysts, and testing personnel who are engaged in space flight hardware production.

15. SUBJECT TERMS

Linear elastic fracture mechanics; Crack growth; International Space Station; Fracture critical items; Stress analysis

16. SECURITY CLASSIFICATION OF:			17. LIMITATION OF ABSTRACT	18. NUMBER OF PAGES	19a. NAME OF RESPONSIBLE PERSON
a. REPORT	b. ABSTRACT	c. THIS PAGE			STI Help Desk (email: help@sti.nasa.gov)
U	U	U	UU	105	19b. TELEPHONE NUMBER *(Include area code)* (443) 757-5802

Standard Form 298 (Rev. 8-98)
Prescribed by ANSI Std. Z39.18